To be published in "Physics Reports"

Ref.TH.1387-CERN

MANY-PARTICLE PRODUCTION *)

D. Horn

CERN - Geneva

and

Tel-Aviv University, Tel-Aviv

A B S T R A C T

Recent developments in the theoretical and experimental analysis of many-particle production are discussed. After a summary of the main characteristics of the high energy reactions, we discuss the features of the multiperipheral model as an introduction to the recent theoretical developments. The longitudinal kinematics and some of their manifestations in the behaviour of cross-sections are reviewed before turning to the concepts of scaling and limiting fragmentation. The implications of these approaches are compared with available experimental data. This leads to the Reggeistic picture developed in Mueller's analysis. Its results are reviewed and analyzed in the regions of limiting fragmentation and pionization. Separate sections are then devoted to the triple-Regge limit and to diffraction dissociation. We close with a section on correlations, pointing out open problems for future research.

---

*) Research supported in part by the U.S. National Bureau of Standards.

Ref.TH.1387-CERN
20 August 1971

1. - INTRODUCTION

The purpose of this report is to cover and summarize some recent developments in the studies of many-particle production. It is based on an invited talk presented at the International Conference on Duality and Symmetry in Hadron Physics which took place on April 1971 in Tel-Aviv. This field is right now in the process of very rapid growth and, therefore, it turns out that even in the short period that passed since that conference took place, a lot of new information was gathered and analyzed. We try to cover a big part of it in this paper. We do not intend to present a comprehensive review of all theories and models which were developed during the years for the analysis and understanding of the production processes of many particles. Instead we concentrate on theoretical models and phenomenological studies that are most strongly connected to those topics that recently became very fashionable. Since the theoretical studies, as well as the experimental analyses, are doing still their first steps, there exists of course the danger that part of what is said here will change within a relatively short time. Nevertheless, this is also the reason for the interest in this field - since everything is in stages of development new research works are called for to establish the character of the phenomena involved.

The main obstacle that many theoretical approaches are faced with is the fact that there are not really so many particles produced in the high energy experiments. We are usually concerned with energy regions where the main contributions to the cross-sections come from reactions in which five to ten particles are produced. This number is too big to allow a simple description in terms of well-defined exchanges as in two-body production, and too small to be treated in a statistical fashion. Since this number of produced particles grows very slowly with energy, we will not be able to avoid this difficulty in the foreseeable future. We have therefore to accept this impasse as a fact of life that we have to learn to cope with. The same problem manifests itself also in a different aspect - the difficulty in proving or disproving models of particle production. Many models differ only in the description of "asymptotic" phenomena and it is unclear yet what their corresponding energy ranges are and when they will be reached. We will therefore follow the common trail of abstracting the general properties from models and then trying to implement them in the analysis of available data. We try to derive these properties in a simple intuitive fashion, and discuss their validity by using many of the recent experimental results.

The study of many-particle production is a pragmatic trend in physics. The reason is simply that in the high energy machines that are developed nowadays, a natural emphasis will be given to the production of relatively large multiplicities. Nevertheless, the developments in the recent years have shown that it presents new challenges and calls for new insights. Part of the achievements are discussed here. Many more will certainly follow in the near future.

2. - GENERAL PROPERTIES

In this section we will point out some of the more basic and well-known properties of many-particle production. For a more comprehensive review, as well as more detailed numerical fits and estimates, we refer the reader to Wroblewski's rapporteur talk at Kiev [1]. Many of the more recent results are covered by Deutschmann [2] in his rapporteur's talk at Amsterdam.

2.1. - Abundance of pions

A striking fact is that most particles that are produced in the high energy collisions are pions. Thus, e.g., at 25 GeV $\pi^- p$ reactions [3] only 16% of the produced channels include strange particle production. Even these strange particles are usually accompanied by pions. We note therefore that the problem at hand is far from being close to the SU(3) limit. This is so although the sums of the various cross-sections, namely the total cross-sections, do obey many symmetry relations. When we discuss many-particle production, we are treating mainly the production of many pions together with one or two baryons, as determined by the quantum numbers of the incoming particles.

2.2. - Poisson-type distributions

A typical distribution [4] of the cross-sections for the production of non-strange particles in 16 GeV $\pi^- p$ reactions is plotted in Fig. 1 vs. the number of prongs observed. They fall on a curve similar to a Poisson distribution. There exist many papers on the question whether it is really a Poisson distribution, and if so in which variable [1]. In order to avoid this problem right now we called it a "Poisson-type" distribution referring to the characteristic structure of a broad peak for low values of $\langle n_c \rangle$ and a steep fall for higher values. One normally leaves out the elastic cross-section from these plots regarding it later as the shadow of all inelastic channels. The elastic point is added in the figure for comparison.

2.3. - Low transverse momenta

The transverse momenta (p_T) of the outgoing particles are usually of the order of 300 MeV or so and do not change appreciably with the incoming energy. In Fig. 2 we present the transverse momentum distributions of pions produced in $\pi^- p$ experiments [5]. One observes a peak at $p_T^2 = 0$ followed by a steep fall with a slope varying between 10 to 3 $(\text{GeV})^{-2}$.

The production processes can be described within a cylinder in momentum space. This is shown in Figs. 3 and 4 which also emphasize the two characteristic modes of production discussed in the following paragraph.

2.4. - Leading particles and pionization

In Fig. 3, we observe that the proton distribution is clearly concentrated near the location of the incoming (target) proton. The π^- distribution (there are two π^- mesons produced) has a strong tail in the direction of the incoming π^-. These two particles that follow the trend of the incoming particles are referred to as "leading particles". In contrast one finds all other pions around the c.m. origin. This phenomenon, namely the existence of a cloud of pions with low c.m. longitudinal momenta (p_L) is sometimes referred to as pionization. This concept was first introduced by Pal and Peters [6] in the context of a production mode in high energy collisions. It is often used for describing a concentration of pions around the c.m. that stays finite as one increases the incoming energy indefinitely. We will use it more freely to describe the phenomenon that exists at available energies.

The description of the process in momentum space has one deceiving aspect to it, namely, one may tend to think that this separation between the leading proton and all the pions exists in configuration space. This is not true since if a proton and a pion move with the same velocity, the ratio between their two momenta is m_p/m_π thus favouring strongly a separation in momentum space. It means also that Fig. 3 does not preclude the existence of resonances in intermediate stages which then decay into the proton and pions.

Figure 4 shows the average momentum vector of the outcoming particles as a function of the multiplicity. One sees again the clear cut-off in p_T. We note also the decrease in the leading particle effect as the multiplicity increases.

Figure 5 shows all the above-mentioned effects in the production spectra of pp reactions [7]. Even after integrating upon all other emitted particles one still clearly observes the leading effect in the proton distribution : it is flat whereas all other distributions peak towards the c.m. The different scales in the various distributions provide the evidence for the abundance of pions. Note also the similarity in the p_T distributions of all emitted particles. They are plotted here vs. p_T rather than p_T^2, the variable used in Fig. 2.

An exception to the rule of leading particles is given by $\bar{p}p$ annihilation and we may justly ask ourselves whether the $\bar{p}p$ reactions fall into the same category with the πp and pp ones where annihilation is absent. Figure 6 shows the relative importance of the various types of channels in $\bar{p}p$ reactions. The total annihilation cross-section is falling with energy. The highest point where this is measured is at 7 GeV. The data up to this point can be fitted by $\nu^{-0.6 \pm 0.03}$ where ν is the incoming laboratory energy [8]. We may expect therefore that, at higher energies, the $\bar{p}p$ reactions will resemble more and more the pp ones. The proportion of the elastic vs. the total cross-sections as well as the amount of strange particle production is similar to that observed for other incoming particles when absorption channels are absent.

2.5. - Increase of the average multiplicity

The average multiplicity of the particles produced grows slowly with energy. A compilation by Czyzewski and Rybicki [9] of data in the ν range of tens of GeV is consistent with a power increase of the multiplicity of charged particles, as $W^{0.7}$, where $W = \sqrt{s}$ is the total c.m. energy. Recent cosmic rays data [10] provide evidence for a logarithmic increase in the ν ranges of hundreds of GeV, as shown in Fig. 7. Such energies are available in the ISR and soon will be available in NAL. One clearly looks forward to a verification of these results, especially since recent emulsion data [11] from Serpukhov seem to follow the $W^{0.7}$ behaviours in contradiction [2] with the cosmic rays results of Ref. [10].

3. - THE MULTIPERIPHERAL MODEL

The logarithmic increase of the multiplicity is one of the well-known results of the multiperipheral model. This model, otherwise known also as the ABFST model [12], was suggested in 1962 and is a straightforward generalization of the peripheral approach to two-particle production amplitudes. A scattering amplitude is described by a diagram of the form of Fig. 8. The two question marks refer to the two basic questions - what is exchanged and what is produced. We know that eventually one observes pions, nevertheless it may be that they come mainly in forms of ρ and perhaps σ mesons. We will return to this question of correlations between the pions in the Section 11. Let us just note here that a model of such meson production would be consistent with pion exchanges. Indeed the original ABFST model dealt with pion exchanges. It was of course soon generalized to include Regge pole exchanges [13]. The trouble with the multi-Regge exchange model is that its application can be justified only for about 10% of the data at conventional energies [14]. Although several successful modifications have been suggested, such as the CLA model [15] and multi-Veneziano formulae [16], we saw in the last two years a return to the old pion-exchange model [17].

The arguments that we are going to bring here for the derivation of the logarithmic increase of the multiplicity are quite general and independent of the exact details of the model. We follow Fubini [18] and note that if one changes all the coupling constants by a continuous parameter then all n particle cross-sections (σ_n) will change accordingly as

$$\sigma_n \to \lambda^n \sigma_n \qquad \sigma_T = \sum_{n=2}^{\infty} \sigma_n \to \sum_{n=2}^{\infty} \lambda^n \sigma_n \tag{1}$$

It follows from Eq. (1) that

$$\langle n \rangle = \frac{\lambda}{\sigma_T} \frac{\partial}{\partial \lambda} \sigma_T \Big|_{\lambda=1} \tag{2}$$

We assume now that the total cross-section has a leading power behaviour, namely

$$\sigma_T(\lambda) \approx \beta(\lambda)\, s^{\alpha(\lambda)-1} \tag{3}$$

and the choice $\lambda = 1$ leads to the expected asymptotic result $\alpha = 1$. It follows then that

$$\langle n \rangle = \left(\lambda \alpha'(\lambda) \ln s + \frac{\lambda \beta'(\lambda)}{\beta(\lambda)}\right)\Big|_{\lambda=1} = a \ln s + b \tag{4}$$

Two main assumptions went into this calculation. The first one is that there exists a simple basic mechanism by which all cross-sections change proportionally. This is characteristic of independent production as well as quasi-independent mechanisms like the multiperipheral model. This leads also to Poisson-like distributions of the type discussed in the previous section. The second assumption is that of the leading power behaviour. Within a specific multiperipheral model, one can of course calculate explicitly the various cross-sections. Figure 9 shows the results of such a calculation by Wyld [19] who looked at $\pi\pi \to n\rho$ mesons via pion exchanges. He calculated the resulting Feynman diagrams using the physical masses of the ρ and π and varying the $\rho\pi\pi$ coupling constant until a constant asymptotic σ_T was reached. We note how quickly σ_T reaches its constant value. The calculation fixes the $\rho\pi\pi$ coupling constant and the total cross-section. Both come out much too big. The discrepancy in the orders of magnitude prevails also in more sophisticated versions of this model [20]. Recently, Abarbanel et al. [21] suggested an interpretation that circumvents this difficulty. They discussed pseudoscalar scattering that results in vector-meson production, in the limit of unitary symmetry. They looked for the leading singularity in a Bethe-Salpeter equation - the equivalent of summing all diagrams of the type of Fig. 8. The only parameter left in their problem was M_V - the mass of the vector mesons, and they derive the result

$$\sigma_T = \frac{16\pi^3}{N}\,\frac{1}{M_V^2} \tag{5}$$

where N is the dimensionality of the multiplet. By choosing $N = 8$ and $M_V = 900$ MeV one gets $\sigma_T = 30$mb. Although the resulting σ_T has a reasonable magnitude one has to remember that the actual situation is very far from the $SU(3)$ limit - as already stressed in the previous section. One may doubt therefore whether this can be regarded as a realistic derivation of the observed magnitude of the total cross-section.

The big advantage of the multiperipheral model, in any of its many variations, is that it is the only simple generalization of the known techniques for two-particle production. Although detailed predictions may fail in experimental applications of the model, it may still serve as a guide to our intuition when discussing the complex phenomena of many-particle production. It is indeed this model [12], [18] that led to the

concept of scaling, now so widely used in discussions of many-particle production. We will therefore discuss some of its predictions for the momentum space distributions of the emitted particles.

Let us use the labels of Fig. 8 to define the momenta involved in the process. We now introduce the quantities $p^{(\pm)}$ and the "transverse mass" m_T defined by

$$p^{(\pm)} = E \pm p_L \qquad m_T^2 = m^2 + p_T^2 \qquad p^{(+)}p^{(-)} = m_T^2 \tag{6}$$

The quantities $p^{(\pm)}$ depend of course on the frame of reference, nevertheless the ratio of quantities like $p^{(+)}$ for two different momenta is invariant under longitudinal boosts [see Eq. (8) below]. It is indeed such a quantity that appears in the calculation of $t_i = k_i^2$. If one stays in the laboratory frame $q_2 = (M_2;\vec{0})$ $q_1 = (\nu;0,0,\sqrt{\nu^2-M_1^2})$ one finds for high ν values that

$$t_1 = k_1^2 = \frac{k_1^{(+)}}{q_1^{(+)}}\left(M_1^2 - \frac{m_{T_1}^2}{1-\frac{k_1^{(+)}}{q_1^{(+)}}}\right) - p_{T_1}^2 \tag{7}$$

The propagator of k_1 exchange restricts the allowed t_1 values and peaks around $t_1 \approx 0$. This reflects itself in a limited range for $p_{T_1}^2$ as well as for the ratio of $k_1^{(+)}/q_1^{(+)}$. Similar relations can be obtained for $k_2^{(+)}/k_1^{(+)}$, etc. A careful analysis leads to the result [18] that the optimal configuration of this model is obtained when all $p_{T_i}^2 \approx 0$ and all ratios $k_{i+1}^{(+)}/k_i^{(+)}$ are roughly equal. Similarly, one will obtain that all $p_{i+1}^{(+)}/p_i^{(+)}$ will be roughly equal.

It is convenient to introduce now a new variable - rapidity [22], [23], [24] - defined by the following equations

$$p^{(\pm)} = m_T e^{\pm y} \qquad \beta_L = \frac{p_L}{E} = \tanh y \qquad \frac{dp_L}{E} = dy \tag{8}$$

in terms of which the prediction of constant ratios between consecutive $p^{(+)}$ values means constant differences between consecutive rapidities (see next section for an extensive study of rapidity). This is borne out by the explicit calculation of De Tar [23] based on a simplified Chew-Pignotti [13] model. The results, shown in Fig. 10 exhibit the asymptotic distribution of particles enumerated by their location on the multiperipheral chain ($p_T = 0$ was assumed). Note that although the peaks are located at equal distances, there is a clear spread of the single particle distributions. In the central region the resulting picture is invariant under small changes of y, namely, under small longitudinal boosts.

We can now use this knowledge in order to get a rough estimate of the cross-sections. If we denote the ratio of consecutive $k^{(+)}$ values by a then, since $q_1^{(+)} \approx 2\nu$ and $q_2^{(+)} \approx M_2$ in the laboratory frame, it follows that

$$a^n = \frac{2\nu}{M_2} \qquad n \ln a = \ln \frac{2\nu}{M_2} \tag{9}$$

where n is the optimal multiplicity. This is an alternative proof of the logarithmic increase of the multiplicity with the energy ν, since a depends only on the properties of the exchanged propagators. Using conventional values of ν, M_2 and n one is led to $\ln a \approx 1$. This is therefore the expected difference in rapidity between neighbouring particles on the multiperipheral chain. In order to get an estimate of the cross-section for the production of $n+2$ particles [25] let us assume that they are distributed equally along the rapidity variable with the simple restriction $y_i > y_{i+1}$. Neglecting the transverse momentum dependence and remembering that $dp/E = dy$ we obtain

$$\sigma_n = \frac{cg^n}{\nu^2} \int_0^{\ln \frac{2\nu}{M_2}} dy_1 \int_0^{y_1} dy_2 \cdots \int_0^{y_{n-1}} dy_n = \frac{cg^n}{\nu^2} \frac{\left(\ln \frac{2\nu}{M_2}\right)^n}{n!} \tag{10}$$

The ν^{-2} factor includes the incoming flux factor as well as the effect of energy momentum conservation (see next section for discussion of phase space integrals). The resulting total cross-section will then exhibit the wanted (Regge) power behaviour

$$\sigma_T = \sum_n \sigma_n \sim \nu^{g-2} \tag{11}$$

which was the basis of the discussion at the beginning of this section.

Summarizing, we see that the main characteristic results of the multiperipheral model are the low p_T values, the logarithmic increase of the multiplicity and the equal distances in the rapidity distribution. (Scaling or limiting fragmentation, which can also be derived in this model, will be discussed below in Sections 6 and 7.) Whatever the exact details of the multiperipheral model are, we would expect it to yield an even distribution of the emitted particles in rapidity.

There are several other ways which lead to an expectation of a dp_L/E distribution. Thus Feynman [22] argues that because the Lorentz contracted field is so sharp in the longitudinal direction in configuration space, its energy must be uniformly distributed in p_L. Therefore, individual particles that carry energy E will have a longitudinal momentum distribution of dp_L/E. Furthermore he points out that the uniform distribution in rapidity has the important character that if a set of particles obeys it, then also the set of their decay products will have this property. The emerging picture is discussed by Wilson [24], who refers to it as a "Feynman gas" of many particles with short range correlations confined to a cylinder in phase space (whose co-ordinates are rapidity and $\vec{p}_T$). A similar conclusion comes also from interpreting the colliding particles as composite objects which therefore should not have any preferred centre of collision [26]. Experimentally, however, such a centre seems to exist, at least in the energy ranges accessible to present day experiments.

In Fig. 11, we show the π^- spectrum obtained [27] in 19 GeV pp collisions. The various p_T cuts show similar patterns of Gaussian shapes in rapidity. When the integrated p_T distribution of the same data is replotted in a linear scale in Fig. 12 it is clear that we are still very far away from a flat distribution. It remains to be seen whether experiments at higher energies will indeed show a significant plateau over wide ranges in rapidity.

4. - LONGITUDINAL KINEMATICS AND DYNAMICAL MODELS

In a realistic model one would naturally associate with the different k_i of Fig. 8, different types of exchanges. The exchange of k_i connects the momenta p_i and p_{i+1}. The energy of this subsystem is proportional to $p_i^{(+)}/p_{i+1}^{(+)}$ since in the rest system of p_{i+1} this ratio becomes $(E_i + p_{L_i})/M_{i+1} \approx (2E_i/M_{i+1})$ in the high energy limit. In this limit one can therefore associate with each such subsystem a factor of $(p_i^{(+)}/p_{i+1}^{(+)})^{\alpha_i(t_i)}$ where α_i is the power corresponding to the relevant exchange. If a single type of exchange α dominates the chain, one may expect therefore that it will be reflected in the cross-section which will then behave as

$$\sigma \approx \nu^{2\alpha-2} \tag{12}$$

Thus pion exchange will lead to $\alpha \approx 0$ and baryon exchanges will reduce this power. A recent analysis of 64 reactions by Hansen, Kittel and Morrison [28] shows that the energy behaviour of the various cross-sections is indeed specified by the exchanged quantum numbers rather than, say, the multiplicity of particles observed. Their analysis is summarized in Table I.

Reaction	Exchange	α
$(\pi, K, p) + p \rightarrow (\pi, K, N) + N + \text{pions}$	Meson S = 0	0
$K^- p \rightarrow \Lambda + \text{pions}$	Meson S = 1	$-\frac{1}{2}$
$K^- p \rightarrow \Xi^- + K + \text{pions}$	Baryon S = 0	- 1

TABLE I - Energy behaviour of cross-sections

To derive their results the authors used a trick, namely, they looked at σ_A defined by

$$\sigma_A \propto \sigma \frac{\nu^{n-2}}{\text{Phase Space}} \tag{13}$$

rather than at the cross-section σ. n is the multiplicity of the channel discussed and A stands for "asymptotic" since asymptotically the phase space term behaves like ν^{n-2}. The behaviour of σ and σ_A for a particular channel is shown in Fig. 13. We see that the effect of the multiplicative factor in (13) is to raise the lower part of σ and, miraculously enough, it leads to simple power behaviour from low energies onward.

The phase space term referred to above is given by the Lorentz invariant expression

$$P.S. = \int \prod_i \frac{d^3 p_i}{E_i} \delta^{(3)}(\sum_i \vec{p}_i) \delta(\sum_i E_i - W) = W^{2n-4} F_{ps}\left(\frac{W}{\mu}\right) \qquad (14)$$

where we used the momenta and energies in c.m. and $W = \sqrt{s}$ is the total c.m. energy. If one assumes for simplicity that all particles have the same mass μ then one can prove the right-hand side equality. The function $F_{ps}(W/\mu)$ is regular in the limit $\mu \to 0$ or $W \to \infty$ and therefore the asymptotic behaviour of P.S. is like W^{2n-4} or ν^{n-2}. Obviously σ does not behave like P.S. since it is decreasing with energy. We know already from the general properties listed in Section 2 that phase space is far from being homogeneously filled. Figures 2 and 3 demonstrate clearly the strong cut-off in the transverse momentum. If one introduces such a cut-off K into the P.S. formula, it will lead to

$$P.S. \xrightarrow{p_T < K} W^{2n-4} \left(\frac{K}{W}\right)^{2n-2} F(W, K, \mu) \qquad (15)$$

which has a leading W^{-2} behaviour provided F. is a regular function in W. [Compare this with the increasing W^{2n-4} behaviour of Eq. (14).] To facilitate calculations one might try instead of this more realistic P.S. formula an approximate expression in which all particles have a fixed (and common) transverse momentum

$$f_n = \int \prod_{i=1}^{n} \frac{dp_{L_i}}{E_i} \delta(\sum_i p_{L_i}) \delta(\sum_i E_i - W) = \frac{1}{W^2} F_n\left(\frac{W}{m_T}\right) \qquad (16)$$

where $m_T^2 = \mu^2 + p_T^2$. Once again we see the decreasing W^{-2} behaviour. The function $F_n(x)$ behaves roughly like $(\ell n\, x)^{n-2}$ and leads therefore to a structure [29] shown in Fig. 14. We note that the shape is very similar to that of σ in Fig. 13. One may therefore correlate the shape of the cross-section with the dynamical bounds on the available transverse momenta.

From the discussion in both this and the previous sections, it is clear that most of the physical effects will have to be looked for in longitudinal momentum distributions. This is true in the analysis of a few outgoing particles as well as the collective effects of many emitted particles [30]. In the previous section, we introduced a variable - rapidity - that, from the point of view of the multiperipheral model, plays

a special simplifying role. Let us here discuss this variable at some length. Rapidity is denoted in the literature by either z or y. We will use y when it is measured in the laboratory frame, and z when it refers to c.m. momenta. Unless otherwise specified, we will use c.m. variables, in terms of which we repeat the definition

$$m_T = \sqrt{m^2+p_T^2} \qquad p_L = m_T \sinh z \qquad E = m_T \cosh z$$

$$\beta_L = \frac{p_L}{E} = \tanh z \qquad \frac{E \pm p_L}{m_T} = e^{\pm z} \qquad \frac{dp_L}{E} = dz \tag{17}$$

A longitudinal boost is equivalent to a linear translation $z \to z - z_o$ which is reflected in the fact that the Lorentz invariant differential element of phase space is $dp_L/E = dz$. The longitudinal velocity β_L is independent of the mass of the particle and is therefore directly given by the rapidity. The relation between several of these variables is demonstrated in Fig. 15. The points A, B, C denote characteristic values of longitudinal momenta of pions (A, B) and a proton (C) that have the same rapidity (and velocity) but completely different longitudinal momenta because of their different transverse masses *). This is a partial reason for the concentration of pions around the c.m. (see Section 2). Whereas the velocity (β_L) can vary between ± 1, the rapidity (z) varies between $\pm \ell n(W/m_T)$. We show also on Fig. 15 a characteristic $1/E$ plot which is the expected shape of a momentum distribution if the rapidity distribution is flat. As already mentioned before, one finds experimentally Gaussian shapes in rapidity.

The rapidity plots have the important property that they expand the region of low $p_L^{c.m.}$ [30]. This can be clearly seen in Fig. 16 which is taken from De Tar [23]. Here we have a comparison between plots in rapidity (where $y = 2$ corresponds to $z = 0$), c.m. longitudinal momentum (denoted in Fig. 16 by $p_{\parallel}^*$) and lab longitudinal momentum ($p_{\parallel}$). The vertical axis is the transverse momentum ($p_\perp$). Comparing Figs 16a and 16b we see that the rapidity plot magnifies the region of low $p_L^{c.m.}$ enormously. On the other hand, we learn that most of the negative $p_L^{c.m.}$ axis is actually a mapping of negative momenta in p_L^{lab} (the line A characterizes this limit). This is a fact that we will have to bear in mind since a lot of attention is given to these two regions. The first is called the central (or pionization) region and the second is the fragmentation region. We learn therefore that in order to study the first one we should use rapidity plots and for the second a $p_L^{c.m.}$ plot.

The shaded areas in Fig. 16 correspond to pionic contributions from $pp \to \Delta\Delta \to \pi$ + anything. We note the regular patterns in rapidity compared to the distorted contours obtained in $p_L^{c.m.}$ and p_L^{lab}. One may say that because longitudinal boosts lead to translational transformations in rapidity, plots in the latter variable conserve the symmetry that is evident in the Δ rest frame. Another way to put

---

*) The name "longitudinal mass" would be more appropriate since it specifies the relation between p_L and E. We continue to denote it by m_T because of its common use in the literature.

this statement is that if there exists one rest frame in which a symmetric distribution is achieved then the rapidity plot will show it. We will use this property in Section 8 when we will look for the frame of reference in which the pionization distribution is symmetric.

Another interesting feature which is manifested in Fig. 16 is that for $p_L^{lab} \gg p_T \gg m$ one finds $y = \ell n(2/\tan\theta_{lab})$. This latter variable was introduced long ago by Lindern [31] because of its usefulness in the analysis of cosmic rays data. Line E in Fig. 16 shows that a measurement of the cross-section at fixed laboratory angle and large momenta is equivalent to looking at the large p_T structure for fixed rapidity. Before leaving this subject of rapidity distributions, we have also to mention the fact that the distance between two points on the rapidity scale determines the invariant mass of the corresponding two momenta. A simple manipulation of Eq. (17) leads to the result that for two particles with equal transverse masses, one finds $(p_1 + p_2)^2 = 2m^2 + 2m_T^2 \cosh(z_1 - z_2) - 2\vec{p}_{T_1}\cdot\vec{p}_{T_2}$.

There seems to be some clear physical distinction between the longitudinal and transverse momenta distributions. The similar transverse distributions of all secondaries can be thought of as a Fourier transform of a Gaussian shaped region of collision in configuration space. Its structure reflects then the structure of the colliding particles [32]. On the other hand, one finds in the longitudinal distributions detailed evidence for the reactions that took place between the two colliding particles. The idea of using longitudinal phase space analyses was proposed by Van Hove [33]. It leads to important information about the correlations between the particles produced in low multiplicity events, and allows one to estimate the dominant exchanges in the production process. We refer to Ref. [30] for a summary of the main results. Various models were proposed in the literature to explain the general characteristics of the distributions in either one of these two directions. Until now, we have concentrated mainly on the results of the multiperipheral model for longitudinal distributions. We have stressed this model because it can serve best as an introduction to the recent results that we will discuss in the following sections. Let us, however, use this place to give a short summary of other models, so as to be acquainted with their ideas and terminology.

The thermodynamical model [34] predicts the form of the transverse momentum distribution. It pictures the particle spectrum as consisting of a black-body radiation from a continuous longitudinal distribution of decay centres (fireballs). In each such centre the spectrum follows Planck's law $c/(e^{E/kT} \pm 1)$ (+ for fermions and - for bosons). A temperature T_o is determined from the structure of the mass spectrum (number of possible hadronic states per mass interval) which is predicted to behave like $m^{-5/2} e^{m/kT_o}$. Fitting present knowledge of hadronic states, the authors conclude that $T_o = 160$ MeV. This is then considered to be the maximal possible temperature. The distributions in momentum space are then fitted by using some distribution in the longitudinal momentum on which the fireball structure is superimposed with a T which varies slowly around $0.8\ T_o$. The longitudinal distribution is chosen so as to fit the different trends evident from the data (Fig. 5). It can be made consistent with limiting fragmentation and pionization pictures which will be discussed in the following sections.

So what is the longitudinal structure after all ? An early attempt by Van Hove [35] pictured the particle emission as the formation of a cloud of independent particles. By using unitarity, one finds that the overlap of this distribution with itself leads to the diffraction shape. Since the elastic scattering is sharply peaked in t one concludes that the distributions of the particles in momentum space must have components that have much higher p_L than p_T values, namely leading particles [36]. An interesting question by itself is whether one can really use a concept of independent emission of pions. This is very suggestive in a model in which the pions are formed in coherent states - the analogue of classical (electromagnetic) radiation. It was first suggested by Lewis, Oppenheimer and Wouthuysen [37] and is still often discussed in the literature. The quantum numbers of the pions form, however, severe constraints which will be partially discussed in Section 11.

Several models of the longitudinal distributions originated in the studies of cosmic rays data. A famous one is the two-fireball model which claims that the hadronic collision results in the formation of two distinct hadronic centres [38]. Each fireball decays symmetrically and the total energy is absorbed by the longitudinal momentum of the fireball. At low energies it is then impossible to distinguish between two fireballs and one fireball, but as the total available energy W increases, one should start to see a dip at $p_L = 0$ which should then develop into a well-pronounced separation between the two decay centres. Cosmic rays data lead, however, also to an orthogonal suggestion [6] - the formation of a pionization cloud in addition to the production of leading isobars. This may lead to an eventual clear separation between two leading clouds and a pionization centre in p_L. We may hope that the new generation of high energy machines will shed some light on these questions and select the right description. Until this becomes available, let us return to the analysis of conventional momentum distributions.

5. - DISTRIBUTIONS IN MOMENTUM SPACE

We would like to start this section by demonstrating that the variable rapidity not only reflects a nice theoretical trick, intended to exhibit invariant quantities, but has also some direct physical importance. This can be seen in Fig. 11 which shows a similar shape in rapidity for all the different p_T cuts. This is a non-trivial result since if plotted vs. p_L the various p_T cuts look completely different. We see in Fig. 17 the p_L distribution of π^- mesons produced in 28.5 GeV pp collisions [39]. The plots show the cross-sections for various numbers of prongs and for various cuts in p_T together with fits by simple exponential functions in p_L. We note three important features :

(1) the strong peaking around $p_L = 0$ precludes a simple phase space $(1/E)$ behaviour ;

(2) the slope of the functions increases as the number of prongs increases ;

(3) the slope decreases as p_T increases. This fact means also that the average p_T is smallest at $p_L = 0$ and increases slightly as p_L increases.

The first point was mentioned already several times and reflects itself in the Gaussian shapes of Fig. 11. The third point is the one responsible for the fact that the various p_T curves in Fig. 11 did show the same shape. The reason for this is that $p_L = m_T \sinh z$ and m_T includes in it the transverse momentum, hence the same value of rapidity stands for a higher p_L value in higher p_T configurations. This leads to a broadening of the p_L distributions seen in Fig. 17. We may conclude that, apart from the clear sharp decrease in p_T values, we may consider the p_L behaviour (at least for low $p_L^{c.m.}$) as determined by the transverse mass of the pions. The same consequence can be drawn also from Fig. 18 which shows the inclusive invariant cross-sections [see Eq. (18) below and the following discussion] for π^+ and π^- in a 16 GeV π^-p experiment [5]. A comparison is made here between distributions in a normalized $p_L^{c.m.}$ (denoted by p_L^* in the Figure) scale and a normalized rapidity scale (ξ). The π^+ data show that the different p_T selections retain their shape in rapidity and change their shape in p_L. The π^- show a similar tendency which is, however, modified by the leading particle effects in this mode.

We define the Lorentz invariant distribution in momentum space by

$$\rho_i(p) = E\frac{d^2\sigma}{2\pi p_T\, dp_T\, dp_L} = \frac{d^2\sigma}{2\pi p_T\, dp_T\, dz} \qquad (18)$$

where i designates a particle of type i (e.g., π^-) and σ is a cross-section out of which ρ_i is extracted. Both Figs. 11 and 18 showed distributions where σ was the total cross-section (σ_T). In this case one discusses an inclusive distribution in Feynman's terminology [22]. Since in the following sections we will discuss mostly inclusive distributions of the type $a + b \to c + \text{anything}$ we will use for them a shorthand notation of the form (ab, c). σ can also present a certain partial cross-section (e.g., $pp \to \pi^- +$ 3 prongs) or even a single channel σ_c (e.g., $pp \to pp\pi^-\pi^+\pi^0$). Let us discuss first σ_c. It can be described by

$$\sigma_c = \int g_c(p_1,\dots,p_n,\vec{q},W)\,\frac{d^3p_1}{E_1}\cdots\frac{d^3p_n}{E_n}\,\delta^{(3)}\Big(\sum_{i=1}^{n}\vec{p}_i\Big)\,\delta\Big(\sum_{i=1}^{n}E_i - W\Big) \qquad (19)$$

where $p_1 \dots p_n$ are the momenta of the emitted particles, W the total c.m. energy and $\vec{q}$ the c.m. momentum of the target. The function g_c corresponds to the square of the wave-function in momentum space and includes also the appropriate flux factor. An (exclusive) experiment that will give us all possible information on this function is in general out of question since the number of (momentum) variables grows so quickly that it makes such a prospect unfeasible. We look therefore first at a distribution of the kind

$$\rho_i^c(p) = n_i\int g_c(p_1,\dots,p_n,\vec{q},W)\,\frac{d^3p_2}{E_2}\cdots\frac{d^3p_n}{E_n}\,\delta^{(3)}\Big(\sum_{j=1}^{n}\vec{p}_j\Big)\,\delta\Big(\sum_{j=1}^{n}E_j - W\Big) \qquad (20)$$

where we assumed that particle 1 was of type i. n_i is the number of particles of type i in g_c. The distribution $\rho_i^c(p)$ reflects both the structure of g_c as well as the restrictions imposed by momentum conservation. The latter ones will also affect the distribution for any partial cross-section as well as the inclusive $\rho_i(p)$. Our intuitive feeling is that the higher the energy in question the less important the phase space restrictions become. Let us prove that this is the case.

We limit ourselves first to the line $p_T = 0$. Let us now define

$$\sigma_A(W) = \sum_{n,\alpha} \int g(p_1,\dots,p_n,\alpha,\vec{q},W)\, \delta^{(3)}\Big(\sum_{j=1}^{n} \vec{p}_j\Big)\, \delta\Big(\sum_{j=1}^{n} E_j - W\Big)\, \frac{d^3p_1}{E_1} \dots \frac{d^3p_n}{E_n} \tag{21}$$

where α is the set of quantum numbers required by a condition A (like "4 prongs"). We then look at

$$\rho_i(p_L,0) = \sum_{n,\alpha} n_i \int g(p_1,\dots,p_n,\alpha,\vec{q},W)\, \delta^{(3)}\Big(\sum_{j=1}^{n} \vec{p}_j\Big)\, \delta\Big(\sum_{j=1}^{n} E_j - W\Big)\, \frac{d^3p_2}{E_2} \dots \frac{d^3p_n}{E_n}\Bigg|_{p_{T_1}=0} \tag{22}$$

Since we look for the effect of energy momentum conservation let us assume for a moment that the various g are constant. In other words we test the assumption that the dependence on p_1 is just given by longitudinal phase space. In that case, Eq. (22) leads to

$$\rho_i(p_L,0) = f(M) \tag{23}$$

where M is the missing mass of all other particles emitted in addition to particle 1 :

$$M = (W^2 - 2WE_1 + m_1^2)^{1/2} \approx W\left(1 - \frac{E_1}{W}\right) \tag{24}$$

Equation (24) shows that for high values of W such that $E_1 \ll W$, $\rho_i(p_L, p_T = 0)$ will be roughly a constant reflecting the assumption of a constant g. This corresponds to the intuitive understanding that for high values of available energies the effects of the other particles do not interfere with the distribution of the particle in question. In the data shown in Fig. 17, we discuss values of W that are of the order of 7 GeV and E of the order of 1 or 2 GeV. If we want a big modification we need a steep function $f(M)$. Before turning to the quantitative analysis let us just note the general characteristic that a peak at $p_L = 0$ means a tendency to produce the highest possible M.

Let us apply this analysis to the data of Fig. 17. The (pp, π^-) has an obvious right-left symmetry in p_L. We will use it by taking into account the sum of the two sides and thus consider only once the range $m_T < E \lesssim W/2$. We take the first group of data with $0 < p_T < 0.2$ from Fig. 17 and use an average $m_T^2 = 0.03$ GeV^2. Multiplying the cross-sections by E and plotting the result vs. M we get Fig. 19. If g were indeed constant then the same functional behaviour should also govern the energy (W) behaviour of ρ for fixed values of E. Therefore, we added in Fig. 19 a scale of q^{lab} which is the equivalent laboratory momentum needed to produce a mass M. We compare now these results with the energy behaviour of the cross-sections for the production of a fixed number of prongs. These are shown in Fig. 20 which includes the data of a pp experiment at five different energies [40]. We see that the four prongs data are slightly decreasing and the six prongs data are roughly constant in the 20-30 GeV range. This is certainly a different behaviour from the one shown in Fig. 19.

The difference between the two figures can be blamed on the fact that g depends both on W and p_1. A trivial dependence on W should be given by the initial flux factor $1/q^{lab}$. As seen from Fig. 19, this factor by itself does not lead to an appreciable change in the results and much stronger variations of g as a function of both W and p_1 are needed. Nevertheless we realize that the trend of the curves of Fig. 19 to become more and more peaked as the number of prongs increases can be correlated with the same type of change in the behaviour of the cross-sections in Fig. 20. This is a partial explanation of the second feature noted at the beginning of this section. The unavoidable conclusion is that the dynamical effects and the kinematical restrictions are intricately interwoven in the structure of the momentum distributions ρ_i.

6. - SCALING AND LIMITING FRAGMENTATION

Let us turn now to a discussion of the inclusive distributions. The next best thing to knowing their functional form is the knowledge of the variables in which the functions obtain their simplest forms. It was recently suggested by Feynman [22] that the inclusive invariant distributions $E(d^3\sigma/d^3p)$ are functions of p_T and $x = (2p_L^{c.m.}/W)$. This hypothesis of scaling in x can be traced back to the ABFST model [12,18] that leads to a similar result. In the next sections we will discuss its derivation. Since actually no derivation exists that requires scaling of the distribution over the whole range of x, let us treat it here as an hypothesis and discuss its phenomenological verifications and implications.

A recent ISR experiment [41] furnished the first partial experimental proof of this concept in the new ranges of energies that now became available. Figure 21 shows the inclusive distributions of (pp, π^+), (pp, p) and (pp, K^+) at several energies (quoted in the figure are the corresponding ν values). The experimental

errors are of the order of 20%, and, within these errors, the (pp, π^+) data are consistent with scaling in x over this whole wide range of energies, which amounts to about a change of one order of magnitude in W (from 5 to about 50 GeV). They all show the expected peak in the direction of $x \approx 0$. The (pp, p) data have a different shape which is consistent with the data of machine energies (see Fig. 5). Note in particular that there is no dramatic increase in the K^+/π^+ ratio (at least in the measured regions) which still remains very low. The transverse momentum curve corresponds also to a phenomenological fit in this p_T range at lower energies.

These encouraging results lead us to an investigation of some of the phenomenological consequences of scaling in x. The consequences of this hypothesis with respect to the energy variation of the average multiplicity and transverse momentum are mentioned by Feynman [22] and discussed by Bali et al. [42]. As can be seen from Eq. (22) one should obtain, by integrating the inclusive distribution

$$\int \rho_i \frac{d^3p}{E} = \langle n_i \rangle \sigma_T \tag{25}$$

where $\langle n_i \rangle$ is the average multiplicity of particles of type i. Some authors prefer to use the total inelastic cross-section rather than σ_T in Eq. (25). This is just a redefinition of $\langle n_i \rangle$. If ρ_i scales in x, then we find

$$\sigma_T \langle n_i \rangle = \pi W \int \rho_i(x, p_T) \frac{p_T \, dp_T \, dx}{E} \tag{26}$$

This quantity is clearly a rising function of W since for $W_1 > W_2$ it turns out that $W_1/E_1 > W_2/E_2$. The question is how fast is it rising ? Expanding $\rho_i(x, p_T)$ in a Taylor series in x one finds that the most divergent term is a logarithmic one, determined by the structure at $x = 0$. For fixed p_T the result is

$$\frac{W}{2}\int_{-1}^{1} \rho(x) \frac{dx}{\left(m_T^2 + \frac{W^2 x^2}{4}\right)^{1/2}} = \int_{-1}^{1} \rho(x) \frac{dx}{\left(x^2 + \frac{4m_T^2}{W^2}\right)^{1/2}} \approx 2\rho(0) \ln\left(\frac{W}{m_T}\right) + \int_{-1}^{1} [\rho(x) - \rho(0)] \frac{dx}{|x|}$$

hence we derive the asymptotic relation

$$\sigma_T \langle n_i \rangle \approx \ln(s) \cdot \int \rho(0, p_T) 2\pi p_T \, dp_T + \text{const.} \tag{27}$$

which allows for a logarithmic increase of $< n_i >$ provided σ_T is constant. Bali et al. [42] have given a factorized expression for ρ_i [of the type $g(p_T)f(x)$] which can be regarded as a crude fit to the (pp, π) data and leads to consistent results for some values of $< n_i >$.

Given the fact that $\sigma_T < n_i >$ changes very slowly with the total energy W, we learn from Eq. (27) that the scaling in x is likely to be true. Any deviations from scaling are detectable in $\sigma_T < n_i >$ unless they vanish when integrated upon. Since ρ_i is positive - definite and smooth, we may expect these deviations to be small. One can of course have fine effects coming in. Thus for those reactions in which σ_T is varying strongly, one may expect ρ / σ_T to be the candidate for scaling. We will come back to these questions when we discuss the experimental results. Meanwhile it should still be pointed out that a consequence of scaling in x is also that

$$\frac{\langle E_i^{c.m.} \rangle}{W} \sigma_T = \int \rho_i(x, p_T)\, \pi\, dp_T^2\, dx \qquad (28)$$

hence the fraction of the total energy absorbed by particles of type i (known as the inelasticity) is expected to be constant. Similar arguments lead to the conclusion that also $< p_{T_i} >$ should increase logarithmically as

$$\sigma_T \langle p_{T_i} \rangle \approx \ln(s) \int \rho_i(0, p_T)\, 2\pi\, p_T^2\, dp_T + \text{const.} \qquad (29)$$

which implies that $< p_{Ti} > / < n_i >$ approaches asymptotically a constant value determined by $\rho_i(0, p_T)$.

In order to derive the above-mentioned results one has to assume scaling over the whole wide range of x. Are these assumptions substantiated by presently available data ? Figure 22 shows results, that only recently became available, of bubble chamber data [5] for the $(\pi^+ p, \pi^-)$ invariant distributions at two different energies. The discrepancy is brought out strongly in the rapidity plot which shows that for low $p_L^{c.m.}$ momenta the data do not scale yet. In the x plot we see that for x outside the range of $(-0.1, 0.2)$ the data seem to scale quite nicely. Although $\sigma_T < n_i >$ may still change considerably, we learn that the falling part of the distribution has presumably reached its limiting behaviour.

This leads us to a discussion of the hypothesis of limiting fragmentation proposed by Benecke, Chou, Yang and Yen [43]. They suggest that the high energy processes look simple when viewed in the target or the projectile frames of reference. When viewed in this way one regards the outcoming particles as the results of the fragmentation of the two original particles into well-defined ratios of hadronic matter under the influence of the collision. The simplicity that we referred to lies in the proposition that the distributions of the outgoing particles reach a limiting value which is independent of the original total energy of the collision (W). Figure 22 verifies

this proposition at least for the p_L values that are in the neighbourhood of the target. To emphasize it, we show the same (π^+p, π^-) data in negative p_L^{lab} region plotted vs. p_L^{lab} in Fig. 23. Once again we see the agreement between the 8 and 16 GeV data. The situation is not so perfect for the same regions of (π^+p, π^+) data, also shown in Fig. 23. It will be explained in the next section how this fact can be correlated with the observation that $\pi^+p\ \pi^+$ has exotic quantum numbers whereas $\pi^+p\ \pi^-$ is a non-exotic channel. This will lead to the expectation that (π^+p, π^+) reaches the asymptotic value slower than (π^+p, π^-).

Comparison between Fig. 22 and Fig. 23 shows that both the scaling in x as well as the limiting fragmentation in p_L^{lab} work. Hence these two ideas have to be consistent with one another. To show that this is indeed the case, we consider the quantitiy $(p^{(-)})/(q_2^{(-)})$ which is invariant under longitudinal boosts. $p^{(-)}$ refers to the particle (e.g., π) tested and $q_2^{(-)}$ refers to the target whose energy and momentum in the c.m. frame are ε and $-q$ respectively.

$$r = \frac{p^{(-)}}{q_2^{(-)}} = \frac{E^{c.m.} - p_L^{c.m.}}{\varepsilon + q} = \frac{E^{lab} - p_L^{lab}}{M_2} \tag{30}$$

where M_2 is the mass of the target. For values of $p_L^{c.m.} \ll -m_T$ we can use $E^{c.m.} \approx -p_L^{c.m.}$ and for high enough W we find $\varepsilon + q \approx W$ hence

$$r \approx \frac{-2p_L^{c.m.}}{W} = -x \tag{31}$$

(note that r is a positive definite quantity and x is negative in this lab region). From Eq. (31) we learn that scaling in x implies approximate scaling in r. This means that if the distribution is drawn in the laboratory frame no trace of W is left since in the relation between r and the lab variables, W does not appear. This, however, is the statement of limiting fragmentation.

Chou and Yang [44] noted that an interesting sum rule is obtained in terms of r. Momentum conservation leads to the result

$$\sum_{particles} r_j = 1 + \frac{E^{lab} - p_L^{lab}}{M_2}\Big|_{projectile} \approx 1 \tag{32}$$

Since the various ρ_i describe the distributions of the particles in the process, this can be rewritten as

$$\sum_i \frac{1}{\sigma_T} \int \rho_i(p)\, r\, \frac{d^3p}{E} \approx 1 \tag{33}$$

where the sum is over all types i of particles emitted. This sum rule emphasizes the region of high values of r where limiting fragmentation is applicable. It can be used to give some invariant meaning to the measure of the relative importance of the various

hadronic fragments emitted in the collisions. The authors [44] called the contribution of each type of particle i to the sum rule (33) its "fragmentation fraction". They estimated the following fragmentation fractions in pp collisions : the proton contributes 40%, the neutron 12%, all pions 40% and all kaons 5%. The relative importance of the proton is of course because it appears as a leading particle and therefore contributes characteristically to higher r values than the pions which are, after all, concentrated around the c.m. The proton contribution includes the elastic term. Since the emitted proton lies in this case around $r \approx 1$ and $(\sigma_{el}/\sigma_T) \approx 1/4$ we see that this term contributes by itself more than half of the proton's 40%.

There are several remarks that are in accord here.

1) The sum over i in Eq. (33) means that we have to determine in advance the types of particles discussed. It is natural to choose as the definition all hadrons that are stable under strong interactions. If one were to include also vector mesons, etc., in Eq. (33), then the question of double counting would come up and the practical way of evaluating such an integral would not be clear. This is so although it may be expected that also the other hadrons reach limiting distributions.

2) The sum rule hinges upon the fact that the projectile contribution in Eq. (32) vanishes at high energies. This is true for any finite mass particle but gets modified in deep inelastic electron scattering where a photon with a large negative q^2 hits the target proton with energy ν in the laboratory frame of reference. In this case

$$\frac{E^{lab.} - p_L^{lab}}{M_2}\Big|_{projectile} = \frac{\nu - \sqrt{\nu^2 - q^2}}{M} \approx \frac{q^2}{2M\nu} = \frac{-1}{\omega} \qquad (34)$$

For small values of ω the sum rule gets strongly reduced and a shift of all distributions towards the lower values of r (high p_L^{lab}) is expected to occur. For $\omega \gg 1$ the sum rule retains its usual form.

3) If the concept of fragmentation has some invariant meaning, one would expect the fragments to show dependence on the target but not on the projectile. In other words, one would assume that their contributions to (33) are independent of the projectile. We will see in the next section that a similar consequence follows from the factorization of the Pomeron. We should therefore compare quantities of the type $(1/\sigma_T(ab))\rho(ab,c)$. In the next section, we will bring evidence for the existence of this effect. As noted in the former paragraph, this will not be true in deep inelastic electron scattering with low ω. How the situation looks for high ω (and also for real photons) is still an open question.

4) In the last comment, let us discuss the various variables that are now at our disposal. Expressing them in terms of rapidity, we find

$$x = \frac{2p_L^{c.m.}}{W} = \frac{2m_T \sinh z}{W} = \frac{2m_T \sinh(y - y_{c.m.})}{W}$$

$$r = \frac{E^{lab} - p_L^{lab}}{M_2} = \frac{m_T e^{-y}}{M_2} = \frac{m_T e^{-(z+y_{c.m.})}}{M_2} \approx \frac{m_T e^{-z}}{W} \qquad (35)$$

where $y_{c.m.}$ is the c.m. point in the rapity distribution as measured in the laboratory frame. As implied by the last equation [derived from Eq. (30)] this is given by $y_{c.m.} \approx \ell n(W/M_2)$. This is an asymptotic result. At low energies the mass (M_1) of the projectile plays a role. Then one finds

$$\tanh y_{c.m.} = \frac{\sqrt{\nu^2 - M_1^2}}{M_2 + \nu}$$

Equations (35) bring out the antisymmetric nature of x in the c.m. and the asymmetric nature of r which singles out the target frame. Whereas x grows for positive z values, r dies out exponentially in the direction of the projectile.

Finally, let us remark that the point $p_L^{lab} = 0$ is of some importance since it is a natural turning point in the fragmentation region. Equation (30) implies that in x it corresponds to

$$x \approx -\frac{m_T}{M_2} \qquad (36)$$

thus confirming what we learned from Fig. 16, namely, that a large portion of the negative x axis corresponds to negative laboratory momenta.

7. - REGGEISTIC APPROACH TO LIMITING FRAGMENTATION

An approach that discusses the inclusive data in the familiar Regge language was recently introduced by Mueller [45]. He pointed out that the inclusive distribution ρ can be regarded as a discontinuity in a six-point "forward scattering" amplitude (shown in Fig. 24) in an analogous fashion to the connection between the total cross-section and the discontinuity of a forward scattering four-point function given by the optical theorem. For certain regions of the kinematical variables one can then assume dominance of Regge behaviour which leads to testable interesting predictions. This provides us with a familiar language and technique with which we can describe and analyze the data. Some of the features of this approach were successfully verified within

the Veneziano model of multiparticle production [46] and within the multiperipheral model, to which it is indeed very close in spirit, as we shall see below. In the present section, we will concentrate on the Reggeistic description of limiting fragmentation. We will follow here a heuristic approach in deriving the formula. The original $O(2,1)$ analysis will be outlined in the next section which deals with pionization. Let us start by defining the notation for the inclusive process

$$(ab,c): \qquad a(q_1)+b(q_2)\longrightarrow c(p)+\text{anything} \tag{37}$$

where we denote the momentum of the projectile by q_1 and the momentum of the target by q_2. We will assume for simplicity that both these particles have the same mass M and that the outgoing particle has mass μ. We may now define the invariant energy variables

$$\nu=\frac{q_1\cdot q_2}{M} \qquad \nu_1=\frac{q_1\cdot p}{M} \qquad \nu_2=\frac{q_2\cdot p}{M} \tag{38}$$

Altogether there are three independent variables which can be expressed in terms of p_L, p_T and W. Indeed, if we define the momenta in the c.m. frame by

$$\begin{aligned} q_1&=\left(\tfrac{W}{2};\,0,\,0,\,q\right)\\ q_2&=\left(\tfrac{W}{2};\,0,\,0,\,-q\right)\\ p&=\left(E;\,\vec{p}_T,\,p_L\right)\end{aligned} \tag{39}$$

we find that

$$\begin{aligned} M\nu&=M^2+2q^2=\frac{W^2}{2}-M^2\\ M\nu_1&=\tfrac{1}{2}WE-qp_L\\ M\nu_2&=\tfrac{1}{2}WE+qp_L\end{aligned} \tag{40}$$

Multiplying the last two equalities by one another, we find

$$\frac{\nu_1\nu_2}{m_T^2}=\frac{\nu}{2M}+\frac{E^2}{m_T^2}-\frac{1}{2} \tag{41}$$

which means that for fixed values of ν and E the values of ν_1 and ν_2 are inversely proportional to one another.

Alternatively, one may just use the known s, t, u variables

$$\begin{aligned} s&=(q_1+q_2)^2=2M^2+2M\nu=W^2\\ t&=(q_1-p)^2=M^2+\mu^2-2M\nu_1\\ u&=(q_2-p)^2=M^2+\mu^2-2M\nu_2\end{aligned} \tag{42}$$

Note, however, that all three are independent since their sum is no longer fixed ; it includes a variable which we met before

$$s+t+u = 2M^2+\mu^2+M^2$$
$$M^2 = W^2-2EW+\mu^2 \qquad (43)$$

Forward (backward) scattering corresponds to small values of $t(u)$ and large values of x near $1(-1)$ thus showing that the outgoing particle is approaching the momentum value of the projectile (target). We find then

$$t = M^2+\mu^2+2qp_L-WE \simeq M^2+\mu^2-M^2x-\frac{m_T^2}{x} \qquad (p_L \gg m_T)$$
$$u = M^2+\mu^2-2qp_L-WE \simeq M^2+\mu^2+M^2x+\frac{m_T^2}{x} \qquad (p_L \ll -m_T) \qquad (44)$$

In the same limits, it turns out also that

$$\nu_2 \to \nu \qquad (p_L \gg m_T)$$
$$\nu_1 \to \nu \qquad (p_L \ll -m_T) \qquad (45)$$

When $\mu < M$ positive values of t can be reached. When $\mu = M$ only negative values of t are allowed. In particular $t = 0$ corresponds then strictly to forward elastic scattering. Using Eq. (44), we note that near the forward direction $\partial t/\partial p_T = -2p_T/x$ hence we can write near the forward direction

$$E\frac{d^2\sigma}{2\pi p_T dp_T dp_L} \simeq \frac{E\,d^2\sigma}{\pi p_L\, dt\, dx} \simeq \frac{d^2\sigma}{\pi\, dt\, dx} \qquad (46)$$

This equality will turn out to be very useful.

Mueller [45] derived the limiting fragmentation result by using an $O(2,1)$ analysis. Instead of following the original derivation we will just use here a plausibility argument based on Fig. 25. The idea is simply that if ν_2 is small then the sum over all particles reduces to an over-all diffractive effect which is to be represented by Regge poles and, in particular, Pomeron exchange. This is very similar to the description of σ_T in two-body scattering amplitudes, the only difference being that an unspecified function of ν_2 and p_T has now to be inserted for the lower vertex. Figure 25 should hold for low u values (fragmentation of the target) and an analogous diagram at the upper vertex could describe fragmentation of the projectile (low t). We expect therefore to find

$$\rho = E\frac{d^2\sigma(a+b\to c)}{2\pi p_T dp_T dp_L} \underset{\text{low } \nu_2}{\propto} \frac{\nu_1^{\alpha(0)}}{\nu} f(\nu_2,p_T) \xrightarrow[\alpha(0)=1]{} f(\nu_2,p_T) \qquad (47)$$

where $\nu_1^{\alpha(0)}$ stands for the Regge behaviour and $1/\nu$ for the incoming flux factor. When we choose $\alpha(0) = 1$, namely Pomeron exchange, then the result is scaling. Hence Pomeron dominance in Fig. 25 ensures limiting fragmentation *).

Equation (47) still leaves the structure in the lower vertex as an open question. We will see below that the "triple-Regge limit" is a Reggeistic attempt to formulate a partial answer. In the meantime, let us, however, note that even if $f(\nu_2, p_T)$ is left as an unknown function there is still more information one can derive from Eq. (47) provided one assumes that the Pomeron contribution factorizes. In that case, one predicts that

$$\frac{\rho(ab,c)}{\sigma_T(ab)} = \frac{\rho(db,c)}{\sigma_T(db)} \qquad (48)$$

in the low u region. This prediction is welcomed from the limiting fragmentation point of view. It means that the fragmentation fractions (see discussion in previous section) are independent of the projectile that caused the fragmentation, and gives therefore an invariant meaning to the fragmentation of the target.

An experimental study by Chen et al. [47] was the first to point out that this may indeed be the case. These authors studied the data of (π^+p, π^-) at 7 GeV, (K^+p, π^-) at 12.7 GeV, (pp, π^-) at 28.5 GeV and $(\pi^-p, \pi^\pm)$ at 24.8 GeV. The first three distributions coincide in the target fragmentation region when normalized by their total cross-sections, thus favouring the consequences of Eq. (48). This can be seen in Fig. 26. (π^-p, π^-) seems to be an exception since it lies somewhat higher. Before discussing this phenomenon we note the limiting fragmentation in the transverse momentum distributions of the reactions as shown in Fig. 27 : the transverse distributions of all these reactions are amazingly similar. Another interesting result was pointed out by these authors for distributions in the projectile fragmentation region. Figures 28 and 29 show a complete equivalence between (π^-p, π^+) and (π^+p, π^-) near $t \approx 0$. This is of course also expected from an analysis based on Fig. 25 since the two reactions are related to one another by charge conjugation of the $\pi\pi$ vertex and should therefore yield the same asymptotic distributions **).

Let us return now to the (π^-p, π^-) distribution of Fig. 26. We note that it roughly coincides with the other distributions for negative p_L^{lab} but deviates from them at positive values. Pomeron dominance would predict of course that all distributions are equal. Nevertheless it is hard to say exactly where the diagram 25 is

---

*) Fine details such as effects of Regge cuts, or possible deviations of $\alpha_p(0)$ from 1, will not be discussed here. The crudeness of the data allows us still to use very simple Reggeistic parametrizations in this field.

**) The fact that (K^+p, π^-) seems so much bigger than (π^+p, π^-) is a fault of the p_L^{proj} plot. The two are similar when plotted vs. x but, because of the different kinematics, a much larger portion of the x plot is converted to the low p_L^{proj} region in the $K^+ \to \pi^-$ case than in the $\pi^+ \to \pi^-$ one [see Eq. (36)]. I would like to thank T. Ferbel for a discussion of this point.

valid. Trying to be as optimistic as possible, one would continue it to the right of $p_L^{lab} = 0$. In any case one should ascribe to the $(\pi^- p, \pi^-)$ distributions the additional effects of lower trajectories. This fits in with the suggestion by Chan et al. [48] that all distributions in which $abc\bar{c}$ have exotic quantum numbers approach their asymptotic (scaling) values much quicker than the non-exotic ones that should have correction terms behaving roughly like $\nu^{-\frac{1}{2}} \approx W^{-1}$. Indeed the $(\pi^- p, \pi^-)$ distribution is the only one out of the four shown in Fig. 26 that has non-exotic $abc\bar{c}$ quantum numbers. If the discrepancy between $(\pi^- p, \pi^-)$ to $(\pi^+ p, \pi^-)$ is given by a lower Regge term, then it should diminish with growing energy like W^{-1}. One should, however, note that the difference between the two distributions for $p_L^{lab} > 0$ is very big, much more than the relative difference between non-exotic and exotic total cross-sections.

The effects of the lower trajectories are brought out in the best way by looking at energy dependence. In Fig. 23, we showed the comparison between $(\pi^+ p, \pi^-)$ and $(\pi^+ p, \pi^+)$ in the $p_L^{lab} < 0$ range for two different energies. One could indeed verify that the exotic $(\pi^+ p, \pi^-)$ reaches its limiting value at 8 GeV whereas the non-exotic $(\pi^+ p, \pi^+)$ continues to decrease. Let us compare now these two distributions over the whole x range in Fig. 30. The trends shown in the fragmentation region of the target are also evident in the fragmentation region of the projectile. In addition we see the growth of $(\pi^+ p, \pi^-)$ near $x \approx 0$. The same effect exists also in $(\pi^+ p, \pi^+)$ but, because of the over-all decrease of this distribution, it leads to an apparent scaling structure in this region. In the right corner of $(\pi^+ p, \pi^+)$ one sees a non-scaling diffractive part to which we will return in Section 10.

The quantity plotted in Fig. 30 is the invariant distribution to which the Mueller analysis and the arguments of Ref. [48] apply. The decrease of σ_T clearly plays a major role in the forms of Fig. 30 and justly so since it affects also the corresponding theoretical analysis. In comparing values of distributions from different sources one divides by σ_T. In principle one should have divided only by the "Pomeron contribution". In practice σ_T is in general varying with the energy and the division by σ_T masks, at least partially, the Regge effects. Therefore it is much easier to derive conclusions from Fig. 30 than, say, from Fig. 26.

Ellis et al. [49] have pointed out that the relevant criterion for the approach to the limiting distribution should be not only exotic $abc\bar{c}$ channel but also exotic ab quantum numbers. To understand this point we turn again to Fig. 24 and note that since the quantity we study is positive definite, we have to choose for each intermediate state, and therefore for the total $\mathcal{M}^2$ discontinuity, the amplitude at a point above the s cut (+) for the incoming ab channel and below the s cut (-) for the outgoing ab channel. This assures the positivity of this term. All other variables in the problem (t and u) are below their physical thresholds and one does not encounter therefore any problems with their definition. Since we may feel uneasy in dealing with a discontinuity in $\mathcal{M}^2$ of an amplitude that connects two different s branches we can put it in a different language. Let us use the notation $A(s_{in}, \mathcal{M}^2, s_{out})$ and symbolically

define the discontinuity in question by $A(++-) - A(+--)$, as implied above. We note that the following decomposition can be made [50]

$$A(++-) - A(+--) = [A(+++) - A(+-+)] + [A(++-) - A(+++) + A(+-+) - A(+--)] \tag{49}$$

The first term in square brackets is a discontinuity with respect to M^2 for $s_{out} = s_{in}$ and the second term is an M^2 discontinuity of the discontinuity in s_{out}. Although these two terms may now have arbitrary phases, they may be the right ones to use for continuing the usual dual arguments from two-body scattering amplitudes to this new domain. Symbolically we can then write

$$\Delta A = \Delta_{M^2} A(s_{out} + i\epsilon) - \Delta_{M^2}(\Delta_s A) \tag{50}$$

If the $ab\bar{c}$ channel is exotic and the ab is non-exotic, then the second term may lead to a contribution that decreases with energy. It is of course difficult to specify a priori what the size of the second term should be. In Fig. 26 we note that $(\pi^+ p, \pi^-)$ seems to reach a limiting distribution quickly although it has a non-exotic ab channel. This seems to imply that the second term leads to small effects. It would be better to test it in reactions that are known to have strong non-leading behaviour in σ_T like $(K^+ p, \pi^-)$ and $(K^- n, \pi^+)$. One would expect both to approach the same limiting distribution at $u \approx 0$ and only the second one to have the effect of the second term of Eq. (50).

8. - PIONIZATION

We start this section with Mueller's derivation [45] of the pionization formula. It is easiest seen in the frame of reference of the emitted particle in which

$$\begin{aligned} q_1 &= M(\cosh\zeta_1 ; \sinh\zeta_1 \cos\varphi, \sinh\zeta_1 \sin\varphi, 0) \\ q_2 &= M(\cosh\zeta_2 ; -\sinh\zeta_2 , 0 , 0) \\ p &= \mu(1; 0,0,0) \end{aligned} \tag{51}$$

where ζ_1 and ζ_2 are the rapidities of q_1 and q_2 in the rest frame of p. Again we choose for simplicity the equal masses case. The connection with the variables of Eq. (38) is given by

$$\begin{aligned} M\nu_1 &= q_1 \cdot p = M\mu \cosh\zeta_1 \\ M\nu_2 &= q_2 \cdot p = M\mu \cosh\zeta_2 \\ M\nu &= q_1 \cdot q_2 = M^2(\cosh\zeta_1 \cosh\zeta_2 + \sinh\zeta_1 \sinh\zeta_2 \cos\varphi) \end{aligned} \tag{52}$$

Comparing these equations with (41) we find that

$$\frac{M\nu}{M^2\nu_1\nu_2} = \frac{2}{m_T^2} + \frac{1}{\nu_1\nu_2}\left(1 - \frac{2E^2}{m_T^2}\right) = \frac{1}{\mu^2} + \frac{\sinh\zeta_1 \sinh\zeta_2}{\mu^2 \cosh\zeta_1 \cosh\zeta_2}\cos\varphi \tag{53}$$

which reduces in the high-energy limit $\nu_1 \gg \mu$ $\nu_2 \gg \mu$ and $E \approx m_T$ to

$$1 + \cos\varphi \approx \frac{2\mu^2}{m_T^2} = \frac{2\mu^2}{\mu^2 + p_T^2} \tag{54}$$

The invariant distribution that we look at in a problem like (pp, π) can be written as

$$\begin{aligned} E\frac{d^3\sigma}{d^3p} &= \frac{(2\pi)^3 M^2}{4M\sqrt{\nu^2 - M^2}} \int d^4x\, e^{-ipx} \langle q_1 q_2 | j_\pi(x)\, j_\pi(0) | q_1 q_2 \rangle \\ &= \frac{M}{2\sqrt{\nu^2 - M^2}}\, A(q_1 q_2 p) \end{aligned} \tag{55}$$

where an average over the spins in the $q_1 q_2$ system is assumed. The quantity A, which is the invariant inclusive distribution multiplied by the flux factor, is a function of the independent variables ζ_1, φ and ζ_2. Expanding A in O(2,1) harmonics according to Toller [51] one obtains

$$A(\zeta_2, \varphi, \zeta_1) = \sum_m \int_{-\frac{1}{2}-i\infty}^{-\frac{1}{2}+i\infty} d\Lambda_2 \int_{-\frac{1}{2}-i\infty}^{-\frac{1}{2}+i\infty} d\Lambda_1\; A_m^{\Lambda_1,\Lambda_2}\, d_{0m}^{\Lambda_2}(\zeta_2)\, e^{im\varphi}\, d_{m0}^{\Lambda_1}(\zeta_1) \tag{56}$$

If both ζ_1 and ζ_2 grow indefinitely, the asymptotic behaviour of Eq. (56) will be governed by the leading singularities α_1 and α_2 in Λ_1 and Λ_2. If one moreover assumes that these are poles, one obtains for the leading term

$$A(\zeta_2, \varphi, \zeta_1) \xrightarrow[\zeta_2, \zeta_1 \to \infty]{} (\cosh\zeta_2)^{\alpha_2} (\cosh\zeta_1)^{\alpha_1} \beta(\varphi) \tag{57}$$

One can now insert in Eq. (57) the invariant variables from Eq. (52) and obtain

$$\rho = E\frac{d^3\sigma}{d^3p} \propto \frac{1}{\nu} A(\zeta_2, \varphi, \zeta_1) \to \frac{\nu_1^{\alpha_1}\, \nu_2^{\alpha_2}}{\nu} f(m_T) \tag{58}$$

where we used also the asymptotic properties of (54). In the high energies limit, we would now expect Pomeron exchange to dominate and therefore choose $\alpha_1 = \alpha_2 = 1$. Using Eqs. (41) or (53), we are led to

$$\rho \to \frac{m_T^2}{2M} f(m_T) \tag{59}$$

which is the same type of result which we often mentioned before - no dependence on p_L in the central region. Using similar arguments, Mueller [45] derived in much the same way the fragmentation formula (47).

Employing an $O(2,1)$ analysis, one has to introduce at some stage the assumption of dominance by a particular Reggeistic structure. Comparing with definite models of production processes one can get a feeling for the validity of such an assumption. Thus the multiperipheral model, as well as many other more complicated versions of tree and loop diagrams, would lead to the result of Fig. 25 and, consequently, to limiting fragmentation. This is no longer true of the pionization result. Although many models may lead to a constant result near $x = 0$ it does not necessarily mean a breaking of the amplitude into two Pomeron exchanges. Figure 31 shows the structure of a model that can lead to a two-Pomeron exchange. We see that it is very restrictive. Indeed, even if two lines cross (Fig. 32a), the two-Pomreon picture may be spoiled. Crossing of such two lines can occur even in a multiperipheral model if there is enough overlap between the amplitudes of different orderings. Figure 10 taught us that such overlaps do exist. Any general production model (Fig. 32b) will usually involve a complicated structure that does not allow a decomposition like Fig. 31. In particular a simple absorptive correction to a multiperipheral model (Fig. 32c) spoils the two-Pomeron picture.

A pionization formula which is based on two-Pomeron exchange carries with it more information than just the result (59) since one may again invoke factorization of the Pomeron that worked so well in the fragmentation region. This leads then to the result

$$\frac{\rho(ab,c)}{\sigma_T(ab)} = F_c(m_T) \tag{60}$$

which clearly is an extremely restrictive relation that depends crucially on the assumption of Fig. 31.

We saw already in Section 6 data which imply that the scaling region was not reached yet in $(\pi p, \pi)$ reactions. Clearly one should not expect then that Eq. (60) holds at present energies. Is there any way to estimate when Eq. (59) is applicable ? Equation (41) tells us that at $E = m_T$ we have $\nu_1 = \nu_2 = m_T\sqrt{(\nu+M)/2M}$. Hence for a ν value around 30 GeV we find that ν_1 and ν_2 are of the order of 1 GeV. For two-body scattering amplitudes this would be a too low energy to expect Pomeron behaviour to show up. One is therefore tempted to say that also in the application of Eq. (59) to experiment we did not reach yet the necessary energy and changing ν by an order of magnitude may do it. We may hope therefore that ISR and NAL data may pass some judgement on the validity of the approach based on Fig. 31.

An obvious correction [52], [53] to Eq. (59) comes from exchanges of non-Pomeron Regge trajectories (P', ϱ, etc.) with $\alpha < 1$. Such contributions may be comparable with the diffractive Pomeron component at low ν_i values. We may then expect a modification of the type

$$\rho \propto \frac{1}{\nu}(\nu_1 + a\nu_1^{\alpha})(\nu_2 + a\nu_2^{\alpha})\, f(m_T) \tag{61}$$

with positive values for a (which may also depend on m_T). The argument for the positivity can be the same used in two-body scattering amplitudes : the correction to the Pomeron behaviour is dual to resonance contributions [54] and must therefore be positive by itself. This leads to the well-known decrease of the total cross-sections towards their asymptotic values, and its effect will be the same here : it leads to a decrease of ρ (x=0) towards its asymptotic value. Moreover, at fixed ν, ρ gets its minimal value at x = 0. Although this is a small effect, it is nonetheless clear that both these trends are in distinct contrast to the available data, and we must conclude that the effects of Eq. (61) were not yet observed.

Anticipating the fact that such effects may be looked for in the ISR and NAL machines, let us investigate further their consequences in some detail [52]. Equation (61) is applicable in an x range that is the border region between pionization and limiting fragmentation. Requiring $\nu_1 \nu_2 \approx (m_T^2/2M)\nu$ we find from Eq. (53) that $x^2 \ll (m_T/M)^2$. To see clear effects of Eq. (61) we would like to be able to allow $(\nu_1/\nu_2) \ll 1$. This means [see Eq. (40)] that $x^2 \gg (2m_T/W)^2$. The combined effect of these two conditions results in

$$\frac{2m_T}{W} < x < \frac{m_T}{M} \qquad\qquad 1 < \sinh z < \frac{W}{2M} \tag{62}$$

(Some authors regard $\sinh z < 1$ or $x < 2m_T/W$ as the definition of the pionization region.) It follows then from Eq. (40) that

$$\nu_1 \approx \frac{m_T^2}{2Mx} \qquad \nu_2 \approx \frac{Sx}{2M} \tag{63}$$

which means that

$$\frac{\nu_1^{\alpha_1}\nu_2^{\alpha_2}}{\nu} = \left(\frac{m_T^2}{2M}\right)^{\alpha_1}\left(\frac{S}{2M}\right)^{\alpha_2-1} x^{\alpha_2-\alpha_1} \tag{64}$$

This formula is asymmetric because we chose $(\nu_1/\nu_2) \ll 1$ (positive x values in the direction of the projectile). We learn that, as expected, the result is scaling if $\alpha_2 = 1$. Hence the important effects of Eq. (61) in this region will be

$$\rho = f(m_T) + x^{1-\alpha} g(m_T) \tag{65}$$

which, with positive g values, leads to a decrease towards $x = 0$.

Like before we may use the conditions $\nu_1 > M$ and $\nu_2 > M$ to give us a (somewhat arbitrary) criterion for the physical threshold of such effects. Imposing this condition on Eq. (63), we find

$$\frac{2M^2}{s} < x < \frac{m_T^2}{2M^2} \tag{66}$$

The upper limit is more stringent than the one in Eq. (62) and leads characteristically to $x < 0.05$. The lower limit of Eq. (66) is at higher energies below that of Eq. (62). We may therefore look for effects of the type of Eq. (65) in the regions where $(2m_T/W) \ll (m_T^2/2M^2)$ or $W \gg (4M^2/m_T)$, a condition satisfied in the ISR and NAL energy ranges.

If such effects will indeed be observable then one may expect also to identify the roles of the various exchanges [53]. Thus, for instance, $(pp, \pi^-) - (pp, \pi^+)$ should be dominated by Pomeron ρ interference. We have already stressed several times that such a behaviour depends on assuming the dominance of diagram 31. Many alternatives are possible, as already discussed above. In particular let us mention the polyperipheral [52] diagram of Fig. 33a. It has several multiperipheral chains which form in the unitarity closure a Mandelstam cut [55], as shown in Fig. 33b. A major effect of the polyperipheral diagrams is that they lead to narrow and overlapping distributions in rapidity (because the total momentum is divided among the various chains) whose sum has then the characteristic tendency to grow towards $x \approx 0$. This difference from the simple multiperipheral model may be a partial explanation for the observed nature of the data. For a discussion of other models and their relation to diffraction scattering, we refer the reader to the extensive survey by Zachariasen [56].

Let us turn now to a different phenomenon that was recently investigated. We repeatedly emphasized that the characteristic pionic distributions have Gaussian shapes in rapidity, which can be fitted roughly with exponentials in $d\sigma/dp_L$. In general one finds that in a reaction like (ab, π) when $a \neq b$ the slopes in these two exponential distributions are different. Elbert et al. [57] analyzed $(\pi^- p, \pi^{\pm})$ data at 25 GeV and noted that by boosting to a frame of reference in which

$$R = -\frac{\text{momentum of target}}{\text{momentum of projectile}} = 1.5 \tag{67}$$

they got a symmetric distribution (excluding leading particle effects). Similar results were obtained by Stone et al. and Biswas et al. [58], and Ko and Lander [59]. Clearly if $d\sigma/dp_L^{c.m.}$ were given mathematically by a two-exponentials formula no boost would have changed the peak at the c.m. The fact that the boosts allow us to pick a better frame means that the central distribution deviates from a two-exponentials behaviour. An alternative way to state this fact would be to say that the rapidity distribution peaks not at the c.m. point but somewhere outside it, namely at the point to which the above-mentioned boost leads us.

To see this structure in more detail we follow the analysis of Ko and Lander [59] of the (K^+p, π^-) data at 12 GeV. Figure 34 shows the familiar two-exponentials structure of $d\sigma/dp_L^{c.m.}$. As we noted before (see Fig. 17), the structure is somewhat different for different numbers of prongs. This is reflected in Fig. 35 that shows the parameters of the two-exponentials fits as a function of the frame of reference, defined by R. The total data reach a position of equal slopes around $R \approx 1.5$ vhereas the data of different numbers of prongs reach the symmetric structure at different values of R. The inclusive distribution at $R = 1.5$ is then shown in Fig. 36.

The value 1.5 is very reminiscent of quark model results. Elbert et al. [57] suggested indeed an interpretation, based on a naïve quark model, according to which the pionic cloud is formed during a collision of a baryonic quark and a mesonic quark or antiquark. Since each quark carries a 1/3 or a 1/2 of the total momentum if it sits in a baryon or a meson respectively, the $R = 1.5$ result follows. This does not explain why the 4, 6 and 8 prongs data do not follow the same rule. Alternatively one may use a parton picture (different from the quark one by allowing a large number of constituents). In such a picture one ascribes more partons to the proton than to the pion just because the proton has bigger cross-sections than the pion. If one further assumes pairwise parton collisions, one finds [52] in the limit where shadowing effects can be neglected, that R is given by the ratio of total cross-sections, e.g., $\sigma_T(pp)/\sigma_T(K^-p)$.

An alternative explanation was recently suggested by Caneschi [60] who shows that a multiperipheral fit with exponential propagators leads to a quite narrow peak in the pionization region. He adds to it diagrams of a fragmentation type which lead to an enhancement of the distribution in the direction of the incoming meson. These relatively small end effects cause the asymmetry of the resulting inclusive distribution.

It is interesting to know how the asymmetry parameter R changes with energy. Figures 37a and 37b show a recent compilation [61] of the known R values in reported analyses of πp and Kp reactions. The data of Ref. [5], namely the πp points at 8 and 16 GeV, favour R values close to 1.8. The energy trends are consistent with being constant but the general situation should still be regarded as preliminary. As the energy W increases we know that $< n_{ch} >$ increases and, therefore, for R to be constant in the inclusive distribution, the R values of fixed numbers of prongs should slowly increase.

Let us now find the rapidity value z_o which corresponds to the symmetry axis of the distribution. Boosting from the c.m. by $-z_o$ one arrives at R through

$$R = \frac{\sqrt{q^2+M_2^2}\sinh z_o + q\cosh z_o}{-\sqrt{q^2+M_1^2}\sinh z_o + q\cosh z_o} \xrightarrow{W\to\infty} \frac{\cosh z_o + \sinh z_o}{\cosh z_o - \sinh z_o} = \frac{1+\beta_{L_o}}{1-\beta_{L_o}} \qquad (68)$$

hence the value $R = 1.5$ corresponds to a symmetry point $z_o \approx 0.2$, which is very small indeed. Note that this is an energy independent result. Hence we may perhaps expect that scaling in this region (if achieved anywhere) should be given in terms of $x' = (2m_T \sinh(z-z_o))/W$ if R is to be constant.

9. - THE TRIPLE REGGE LIMIT

We saw in Section 7 that a Pomeron exchange in Mueller's analysis leads to the general result of limiting fragmentation. Although this fact, together with the factorization results, is indeed very satisfying, one is still left with an arbitrary function describing the lower vertex of Fig. 25. A step in the direction of understanding its structure is given by the triple Regge formula. The formula was recently suggested on the basis of a Mueller analysis by DeTar et al. [62] and was previously derived by investigations of the multiperipheral model [63].

This approach is supposed to hold for very low momentum transfers. In this case one may expect that the general structure which is left unspecified in Fig. 25 can be further decomposed in terms of Regge exchanges. We show such a diagram in Fig. 38. This describes the fragmentation of the projectile at low values of t with the assumed Regge exchange $\alpha(t)$. Since in addition we have the diffractive (Pomeron) exchange [$\bar{\alpha}(0)$ in this picture], which describes the effect of all the missing masses, we are led to a triple Regge diagram.

The expressions for the invariant amplitude will now contain $(M^2)^{\bar{\alpha}(0)}$ for the effective sum over all missing masses as expected from a regular diffractive picture. In addition one encounters twice the Regge term $(s/M^2)^{\alpha(t)}$. Here one uses a decomposition analogous to Eq. (41) namely, one argues that if there is a gap in the rapidity distribution between the M^2 blob and the outgoing p, one expects the product of the relevant energies to give s. Many applications that we will mention depend crucially on the M^2 dependence of $(s/M^2)^{\alpha(t)}$ and their success or failure hinges upon the applicability of this approach. In addition we should remember that some transverse masses appear in the relations among the various energy terms and they are left out by using the dimensionless expression $(s/M^2)^{\alpha(t)}$. It is hard to estimate when such an approximation is indeed valid. In this sense the situation here is worse than in the pionization case since there the validity of the approximation $\nu_1 \nu_2 = (m_T^2/2M)\nu$

depended on measurable quantities ($|x| \ll m_T/M$). Here the validity of the approximation implied by using $s/\mathcal{M}^2$ depends on the properties of the set of particles that is summed upon and does no longer appear in the final configuration of the triple Regge amplitude. We may just hope that in the low t and high $s/\mathcal{M}^2$ regions it will be valid. If, in analogy with Eq. (41) one uses an average m_T^2/M to determine the connection between $s/\mathcal{M}^2$ to the relevant energy variable, one would estimate $s/\mathcal{M}^2 > 10$ as the region of possible applicability of a Regge picture. After adding the $1/s$ flux factor and the conventional arbitrary t dependence which goes with the Regge pole we are then led to

$$\frac{E\,d^2\sigma}{2\pi p_T\,dp_T dp_L} = \frac{2q_1^{lab} M_2\, d^2\sigma}{\pi\, dt\, d\mathcal{M}^2} \approx \frac{s\, d^2\sigma}{\pi\, dt\, d\mathcal{M}^2} = \left(\frac{s}{\mathcal{M}^2}\right)^{2\alpha(t)} \frac{(\mathcal{M}^2)^{\bar{\alpha}(0)}}{s}\,\beta(t) \qquad (69)$$

Let us recall now that

$$\frac{\mathcal{M}^2}{s} = \frac{W^2 - 2WE^{c.m.} + m^2}{W^2} \approx 1 - x$$

(note that for negative $p_L^{c.m.}$ this is actually $1+x$). Substituting this relation in Eq. (69), we can rewrite it as

$$-\frac{d^2\sigma}{\pi\, dt\, dx} \approx \left(\frac{s}{\mathcal{M}^2}\right)^{2\alpha(t)-1} (\mathcal{M}^2)^{\bar{\alpha}(0)-1}\,\beta(t) \approx (1-x)^{-2\alpha(t)+1} (\mathcal{M}^2)^{\bar{\alpha}(0)-1}\,\beta(t) \qquad (70)$$

Equation (70) includes the expected result that only for Pomeron exchange, $\bar{\alpha}(0) = 1$, a scaling distribution is obtained.

We now look for applications of this formula in the domain of low t, high s and high $s/\mathcal{M}^2$. The last restriction, due to the use of a Regge expression, limits x to the vicinity of ± 1. Clearly it is then advisable to start testing the formula in such cases where the distribution near ± 1 is sizeable. We saw in Fig. 5 the inclusive c.m. distributions for particle productions in a 19.2 GeV pp experiment [7]. The leading particle effect of the proton resulted in a distribution that continues strongly towards the $x = 1$ edge. All other distributions show a clear strong damping while approaching this limit. The qualitative hints of Eq. (70) are actually in the right direction. For (pp,p) near $t \simeq 0$ one should expect Pomeron and mesonic exchanges in the Regge vertex leading to $-1 \leq 1 - 2\alpha(t) \lesssim 0$ whereas for meson production one needs baryon exchanges leading to high values of $1 - 2\alpha(t)$ and strong damping near $x \approx 1$. We will therefore concentrate first on (pp,p) distributions.

Before turning to the experimental tests let us see how the distributions will look for characteristic values of the different Regge intercepts. The situation is summarized in Table II.

	$\alpha(t)$	$\bar{\alpha}(0)$	$\frac{-d^2\sigma}{dt\ dx}$	$\frac{-d^2\sigma}{dt\ dx}$ | fixed s
I	1	$\frac{1}{2}$	$\frac{c}{M(1-x)}$	$\frac{d}{(1-x)^{\frac{3}{2}}}$
II	$\frac{1}{2}$	$\frac{1}{2}$	$\frac{c}{M}$	$\frac{d}{(1-x)^{\frac{1}{2}}}$
III	1	1	$\frac{c}{1-x}$	$\frac{c}{1-x}$
IV	$\frac{1}{2}$	1	c	c
V	0	1	$c(1-x)$	$c(1-x)$
VI	-1	1	$c(1-x)^3$	$c(1-x)^3$

TABLE II : Characteristic distributions in the triple-Regge limit.

Cases I and II correspond to a non-scaling behaviour (P' or other exchanges with $\bar{\alpha} = \frac{1}{2}$). Because of the explicit M dependence in the denominator one would expect now $-M(d^2\sigma/dt\ dx) = (s\ d^2\sigma/dt\ dM)$ to show a scaling behaviour. Alternatively, if one looks at $d^2\sigma/dt\ dx$ at fixed s values (varying M^2 only), one finds stronger singularities near $x \simeq 1$. The $(1-x)^{-1}$ singularity in cases I and III corresponds to diffraction dissociation [$\alpha(t)$ being identified with the Pomeron] to which we will return in the next section. In the scaling region (dominance of $\bar{\alpha} = 1$) one would expect a smooth constant distribution for natural parity Regge exchanges (case IV) and a dip developing for unnatural exchanges (case V) near $t \simeq 0$. As one moves to higher -t values this dip increases and when $\alpha \approx -1$ one expects already a $(1-x)^3$ behaviour (case VI).

The (pp,p) data of the BNL-CMU experiment were analyzed in this spirit by Edelstein, Rittenberg and Rubinstein [64]. Their results, shown in Figs. 39 and 40, display the effects obtained by compiling the data at five different laboratory energies (6.2, 9.9, 15.1, 20.0 and 29.7 GeV) and at various t values both in the form of $sd^2\sigma/dt\ dM^2$ (Fig. 39) and $sd^2\sigma/dt\ dM$ (Fig. 40). The authors conclude that although there is no rigorous scaling for either set of plots, both sets give a reasonable qualitative scalelike description of the data, indicating that both $\bar{\alpha}(0) = 1$ and $\frac{1}{2}$ contribute. For the low t values we note the increase near $x = 1$ expected from the

diffraction dissociation. For higher -t values a strong dip develops near $x \simeq 1$ as expected because of the decrease in all the $\alpha(t)$ involved. Actually this dip structure can tell us about the type of Regge exchanges involved in this approach. Thus at $t = -0.814$ a normal trajectory $\alpha(t) = 0.5 + 0.9\,t$ would produce an x dependence $-(d^2\sigma/dt\,dx) = (1-x)^{1.5}$ which decreases sharply towards $x = 1$, whereas the data in Fig. d show a roughly constant behaviour. The authors conclude therefore that the data indicate the presence of higher contributions (Pomeron) in this region and may therefore imply the presence of a triple-Pomeron coupling in the high -t region.

One of the lessons of these figures is that even in the resonance regions the data tend to oscillate around some universal curve. This implies that there is some hope of applying the triple Regge treatment down to very low M^2 values. If one uses the approach of diagram 38 in the resonance region, then one would expect, by the usual duality arguments [53], that $\bar{\alpha}(0) \approx \frac{1}{2}$ corresponding to a natural Regge exchange. Hence the resonances do not contribute to the scaling limit. The two low -t regions in Fig. 40 seem to show a strong non-scaling ($\bar{\alpha} \simeq \frac{1}{2}$) component. One can then rewrite Eq. (70) in the form

$$\frac{d^2\sigma}{dt\,dM^2} \approx s^{2\alpha(t)-2} f(M^2,t) \qquad f(M^2,t) \approx (M^2)^{\bar{\alpha}(0)-2\alpha(t)} \beta(t)$$

thus implying that the coupling of the various produced resonances is determined by the triple-Regge vertex. This approach is presumably mostly useful in the discussion of diffraction dissociation to which we will return in the next section.

The set of experiments on which this analysis [64] was based, allows one to probe both the s as well as the M^2 behaviours. We are not yet in a position where such extensive data exist for many other inclusive reactions. Several authors [65], [66] resorted therefore to the analysis of only the M^2 dependence at fixed s, facing the obvious difficulty that they cannot check whether the resulting distributions scale or not. Such an analysis of the 19.2 GeV pp data shown in Fig. 5 was recently carried out by Chen Wang and Wong [66]. They analyzed the M^2 dependence for different t values and inferred from this analysis the $\alpha_{eff}(t)$ values where $\alpha_{eff}(t)$ is defined by

$$\frac{s\,d^2\sigma}{dt\,dM^2} = f(s)(M^2)^{1-2\alpha_{eff}(t)} \tag{71}$$

The results of their fits are shown in Table III and have the general characteristics of very low values of $\alpha_{eff}(t)$. Clearly the range of their x values is (at least partially) responsible for this fact. All these fits were made in regions of $x \lesssim 0.8$ where the triple Regge formula cannot apply. The parametrization is nonetheless interesting and useful and warrants further studies along these lines. We see the

general hierarchy of Regge exchanges reflected also here, namely the order of mesonic > baryonic > exotic α values. This is, however, where the analogy to usual Regge fits stops. None of the other features, like clear dips, can be seen.

Reaction	$\alpha_{eff}(t)$	$(\frac{M^2}{s})_{min}$	Remarks
(pp,p)	-0.1 + 0.43 t	0.19	see previous discussion
(pp, π^+)	-1.32 + 0.53 t	0.16	compare : $\alpha_N(t) \simeq -0.38 + 0.88$ t
(pp, π^-)	-2.0 + 0.78 t	0.27	compare : $\alpha_\Delta(t) \simeq 0.20 + 0.85$ t
(pp, K^+)	-1.11 + 0.63 t	0.18	consistent with $K^+p \to pK^+$
(pp, K^-)	-3.55 + 0.7 t	0.31	exotic
(pp, $\bar{p}$)	-5.7 + 0.7 t	0.34	exotic

TABLE III : Results of the analysis of Ref. [66]. $(\frac{M^2}{s})_{min}$ designates the lowest value of this parameter in the data fitted by Eq. (71).

Actually, Fig. 5 shows that almost all inclusive distributions in this experiment are very smooth. The two exceptions to the rule are the (pp,p) distribution that shows diffractive production of resonances, and the (pp, π^+) data that show some unexplained structure. The clear shoulder in these latter data is evident in Fig. 41, in which the (pp, π^+) distributions extrapolated to $p_T = 0$ are shown in the laboratory frame. We note the clear indication of scaling in the data taken at the three different energies by Allaby et al. [67]. By comparing p_L and p_T distributions, it looks like the shoulder effect is a p_L rather than a t effect. In addition it may be a transient effect since it is more pronounced in the 14 GeV data than in the 24 GeV data. The authors included in Fig. 41 arrows showing the location of π^+ emitted from baryonic resonance production. The position of the dip occurs, however, where a peak (of the 2190) would be expected. The authors conclude therefore that the structure lacks a quantitative explanation at present.

The triple-Regge formula was used by Chliapnikov et al. [68] to analyze data of (K^+p,K^o) at 5 and 8.2 GeV [69]. The data are roughly consistent with scaling. Put in another way, if one calculates $\bar{\alpha}(0)$ then the result is consistent with 1 within one or two standard deviations. Nevertheless it is yet impossible to determine exactly the amount of, say, $\bar{\alpha}(0) = \frac{1}{2}$. The authors used the data to calculate $\alpha(t)$ by looking at the energy dependence of two separate regions in M, namely, $1 < M < 1.7$ GeV and $1.7 < M < 2.2$ GeV. It turned out that the first region gave results consistent with a normal trajectory passing through $\alpha(0) \simeq \frac{1}{2}$. This is the expected result from ρ and A_2 exchanges. The higher M data lead to $\alpha(t)$ values that lie lower

than the expected curve. This is consistent with the other analyses that we described in this section. It is therefore fair to conclude that the triple Regge formula may provide a good description at the high values of x. We need much better data, which allow an analysis in both s and M^2, to determine its exact ranges of validity.

Several remarks of the authors [68] point out further crucial uses of Regge fits : $\rho - A_2$ exchange degeneracy implies that the (K^+p, K^o) and $(K^-p, \bar{K}^o)$ data should be equal in the range of validity of the triple Regge limit. The same pattern of behaviour is predicted also for (K^+p, K^*) inclusive reactions which should be dominated by similar exchanges in the triple-Regge limit. Here one can furthermore distinguish between normal Regge exchanges, which should contribute to $(\rho_{11} + \rho_{1-1})\sigma$, and pion exchanges that will appear only in $\rho_{oo}\sigma$.

Let us close this section with a look at a different kind of distribution, namely, $K^+p \to \Lambda +$ pions. The data [70] are shown in Fig. 42. This reaction is of an annihilation type and therefore it decreases with energy (from 4.2 ± 0.1 mb at 4.2 GeV to 2.2 ± 0.1 mb at 10.1 GeV). Hence conventional scaling cannot be achieved. Nevertheless the shape of the distribution does not change very much and, therefore, if one divides it by its total area [$\sigma(\Lambda)$ in the figure] the result is scaling. In the region of $x \approx -1$ we may still try to apply the triple Regge approach writing

$$\frac{d^2\sigma}{dt\,dx} \approx \left(\frac{s}{M^2}\right)^{2\alpha(t)} \left(\frac{M^2}{s}\right)^{\bar{\alpha}(0)} f(t) \approx (1+x)^{\bar{\alpha}(0) - 2\alpha(t)}\, s^{\bar{\alpha}(0)-1}\, f(t) \qquad (72)$$

The over-all s behaviour of $\sigma(\Lambda)$ is like $s^{-0.8}$. If this would have been uniform we could insert in (72) $\bar{\alpha} = 0.2$. However, we see from Fig. 42 that near $x \approx -0.9$ a different energy behaviour sets in. This may be comparable with $\bar{\alpha} = \frac{1}{2}$ consistent with a normal trajectory exchange, dual to resonance production. The functional behaviour in x near $x = -1$ is roughly like $(1+x)^{\frac{1}{2}}$ which means that exchanges with $\alpha(t)$ near zero play the leading roles. It is of course interesting to analyze separately the $\bar{\alpha} \simeq 0.5$ and the $\bar{\alpha} \simeq 0.2$ parts but present data do not allow yet such fine distinctions.

10. - DIFFRACTION DISSOCIATION

Diffraction dissociation has always been, and still is, an important and fascinating subject by itself. The nature of the Pomeron is still a puzzle but it is known to contribute to inelastic processes which are then given the name of diffraction dissociation. Figure 43 shows total cross-sections [71] of nucleon resonances that are produced diffractively. Note their constant behaviour with energy compared to the decrease in the cross-section for Δ production. Comparing the magnitudes of these cross-sections with the known $\sigma_T(pp)$, which is about 39 mb in this energy range, one concludes that the identified resonances which are diffractively produced play a very small role in building the total cross-section. Nevertheless they are standing out because of their clear energy behaviour. Moreover the fact that their production is constant with energy may lead to diverging contributions to σ_T if their occurence at higher masses is not sufficiently damped. They are therefore the subject of interesting theoretical speculations and experimental observations that will be discussed in this section. We will not dwell upon the question of the nature of the produced resonances and will restrict ourselves to a discussion in the general framework of the triple-Regge formula.

We recall from the previous section that the triple Regge formula leads to a specific prediction for the production of masses M via the exchange $\alpha(t)$

$$-\frac{d^2\sigma}{dt\,dx} = \frac{s\,d^2\sigma}{dt\,dM^2} \approx \left(\frac{s}{M^2}\right)^{2\alpha(t)-1} (M^2)^{\bar{\alpha}(0)-1}\,\beta(t)$$

$$\frac{d^2\sigma}{dt\,dM^2} \propto s^{2\alpha(t)-2}\,(M^2)^{\bar{\alpha}(0)-2\alpha(t)}\,\beta(t) \qquad (73)$$

We show again the relevant variables in Fig. 44 to point out that this formula applies to the distribution of p in the upper vertex and therefore to diffractive dissociation [if $\alpha(t)$ is identified with Pomeron exchange] in the lower vertex. The mass M can represent either resonance or background production. Let us now calculate the contribution of this mode to the total cross-section. The derivation of the triple-Regge formula implies the existence of a single identifiable particle p in the region where the formula is applicable, therefore its integration leads to the contribution to σ_T rather than to $\langle n_i \rangle \sigma_T$ since $n_i = 1$ in the region of integration. Substituting $\beta(t) = e^{at}$ and $\alpha(t) = 1 + \alpha' t$ in Eq. (73) we obtain

$$\sigma_{Diff} = \int_1^s \frac{dM^2}{(M^2)^{2-\bar{\alpha}(0)}} \int dt\, e^{t\left(a + 2\alpha' \ln \frac{s}{M^2}\right)} \qquad (74)$$

$$\approx \int_1^s \frac{dM^2}{(M^2)^{2-\bar{\alpha}(0)}} \frac{1}{a + 2\alpha' \ln \frac{s}{M^2}}$$

Clearly if $\bar{\alpha}(0) < 1$ this integral leads to a decreasing contribution with s. If, however, $\bar{\alpha}(0) = 1$ (triple Pomeron amplitude) then the s dependence is singular. In this case a direct evaluation of the integral results in

$$\sigma_{Diff} = \frac{1}{2\alpha'} \ln\left(1 + \frac{2\alpha'}{a} \ln s\right) \tag{75}$$

The $\ln(\ln s)$ increase with energy was first pointed out by Finkelstein and Kajantie [72] in a two-Pomeron peripheral model. It was recently reemphasized by Abarbanel et al. [73] as an argument against a triple Pomeron coupling [or rather for a small triple Pomeron coupling dependent on the deviation of $\alpha_P(0)$ from 1]. The reason is that although, in principle, one may allow a logarithmic increase of the cross-section with energy, it is disturbing to find in a self-consistent model a cross-section that increases faster than the Pomeron and any of its cuts.

The edge of the diffraction dissociation region can be seen in Figs. 39 and 40 (parts a and b). As we already noted before, one would expect the resonating part to be dual to a normal trajectory and, therefore, to contribute to a non-scaling mode. ($\bar{\alpha} \approx \frac{1}{2}$). This trend seems to exist there. As the energy increases the resonances tend to higher x values building a universal curve in $M\, d^2\sigma/dt\, dx$. If we try to fit a $(1-x)^{-1}$ curve to the left part of Fig. 40a, we will realize that as soon as we reach $x = 0.9$ the curve will deviate from the data and fall below the general constant trend. This is consistent with the observation that we made at the begining of this section, namely that the total diffractive cross-section is in practice very small.

Wang and Wang [74] as well as Ting and Yesian [75] analyzed the effect of the background production. This is the part that may be identified with a triple Pomeron coupling. The data of Ref. [71] for (pp,p) and ($\pi^- p, \pi^-$) distributions at various energies are shown in Figs. 45 and 46. Plotting $d^2\sigma/dt\, dM$ vs. M one finds a clear variation at lower energies which may stabilize at higher energies. Whether or not there is a background present in the final stable curve is the question at hand. The interpretation of the data is still somewhat ambiguous. The authors [74] claim it is consistent with no triple Pomeron coupling.

If the Pomeron factorizes (barring any spin complications) one would expect the distributions in Fig. 45 to be equal in shape to those in Fig. 46 and to obey the the relation

$$(pp, p) : (\pi^- p, \pi^-) = \sigma_T(pp) : \sigma_T(\pi^- p) \tag{76}$$

The two relevant curves in Fig. 46 do indeed show similar features and their normalization agrees with this relation. Note that this relation does not depend on scaling since it follows from the identification of $\alpha(t)$, rather than $\bar{\alpha}(0)$, with the Pomeron. The comparison of diffractive resonance production, as pointed out by Freund [76], was the first experimental verification that the Pomeron factorizes.

The analysis of the triple Regge formalism can be readily extended to the case of double diffractive production. Let us first derive the formalism for general two Regge exchanges. This situation is depicted in Fig. 47, showing the emission of p_1 with very low momentum transfer (t_1) from q_1 and the emission of p_2 with very low momentum transfer (t_2) from q_2 simultaneously. If we define now [77]

$$s_1 = (q_1+q_2-p_2)^2 \quad , \quad s_2 = (q_1+q_2-p_1)^2 \, , \quad M^2 = (q_1+q_2-p_1-p_2)^2 \tag{77}$$

then it follows that in the limit when all energies are large and t_1 and t_2 are small, we may write, using by definition only positive x values, $x_{1,2} = 2E^c_{1,2}\cdot m_{1,2}/W$,

$$\frac{M^2}{s} \approx (1-x_1)(1-x_2) \qquad \frac{M^2}{s_{1,2}} \approx 1-x_{1,2} \qquad s = \frac{s_1 s_2}{M^2} \tag{78}$$

We can now write the corresponding distribution in complete analogy to the triple Regge formula as

$$\frac{d^4\sigma}{dt_1\, dx_1\, dt_2\, dx_2} = \left(\frac{s_1}{M^2}\right)^{2\alpha_1(t_1)} \left(\frac{s_2}{M^2}\right)^{2\alpha_2(t_2)} \frac{(M^2)^{\bar{\alpha}(0)}}{s} f(t_1,t_2) \tag{79}$$

Using a general $O(3,1)$ expansion [77] one can show that the general di-triple Regge formula should be somewhat more complicated, namely

$$\frac{d^4\sigma}{dt_1\, dx_1\, dt_2\, dx_2} = \sum_{M=0}^{\infty} \left(\frac{s_1}{M^2}\right)^{2\alpha_1(t_1)} \left(\frac{s_2}{M^2}\right)^{2\alpha_2(t_2)} \frac{(M^2)^{\bar{\alpha}(0)}}{s} \cos M\varphi \; f_M(t_1,t_2) \tag{80}$$

where

$$\cos\varphi = \frac{\vec{p}_{T_1}\cdot\vec{p}_{T_2}}{|\vec{p}_{T_1}||\vec{p}_{T_2}|}$$

and M is Toller's quantum number [78]. Indeed if the leading singularity (Pomeron) has $M = 0$ then the more simple formula (79) follows. It clearly must have a component with $M = 0$ since otherwise the cross-section has negative values for some φ ; it may, however, have components with different M values. In the latter case, there will be a definite correlation between $\vec{p}_{T1}$ and $\vec{p}_{T2}$ that should be experimentally observable. The same arguments apply not only in the di-triple Regge region but also in the more general double fragmentation regions. The simplest case would be of course if the Pomeron has an $M = 0$ character implying that no correlations exist between the two different fragmentation regions.

One of the results of Eqs. (79) and (80) is that once again scaling is achieved if $\bar{\alpha}(0) = 1$. Turning now to the problem of double diffraction dissociation we realize that Fig. 47 describes Pomeron-Pomeron scattering. According to the arguments brought above this may very well be dominated by P' exchange and have therefore a

non-scaling behaviour because $\bar{\alpha}(0) \sim \frac{1}{2}$. Undoubtedly one may expect the double diffraction amplitude to be very small recalling that the single diffraction dissociation accounts only for a couple of per cent of the total cross-section (at energy ranges of tens of GeV). One would therefore expect that double diffraction dissociation is of the order of 1‰ or less, which is the reason that this process has yet to be detected. Applying duality arguments to Fig. 47, one can understand [79] why the PPf^o coupling would be much smaller than the $PP'f^o$, thus accounting for the well-known fact [14] that the analysis of production data in terms of Regge pole exchanges did not show any sign of a double Pomeron coupling to a meson like f^o.

11. - CORRELATIONS

Clearly the next topic to be discussed after the single particle distributions is the two-particles' correlation function. If we define a normalized distribution by

$$f_i(p) = \frac{1}{\sigma_T(ab)} \rho_i(p) = \frac{1}{\sigma_T(ab)} E \frac{d^3\sigma(ab, i)}{d^3p} \tag{81}$$

(alternatively one could use the total inelastic cross-section instead of σ_T) then we find

$$\int f_i(p) \frac{d^3p}{E} = \langle n_i \rangle \tag{82}$$

Let us now define [80]

$$\frac{1}{\sigma_T} \rho_{ij}(p_1, p_2) = \frac{E_1 E_2}{\sigma_T(ab)} \frac{d^6\sigma(ab, ij)}{d^3p_1\, d^3p_2} = f_i(p_1) f_j(p_2) + f_{ij}(p_1, p_2) \tag{83}$$

Note that $f_i(p)$ has dimensions of p^{-2} and $f_{ij}(p_1p_2)$ has dimensions of p^{-4}. Upon integration of Eq. (83) one finds

$$f_{ij} = \int f_{ij}(p_1, p_2) \frac{d^3p_1}{E_1} \frac{d^3p_2}{E_2} = \begin{cases} \langle n_i n_j \rangle - \langle n_i \rangle \langle n_j \rangle & \text{if } i \neq j \\ \langle n_i (n_i - 1) \rangle - \langle n_i \rangle^2 & \text{if } i = j \end{cases} \tag{84}$$

One can say that particles i and j are produced independently if $f_{ij}(p_1p_2) = 0$. Indeed we see from (84) the characteristic equality of a Poisson distribution $\langle n^2 \rangle - \langle n \rangle^2 = \langle n \rangle$ come out if $f_{ij} = 0$. As one might expect it is impossible to have all these $f_{ij}(p_1p_2)$ vanish. This may be seen in the following way due to Predazzi and Veneziano [81]. In the c.m. frame the relation

$$\sum_{\text{particles}} E_j = W \tag{85}$$

translates into

$$\sum_i \int f_i(p)\, E\, \frac{d^3p}{E} = W \tag{86}$$

where the sum is over all types of particles i. Such arguments were used in deriving the Chou-Yang sum rule (33). We may now square the relation (85) and rewrite it in the form

$$\sum_{ij} \int E_1 E_2\, \frac{d^6\sigma(ab, ij)}{\sigma_T(ab)\, d^3p_1 d^3p_2}\, d^3p_1\, d^3p_2 + \sum_i \int E_i^2\, f_i(p)\, \frac{d^3p}{E} = W^2 \tag{87}$$

The second term on the left of this equation is needed in order to take into account the diagonal terms in the square of Eq. (85). If one substitutes the definition (83) into (87) one obtains, after using equality (86), the result

$$\sum_{ij} \int E_1 E_2\, f_{ij}(p_1 p_2)\, \frac{d^3p_1}{E_1} \frac{d^3p_2}{E_2} + \sum_i \int E^2\, f_i(p)\, \frac{d^3p}{E} = 0 \tag{88}$$

Since the second term is positive definite, the first one has to have a net result different from zero. Following similar consideration with the longitudinal momentum, the authors [81] show that the resulting sum rules are compatible with no correlation in the double fragmentation region but demand negative correlation if both detected particles are fragments of the same initial particle. Using the transverse momentum in such equations, one can show that $\sum_{ij} f_{ij}(p_1 p_2)$ must have an azimuthal dependence. The azimuthal correlations and their connection to the nature of the exchanged poles are discussed in Ref. [82].

The functions $f_{ij}(p_1 p_2)$ are obviously functions of six variables. There are, however, clear favourable ways of presenting them. The first natural way is to look for correlations as a function of the mass of the two particles

$$\frac{df_{ij}}{dm^2} = \int f_{ij}(p_1 p_2)\, \delta((p_1+p_2)^2 - m^2)\, \frac{d^3p_1}{E_1} \frac{d^3p_2}{E_2} \tag{89}$$

$$= \int \frac{d^3p_1}{E_1} \frac{d^3p_2}{E_2}\, \delta((p_1+p_2)^2 - m^2) \left[\frac{1}{\sigma_T} \rho_{ij}(p_1 p_2) - \frac{1}{\sigma_T} \rho_i(p_1) \frac{1}{\sigma_T} \rho_j(p_2) \right]$$

$f_{ij}(m^2)$ will in general depend on the incoming energy as well. We may expect it to have some structure similar to the total cross-section of particles i and j. Note that in the second equality in Eq. (89) one subtracts from the conventional m^2 distribution the part which would exist if the particles i and j were produced independently. In particular, looking at $\pi^+\pi^+$ correlations, one would expect a small result with no structure, while a $\pi^+\pi^-$ correlation should peak strongly around the ρ and f^o masses.

An alternative way to plot the correlation function would be vs. the difference in rapidity between particles i and j

$$\frac{df_{ij}}{dz} = \int f_{ij}(p_1 p_2)\, \delta(z_1 - z_2 - z)\, \frac{d^3p_1}{E_1}\, \frac{d^3p_2}{E_2} \qquad (90)$$

We expect also this plot to be peaked around low values of its argument (say $|z| < 1$) because this is when the low mass resonances can be produced. In a "Feynman gas" picture, one would expect the correlations to fall off exponentially [24] at high values of z. This defines then for each pair of particles (ij) a characteristic length in rapidity, reflecting the strength of the correlation between the two. Berger and Krzywicki [83] emphasize that kinematical correlations are expected to have the same range as the dynamical ones, thus promising us a confusion between the two also in this new field. It may very well turn out that, similar to our experience with $f_i(p)$ one will use for convenience a distribution in z for low z values, and a distribution in x at higher separations.

$$\frac{df_{ij}}{dx} = \int f_{ij}(p_1 p_2)\, \delta(x_1 - x_2 - x)\, \frac{d^3p_1}{E_1}\, \frac{d^3p_2}{E_2} \qquad (91)$$

x can vary between -2 and 2.

In the limiting fragmentation picture [43] one would expect $\rho_{ij}(p_1 p_2)$ to scale in x_1 and x_2. If eventually such a scaling property is reached for all x values, then f_{ij} may have a singularity of $\log^2 s$ which will call for a non-scaling ($\log s$) factor in df_{ij}/dx. All these properties are of course the subjects of future investigations.

Of a completely different nature will be the distribution with respect to the transverse angle between the two particles :

$$\frac{df_{ij}}{d\cos\varphi} = \int f_{ij}(p_1 p_2)\, \delta\left(\frac{\vec{p}_{T_1} \cdot \vec{p}_{T_2}}{|\vec{p}_{T_1}||\vec{p}_{T_2}|} - \cos\varphi\right) \frac{d^3p_1}{E_1}\, \frac{d^3p_2}{E_2} \qquad (92)$$

We can no longer use arguments based on the invariant squared mass of the set of particles, to predict the shape of this distribution.

Experimental data for the correlation function are not available yet. However, recent first trials of such problems show that some new interesting and unexpected structures may emerge. In Fig. 48 we show recent data of the ABBCCHW collaboration [5] where an analysis of $(\pi^- p, \pi_f^- p)$ at 16 GeV is presented. π_f^- is the fastest pion emerging from the reaction in the laboratory frame. The lines present the density of the events plotted in an x_f (refering to π_f) and x_p plane. One observes a clear structure in the x_f distribution varying from a single maximum at low x_p to a two-maxima curve at intermediate x_p and finally arriving at a broad curve with a single maximum for high x_p. The reasons for this structure are still unclear. It teaches us, however, that correlations might exist even at high separations in x. Another important and well-known lesson is that clear signals of correlations are best seen when the two particles are well identified - in some opposition to an inclusive approach. This is also brought up in Fig. 49 where data [84] from $\pi^- p \rightarrow$ six prongs events are compared by choosing once $(\pi^+ \pi^-)$ forward pairs and all the rest in the backward direction, and then doing the same choice for $(\pi^- \pi^-)$ pairs. The latter case looks like a "background" of the former one, out of which clear ρ^0 and f^0 signals form the bulk of the $(\pi^+ \pi^-)$ events [85]. It remains to be seen whether inclusive correlation tests will also be able to give such clear signals.

We saw in Eq. (88) that there are clear kinematic constraints on the correlation functions. Actually there are three general categories of such constraints :

1) conservation of four momenta ;

2) conservation of additive and multiplicative quantum numbers (such as charge, hypercharge, parity and charge conjugation) ;

3) conservation of isospin.

Equation (88) was a consequence of the first type of constraints. As far as the pions are concerned, it may be a mild constraint since the main bulk of their distribution is anyway concentrated around the c.m. and dies out quickly toward the edges of phase space. The points 2) and 3) can be simply avoided in a model that produces pion pairs with vacuum quantum numbers $(I = 0\ J^{PC} = 0^{++})$. Although this looks like the simplest way out it is not necessarily Natures' solution to the problem. The data of Fig. 49 for example do not show any clear evidence for such a state. This is admittedly a poor proof since these are only selected events of a very special type and our knowledge of the structure of the cloud of pions near the c.m. is still very limited.

Let us, however, see how the condition of charge conservation [type 2) in the classification above] leads to immediate constraints on random distributions. Let us in particular discuss the possibility of independent emission of charged pions [86]. If this could be achieved we would expect a Poisson distribution for each kind of pion separately. Such distributions can be defined in terms of the parameters $c_\pm$ in the form

$$P_n^{(\pm)} = e^{-c_\pm} \frac{c_\pm^n}{n!} \tag{93}$$

where n is the number of charged pions emitted. If one asks, however, for the conditional probability of emitting independent pions such that their over-all charge is zero, one finds [86] the following distribution of n pion pairs

$$P_n = \frac{1}{J_0(2ic)} \frac{c^{2n}}{(n!)^2} \tag{94}$$

where $c^2 = c_+ c_-$ and each term in (94) is just the product of the two corresponding ones in Eqs. (93). The normalization function turns then out to be a Bessel function $J_0(2ic)$. The average number of pairs $< n >$ is given by

$$\langle n \rangle = \sum_n n P_n = -ic \frac{J_1(2ic)}{J_0(2ic)} \tag{95}$$

and one finds

$$\begin{aligned} \langle n^2 \rangle &= c^2 \\ \sigma = \langle n^2 \rangle - \langle n \rangle^2 &= c^2 \left(1 + \frac{J_1^2(2ic)}{J_0^2(2ic)}\right) \end{aligned} \tag{96}$$

For high values of n one can use Stirling's formula to obtain

$$P_n \to \frac{1}{J_0(2ic)} \frac{(2c)^{2n}}{(2n)! \sqrt{\pi n}} \tag{97}$$

which differs slightly from a Poisson distribution.

The predictions of Eq. (94) are compared with data compiled by Wang [87] in Fig. 50. This is a compilation of inelastic production experiments below 27 GeV. The number of charged prongs should be related to our n by $n_c = 2n + 2$ (but for the case of nn collisions where it is assumed that $n_c = 2n$). Comparing the data with these distributions corresponds to assuming a model in which the two incoming particles leave as two outgoing leading particles plus a cloud of pions that obey the distribution law (94). To obtain a consistent picture one has to assume the elastic scattering is not given by this model directly (the $n = 0$ case corresponds to many π^0 production) and is related to it only via unitarity. The other two curves on the figure correspond to two distributions proposed by Wang : W^I is a Poisson distribution in $\frac{1}{2}(n_c - 2)$ describing independent production of pion pairs, and W^{II} is built out of the even terms in a Poisson distribution in $(n_c - 2)$. The data are assembled in a way that tests the character of the distribution, namely the figure shows the probability for a certain n_c to occur provided $< n_c >$ is given. Although the distribution (94) seems to work

somewhat better than W^I and W^{II} one can by no means say that it fits successfully all data. The latter do seem to follow some universal trends but they show significant fluctuations characterizing the specific structure of the various channels. It is therefore difficult to draw unambiguous conclusions from these fits. A formula which fits well all known data was suggested by Czyzewski and Rybicki [88]. Defining the quantities $D^2 = \langle n^2 \rangle - \langle n \rangle^2$ and $xD = n - \langle n \rangle$, where n is the number of charged prongs, they suggest the distribution law

$$P(n) = \frac{2d e^{-d^2}}{D} \frac{d^{2(dx+d^2)}}{\Gamma(dx+d^2+1)} \tag{98}$$

where d is a free parameter. This complicated formula is not suggestive of any simple physical interpretation and reflects the complexity of the problem at hand.

Let us turn now to the last type of constraints that was mentioned above - isospin conservation. This is a non-linear condition and leads therefore to more complicated mathematical structures. If one deals with a simple model that consists of leading particles + independent pion production, then one inevitably clashes with isospin conservation even if charge conservation is taken into account in the way described above. Nevertheless one may ask if such a model can be regarded as an approximation. This question was analyzed in Ref. [89]. It turns out that the best choice of parameters still leads to a growth of the isospin of the cloud of pions like

$$\langle \vec{I}^2 \rangle \approx \langle n \rangle \tag{99}$$

where n is the number of emitted pions. This is not unexpected since it just describes a random walk in isospace. Since actually low multiplicities are involved, such a model has some chance to serve as a crude approximation. The experimental check should be given by comparing π^0 with $\pi^\pm$ behaviour. We refer to results like those [90] shown in Fig. 51. Here one sees the average number of π^0 produced in 25 GeV $\pi^- p$ reactions plotted against the number of charged particles in the same event. An independent emission of π^0 would result in a constant value. If, however, the pions are produced in resonances, correlations may occur. In a multiperipheral model [91] in which pions are produced in $I = 1$ and $I = 0$ resonances, one finds clear correlations from the $I = 1$ part. Caneschi and Schwimmer [91] obtained in this way a fit to the data of Fig. 51 in which a minimum occurs at two prongs followed by a rise towards $\bar{n}_{\pi^0} \approx 3$ for the higher prongs. The available data are clearly inconclusive yet.

The correlations that we discussed in this section are obviously just the beginning of a new domain of research. Once again we may expect to learn first about the general properties of the correlation and distribution functions before any specific models will be proved or disproved. With the study of inclusive distributions reaching recently the first stages of maturity, we may hope that the knowledge and understanding of correlations will soon follow.

REFERENCES

1) A.K. Wroblewski - Rapporteur's talk at the Kiev Conference (1970).

2) M. Deutschmann - Rapporteur's talk at the Amsterdam Conference (1971).

3) J.W. Waters, W.D. Walker, A.R. Erwin, J.W. Elbert - University of Wisconsin Paper, submitted to Lund Conference (1969).

4) R. Honecker et al., ABBCCHW Collaboration - Nuclear Phys. B13, 571 (1969) ;
M. Deutschmann et al., ABBCCHW Collaboration - submitted to the Kiev Conference (1970).

5) ABBCCHW Collaboration - Papers submitted to the Amsterdam Conference (1971) ; see also Ref. 2).

6) Yash Pal and B. Peters - K. Danske Vidensk.Selsk.Mat.-Fys.Medd. 33, 15 (1964).

7) J.V. Allaby et al. - CERN Report 70-12 (1970).

8) E. Flaminio, J.D. Hansen, D.R.O. Morrison and N. Tovey - CERN-HERA Report 70-3 (1970).

9) O. Czyzewski and K. Rybicki - Paper submitted to the Kiev Conference (1970) ; see also Ref. 1).

10) L.W. Jones et al. - Phys.Rev.Letters 25, 1679 (1970).

11) Data presented by K. Rybicki at the Amsterdam Conference (1971) ; see also Ref. 2).

12) L. Bertocchi, S. Fubini and M. Tonin - Nuovo Cimento 25, 626 (1962) ;
D. Amati, S. Fubini and A. Stanghellini - Nuovo Cimento 26, 896 (1962).

13) T.W.B. Kibble - Phys.Rev. 131, 2282 (1963) ;
K.A. TerMartirosyan - Zh.Eksper.Teor.Fiz. 44, 341 (1963) ; Soviet Phys. JETP (USA) 17, 233 (1963) ;
F. Zachariasen and G. Zweig - Phys.Rev. 160, 1322, 1326 (1967) ;
G.F. Chew and A. Pignotti - Phys.Rev. 176, 2112 (1968).

14) See, e.g., :
R. Lipes, G. Zweig and W. Robertson - Phys.Rev.Letters 22, 433 (1969).

15) Chan Hong-Mo, J. Loskiewicz and W.W.M. Allison - Nuovo Cimento 57A, 93 (1968).

16) C. Lovelace - Review talk at Regge Pole Conference, U.C. Irvine (1969).

17) G.F. Chew, T. Rogers and D.R. Snider - Phys.Rev. D2, 765 (1970).

18) S. Fubini - "Strong Interactions and High Energy Physics", Scottish Universities' Summer School (1963), edited by R.G. Moorhouse, Oliver and Boyd (1964), p. 259.

19) H.W. Wyld Jr. - University of Illinois, Urbana Preprint ILL-(TH)-71-2.

20) D.M. Tow - Phys.Rev. D2, 154 (1970).

21) H.D.I. Abarbanel, G.F. Chew, M.L. Goldberger and L.M. Saunders - Phys.Rev.Letters 25, 1735 (1970).

22) R.P. Feynman - Phys.Rev.Letters 23, 1415 (1969) ; "High Energy Collisions", edited by C.N. Yang et al., Gordon and Breach, New York (1969), p. 237.

23) C.E. DeTar - Phys.Rev. D3, 128 (1971).

24) K.G. Wilson - Cornell Preprint CLNS-131 (1971).

25) I would like to thank S. Nussinov for suggesting this derivation.

26) H. Cheng and T.T. Wu - Phys.Rev.Letters 23, 1311 (1969) ; Phys.Rev. D3, 2195 (1971).

27) H. Bøggild, E. Dahl-Jansen, M. Gavrilas, K.H. Hansen and H. Johnstad - Paper submitted to the Amsterdam Conference (1971).

28) J.D. Hansen, W. Kittel and D.R.O. Morrison - Nuclear Phys. B25, 605 (1971).
See also :
T. Hofmokl and A. Wroblewski - Phys.Letters 31B, 391 (1970).

29) J. Grunhaus, D. Horn and S. Nussinov - unpublished.

30) L. Van Hove - Physics Reports 1, 347 (1971).

31) L. von Lindern - Nuovo Cimento 5, 491 (1957).

32) M. Kugler - unpublished.

33) L. Van Hove - Phys.Letters 28B, 429 (1969) ; Nuclear Phys. B9, 331 (1969).

34) R. Hagedorn - Suppl.Nuovo Cimento 3, 147 (1965) ; 6, 311 (1968) ;
R. Hagedorn and J. Ranft - Suppl.Nuovo Cimento 6, 169 (1968) ;
For recent summaries, see :
H. Grote, R. Hagedorn and J. Ranft - "Particle Spectra", CERN (1970) ;
G. Ranft and J. Ranft - Leipzig Preprint (1970).

35) L. Van Hove - Nuovo Cimento 28, 798 (1963).

36) A. Białas - Nuovo Cimento 33, 972 (1964).

37) H.W. Lewis, J.R. Oppenheimer and S.A. Wouthuysen - Phys.Rev. 73, 127 (1948).

38) See, e.g. :
G. Cocconi - Phys.Rev. 111, 1699 (1958).

39) R.R. Kinsey, T.W. Morris, R.S. Panvini - Paper submitted to the Kiev Conference (1970).

40) D.B. Smith, R.J. Sprafka and J.A. Anderson - Phys.Rev.Letters 23, 1064 (1969).

41) L.G. Ratner, R.J. Ellis, G. Vannini, B.A. Babcock, A.D. Krisch and J.B. Roberts - Phys.Rev.Letters 27, 68 (1971).

42) N.F. Bali, L.S. Brown, R.D. Peccei and A. Pignotti - Phys.Rev.Letters 25, 557 (1970).

43) J. Benecke, T.T. Chou, C.N. Yang and E. Yen - Phys.Rev. 188, 2159 (1969).

44) T.T. Chou and C.N. Yang - Phys.Rev.Letters 25, 1072 (1970).
Note that our ρ_i differ from their ρ_1 by a factor of E.

45) A.H. Mueller - Phys.Rev. D2, 2963 (1970). For details on the group theoretical approach, see :
H.D.I. Abarbanel - Phys.Rev. D3, 2227 (1971).

46) C.E. DeTar, K. Kang, C.I. Tan and J.E. Weis - MIT Preprint CTP No 180 (1971) ;
D. Gordon and G. Veneziano - Phys.Rev. D3, 2116 (1971) ;
M.A. Virasoro - Phys.Rev., to be published;
R.C. Brower and R.E. Waltz - Nuovo Cimento, to be published.

47) M.S. Chen et al. - Phys.Rev.Letters 26, 1585 (1971).

48) Chan Hong-Mo, C.S. Hsue, C. Quigg and J.M. Wang - Phys.Rev.Letters 26, 672 (1971).

49) J. Ellis, J. Finkelstein, P.H. Frampton and M. Jacob - Phys.Letters 35B, 227 (1971).

50) M. Jacob - CERN Preprint TH. 1340 (1971).

51) M. Toller - Nuovo Cimento 37, 631 (1965).

52) M. Bishari, D. Horn and S. Nussinov - CERN Preprint TH. 1385 (1971).

53) H.D.I. Abarbanel - Phys.Letters B34, 69 (1971).

54) P.G.O. Freund - Phys.Rev.Letters 20, 235 (1968) ;
H. Harari - Phys.Rev.Letters 20, 1395 (1968).

55) S. Mandelstam - Nuovo Cimento 30, 1127, 1148 (1963).

56) F. Zachariasen - Physics Reports 2, 1 (1971).

57) J.W. Elbert, A.R. Erwin and W.D. Walker - Phys.Rev. D3, 2042 (1971).

58) S.L. Stone et al. - Rochester University Preprint (1971) ;
N.N. Biswas et al. - Phys.Rev.Letters 26, 1589 (1971).

59) W. Ko and R.L. Lander - Phys.Rev.Letters 26, 1284 (1971).

60) L. Caneschi - Phys.Rev. D3, 2865 (1971).

61) R. Stroynowski - Paper presented at the Amsterdam Conference (1971). See also Ref. 5).

62) C.E. DeTar, C.E. Jones, F.E. Low, J.H. Weis, J.E. Young and C.I. Tan - Phys.Rev. Letters 26, 675 (1971).

63) G.F. Chew and A. Pignotti - 1968 Summer Study, Vol. 3, NAL (1968) ;
L. Caneschi and A. Pignotti - Phys.Rev.Letters 22, 1219 (1969) ;
D. Silverman and C.I. Tan - Phys.Rev. D2, 233 (1970) ;
A different derivation of this formula was also given by : R.P. Feynman, Ref. 22).

64) R.M. Edelstein, V. Rittenberg and H.R. Rubinstein - Preprint WIS-71/19/Ph.

65) R.D. Peccei and A. Pignotti - Phys.Rev.Letters 26, 1076 (1971).

66) M.S. Chen, L.L. Wang and T.F. Wong - BNL Preprint (1971).

67) J.V. Allaby et al. - Paper submitted to the Amsterdam Conference (1971).

68) P. Chliapnikov, O. Czyzewski, J. Finkelstein and M. Jacob - CERN Preprint TH. 1336 (1971).

69) J.V. Beaupré et al. - CERN/DPhII/70-52 (1971).

70) Aachen-Berlin-CERN-London-Vienna and Amsterdam-Nijmegen collaborations - CERN/DPh.II-Phys. 71-26 (1971), submitted to the Amsterdam Conference (1971).

71) E.W. Anderson et al. - Phys.Rev.Letters 16, 855 (1966) ; 25, 699 (1970).

72) J. Finkelstein and K. Kajantie - Nuovo Cimento 56, 659 (1968).

73) H.D.I. Abarbanel, G.F. Chew, M.L. Goldberger and L.M. Saunders - Phys.Rev.Letters 26, 937 (1971).

74) J.M. Wang and L.L. Wang - Phys.Rev.Letters 26, 1287 (1971).

75) P.D. Ting and J.H. Yesian - Phys.Letters 35B, 321 (1971).

76) P.G.O. Freund - Phys.Rev.Letters 21, 1375 (1968).

77) D.Z. Freedman, C.E. Jones, F.E. Low and J.E. Young - Phys.Rev.Letters 26, 1197 (1971).

78) M. Toller - Nuovo Cimento 53A, 671 (1968).

79) C-li Jen, K. Kang, P. Shen and C.I. Tan - Preprint NYO-2262TA-247 (1971).

80) A.H. Mueller - BNL Preprint 15706 (1971).

81) E. Predazzi and G. Veneziano - CERN Preprint TH. 1378 (1971).

82) A. Bassetto and M. Toller - CERN Preprint TH. 1337 (1971).

83) E.L. Berger and A. Krzywicki - Orsay Preprint LPTPE 71/36 (1971).

84) European Collaboration for Analysis of High Multiplicity Events, submitted to the Colloquium on Multiparticle Dynamics, Helsinki (May 1971).

85) See also discussion in :
L. Van Hove - CERN Preprint TH. 1365 (1971), lecture delivered at the Helsinki Conference (1971).

86) H.A. Kastrup - Nuclear Phys. B1, 309 (1967);
D. Horn and R. Silver - Phys.Rev. D2, 2082 (1970).

87) C.P. Wang - Phys.Rev. 180, 1463 (1968).

88) O. Czyzewski and K. Rybicki - Paper submitted to the Kiev Conference (1970).

89) D. Horn and R. Silver - CERN Preprint TH. 1226 (1970), to be published in Ann. Phys. 66 (1971).

90) J.W. Elbert et al. - Nuclear Phys. B19, 85 (1970).

91) L. Caneschi and A. Schwimmer - Phys.Letters 33B, 577 (1970).

FIGURE CAPTIONS

Figure 1 Cross-sections for non-strange particle production in 16 GeV $\pi^- p$ collisions (from Ref. [4]) plotted vs. the number of prongs. The curve has the characteristic shape of a Poisson distribution. The cross (x) at $n_{ch} = 2$ corresponds to the value of σ_T that includes the elastic cross-section while the circle designates only the inelastic cross-section.

Figure 2 Transverse distributions of π production. Data of Ref. [5]. Note the sharp peak at $p_T^2 = 0$ and the varying slope of this (inclusive) distribution.

Figure 3 Peyrou plot taken from Ref. [4]. Note the clear effect of leading particles in the p and π^- distributions, the cut-off in transverse momenta, and the concentration of pions near the c.m. origin.

Figure 4 Vectors of average momenta of various particles in different modes observed in 16 GeV $\pi^- p$ collisions (from Ref. [4]). The leading particle effect diminishes with increasing multiplicity and the p_T cut-off is roughly invariant.

Figure 5 Particle spectra in 19.2 GeV pp collisions. Figure taken from Ref. [7]. The proton distribution shows a characteristic leading effect whereas all other distributions peak around the c.m. Note the similarity in p_T distributions and the different scales for the different particles.

Figure 6 Sizes of cross-sections observed in $\bar{p}p$ collisions. This plot is taken from the lecture by W.A. Cooper in Symposium on Nucleon-Antinucleon Interactions, Argonne, Ill., (1968), p. 108.

Figure 7 The average charged multiplicity in the pp cosmic rays experiment [10] which shows a logarithmic increase with energy.

Figure 8 Multiperipheral diagram.

Figure 9 Results of a multiperipheral calculation by Wyld [19] of the process $\pi\pi \to n\rho$ $n = 2,3,\ldots$, based on elementary pion exchange. The only free parameter was the $\rho\pi\pi$ coupling which was chosen so as to give an asymptotic constant total cross-section.

Figure 10 Distribution of the i^{th} produced particle in a simplified Chew-Pignotti [13] model. Taken from DeTar [23]. y denotes the rapidity measured in the laboratory frame and Y its maximal range. Distributions are shown for (a) six and (b) eleven produced particles. All add up to a constant inclusive distribution.

Figure 11 Inclusive distribution of 19 GeV (pp, π^-) data of the Scandinavian collaboration [27]. The cross-section is plotted vs. rapidity in the c.m. for different p_T cuts.

Figure 12 Same data as in Fig. 11 are now integrated over p_T and shown on a linear scale.

Figure 13 Characteristic variation of a cross-section (σ) with energy, and the quantity σ_A defined in Eq. (13). Taken from Ref. [28].

Figure 14 The variation of longitudinal phase space, Eq. (16), with total c.m. energy W [29].

Figure 15 Diagrammatic relation of the rapidity z to momentum variables. The points A and B denote characteristic momentum values of pions which have the same longitudinal velocity as a proton of $p_L = C$. The $1/E$ curve is the momentum distribution of phase space (homogeneous z distribution).

Figure 16 Comparison of a rapidity plot (a), with the Peyrou plots in c.m. (b), and in lab (c). Taken from DeTar [23]. The phase space boundary is indicated with a heavy line for the process (pp, π) with beam momentum of 25.6 GeV. The shaded band denotes the position of pions that result from the process $pp \to \Delta\Delta$ in the near forward direction. Note how the main part of the rapidity plot is mapped into a very small region in $p_L^{c.m.}$. The latter plot shows mostly negative p_L values in the target and projectile frames (left of line A and right of line E respectively).

Figure 17 π^- momentum distribution in 28.5 GeV pp collisions, from Ref. [39]. Numerical values of the different slopes (b) are given.

Figure 18 $(\pi^- p, \pi^\pm)$ data [5] are plotted vs. x and normalized lab rapidity ξ. The latter plots show roughly the same shape for the various p_T cuts.

Figure 19 Test of Eq. (23) showing the plot of $\rho_i(p_L)$ for the lowest p_T bin of Fig. 17, vs. M. The equivalent q^{lab} values are added for comparison with Fig. 20.

Figure 20 Cross-sections of pp collisions, from Ref. [40].

Figure 21 Recent ISR data [41] verify scaling in the region of $0.1 \lesssim x \lesssim 0.3$. The quoted P_o values are the equivalent ν values of the ISR data which are here compared with results in the 12-19 GeV range.

Figure 22 $(\pi^+ p, \pi^-)$ data [5], plotted vs. x and vs. normalized lab rapidity ξ, show lack of scaling in the central region in the 8-16 GeV range.

Figure 23 (π^+p, π^+) and (π^+p, π^-) data [5] are compared in the negative p_L^{lab} region. Whereas (π^+p, π^-) shows limiting fragmentation behaviour in these ν ranges, (π^+p, π^+) still decreases slowly with energy.

Figure 24 Diagrammatic representation of Mueller's generalized optical theorem [45] for inclusive distributions.

Figure 25 Diagrammatic representation of limiting fragmentation.

Figure 26 p_L^{lab} distributions (from Ref. [47]) of (π^-p, π^-) at 24.8 GeV, (pp, π^-) at 28.5 GeV, (K^+p, π^-) at 12.7 GeV and (π^+p, π^-) at 7 GeV, normalized by their σ_T. The plot verifies limiting fragmentation as well as factorization.

Figure 27 The p_T^2 distributions of the data shown in Fig. 26 in the range of $p_L^{lab} < 0.5$ GeV.

Figure 28 Similar distributions [47] are plotted vs. p_L^{proj}. See footnote in the text.

Figure 29 Same data as in Fig. 28 are plotted vs. p_T^2 for $p_L^{proj} < 0.5$ GeV.

Figure 30 $(\pi^+p, \pi^\mp)$ data [5] are compared over the entire x range. One observes lack of scaling near $x \approx 0$, and non-limiting effects in (π^+p, π^+).

Figure 31 The two-Pomeron limit for the pionization region.

Figure 32 Several possible graphs that do not lead to the decomposition of Fig. 31.

Figure 33 (a) A polyperipheral diagram.
(b) Its contribution to a Mandelstam cut.

Figure 34 (K^+p, π^-) data [59] show asymmetric distributions in $p_L^{c.m.}$.

Figure 35 The slopes of the two sides of the distributions shown in Fig. 34 are given in various reference frames, specified by the ratio of momenta of the incoming particles.

Figure 36 A symmetric inclusive (K^+p, π^-) distribution is obtained in the R = 1.5 frame [59].

Figure 37 R values of different reactions are compiled for $(\pi p, \pi)$ and (Kp, π) data. Taken from Ref. [61]. The notation $\pi^-p \to \pi^+/\pi^- + \ldots$ means that π^+ data were used in the incoming π^- direction and π^- data in the incoming p direction.

Figure 38 The triple Regge diagram.

Figure 39 Analysis of (pp,p) data, taken from Ref. [64]. y in this plot means $M^2/s \approx 1-x$.

Figure 40 Same data shown in Fig. 39 are plotted for the non-scaling quantity $-M\,(d^2\sigma/dt\,dx)$.

Figure 41 (pp, π^+) data [67] show limiting fragmentation and an intriguing transient structure. Arrows denote the region where π distributions from the quoted resonances should peak. The $p_T = 0$ invariant distribution is plotted vs. p_L^{proj}.

Figure 42 Annihilation cross-sections $K^-p \to \Lambda$ + pions [70] show invariant shapes but decreasing magnitudes.

Figure 43 Cross-sections [71] for diffraction dissociation are compared with the non-diffractive $pp \to p\Delta$ process.

Figure 44 Momentum distribution at low t values corresponds to the dissociation of q_2.

Figure 45 Missing mass distributions in (pp,p) data [71] at the different energies shown in the figure. The data are given for fixed angles in the laboratory rather than fixed t (see footnote b in Ref. [64]).

Figure 46 Missing mass distributions in (πp,π) data [71]. A comparison with one (pp,p) curve is in agreement with factorization of the Pomeron.

Figure 47 Di-triple Regge exchange.

Figure 48 Invariant distribution of fastest π^- and p in π^-p experiments [5] shows intriguing correlations. The value of the distribution is represented by the length of the line which is attached to its corresponding x_p x_f location.

Figure 49 $\pi^+\pi^-$ and $\pi^+\pi^+$ mass distributions are extracted from the data in the way explained in the figure. These results [84] show the expected resonances in $\pi^+\pi^-$ and the corresponding background distribution in $\pi^+\pi^+$.

Figure 50 Theoretical distributions of cross-sections for charged particle emission are compared with Wang's compilation of inelastic production data [87]. W^I and W^{II} are different types of Poisson distributions from Ref. [87] and the solid curve is a Bessel distribution from Ref. [86].

Figure 51 The average number of π^0 produced in π^-p reactions at 25 GeV vs. the number of charged particles. Taken from Ref. [90].

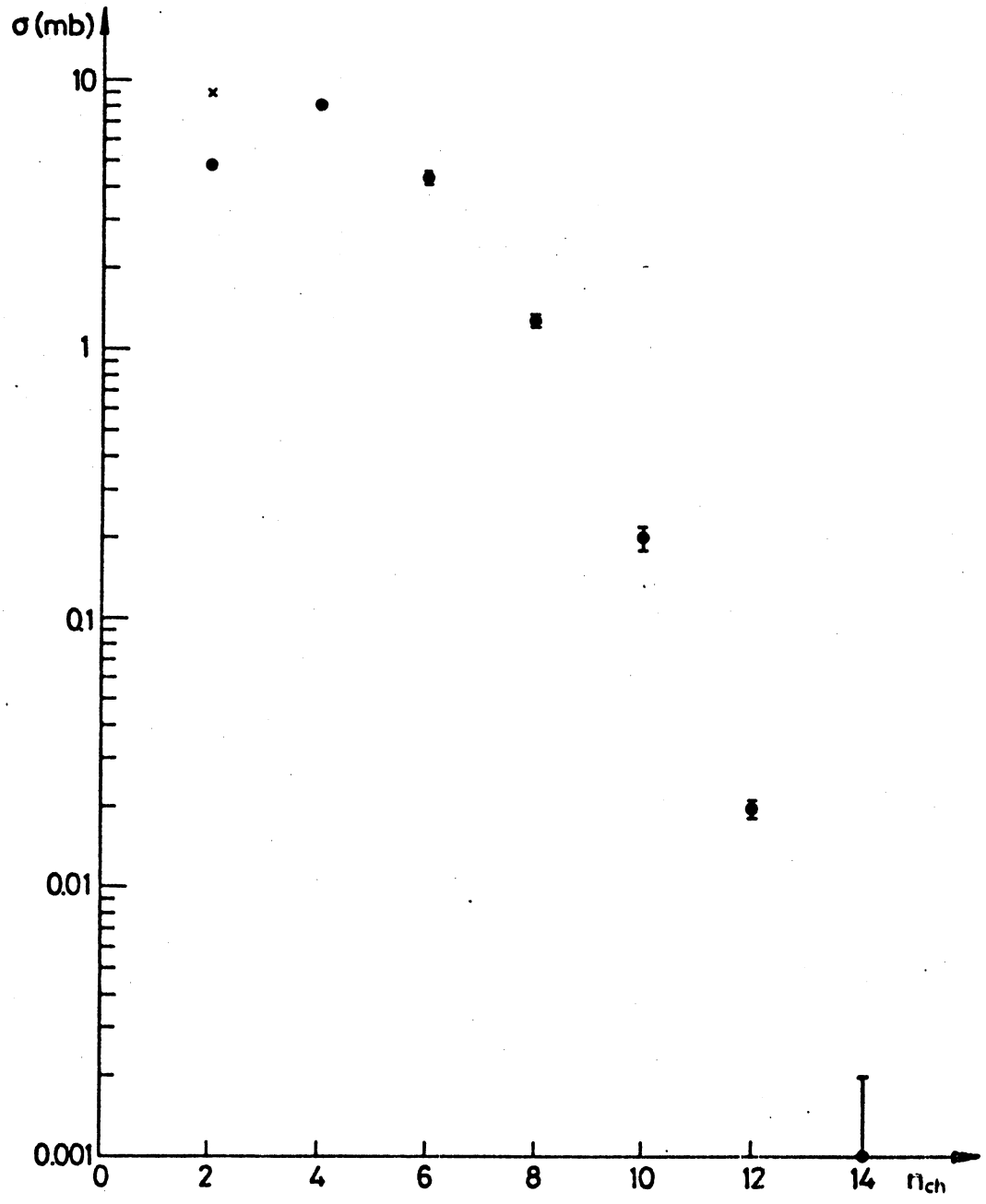

- Figure 1 -

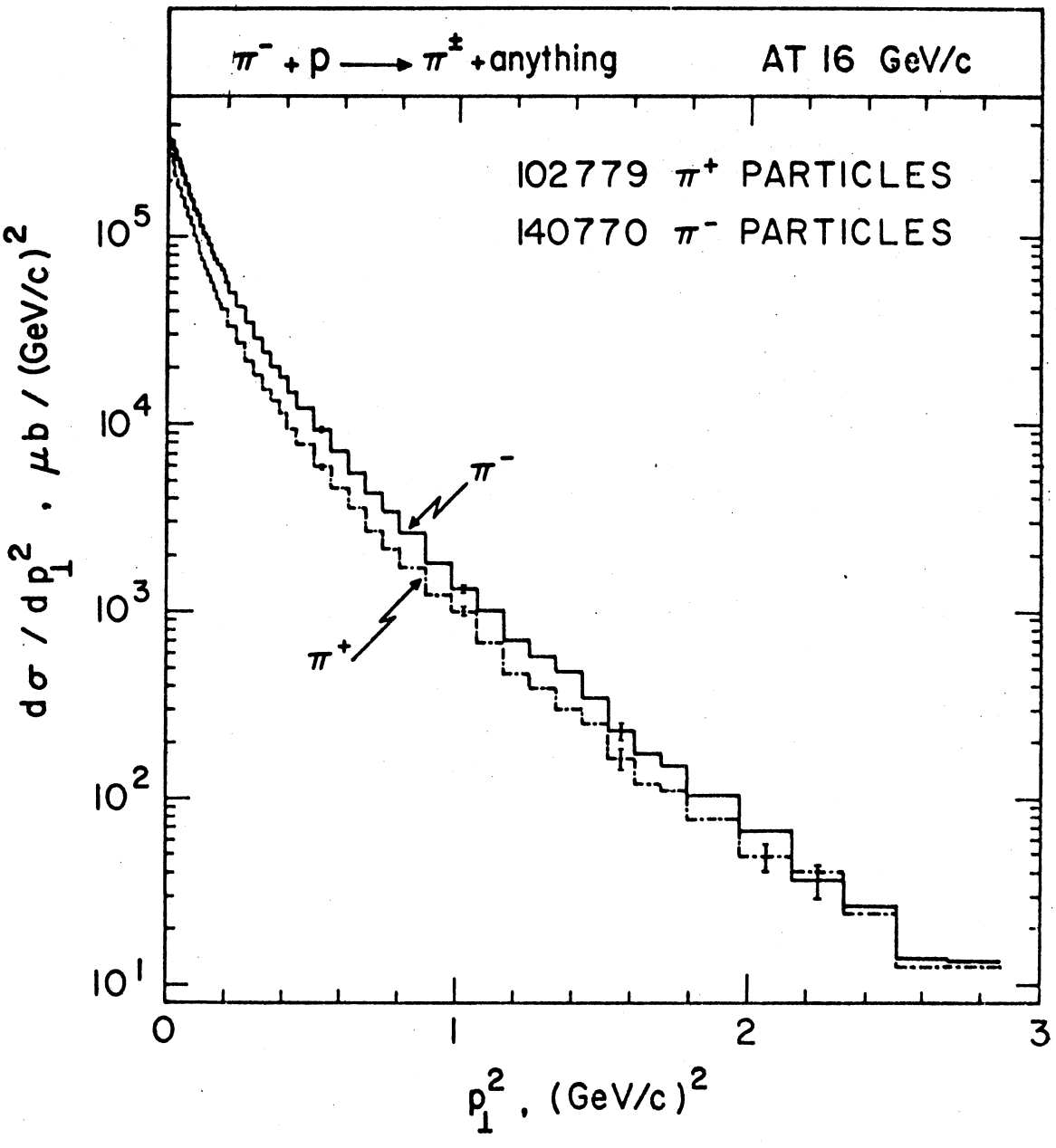
$\pi^- + p \longrightarrow \pi^\pm +$ anything
AT 16 GeV/c
102779 π^+ PARTICLES
140770 π^- PARTICLES
π^-
π^+
$d\sigma / dp_\perp^2$. $\mu b / (GeV/c)^2$
10^5
10^4
10^3
10^2
10^1
0
1
2
3
$p_\perp^2$, $(GeV/c)^2$

- Figure 2 -

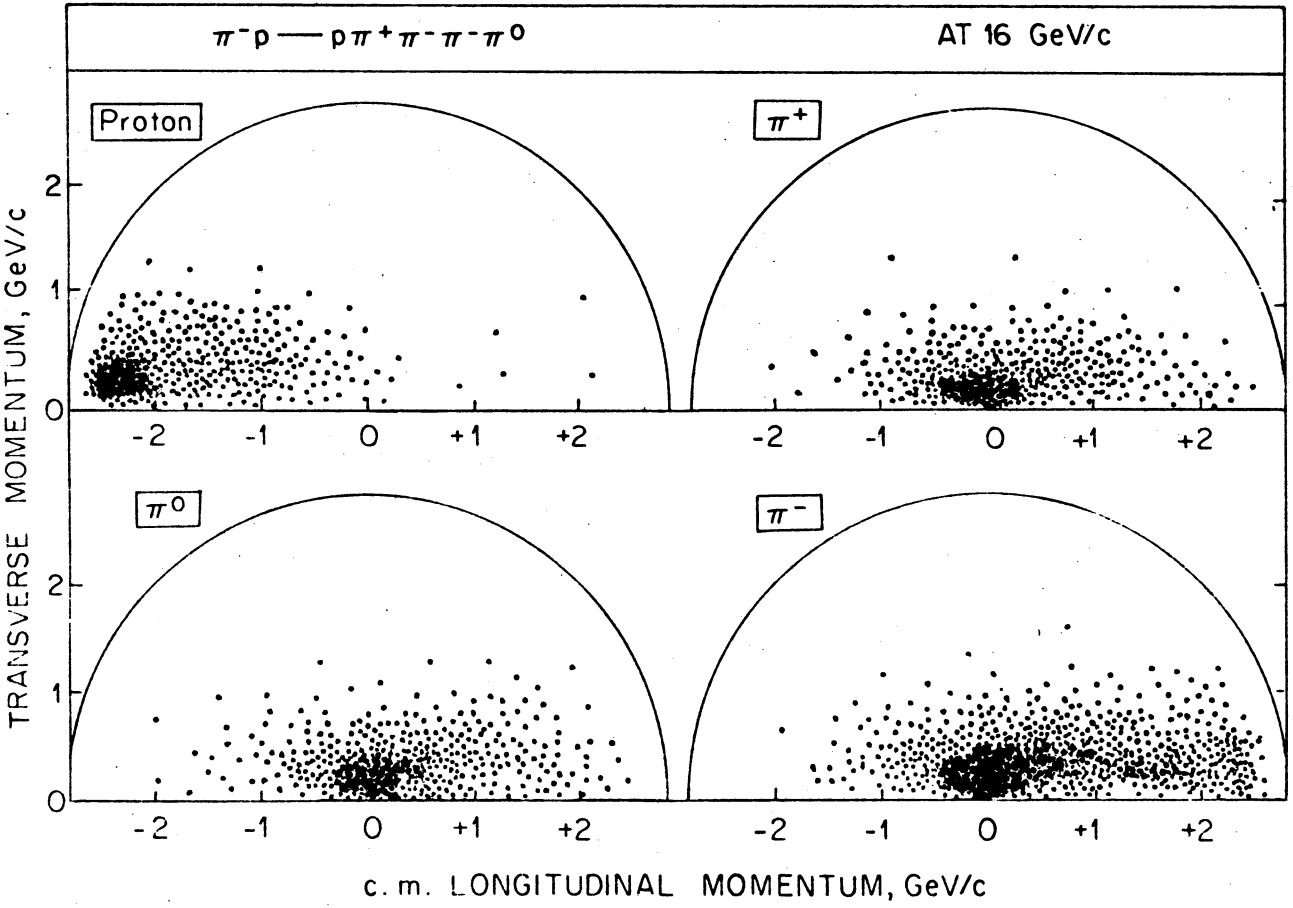
$\pi^- p \rightarrow p\pi^+\pi^-\pi^-\pi^0$
AT 16 GeV/c
Proton
π^+
π^0
π^-
TRANSVERSE MOMENTUM, GeV/c
c. m. LONGITUDINAL MOMENTUM, GeV/c
0
1
2
-2
-1
0
+1
+2

- Figure 3 -

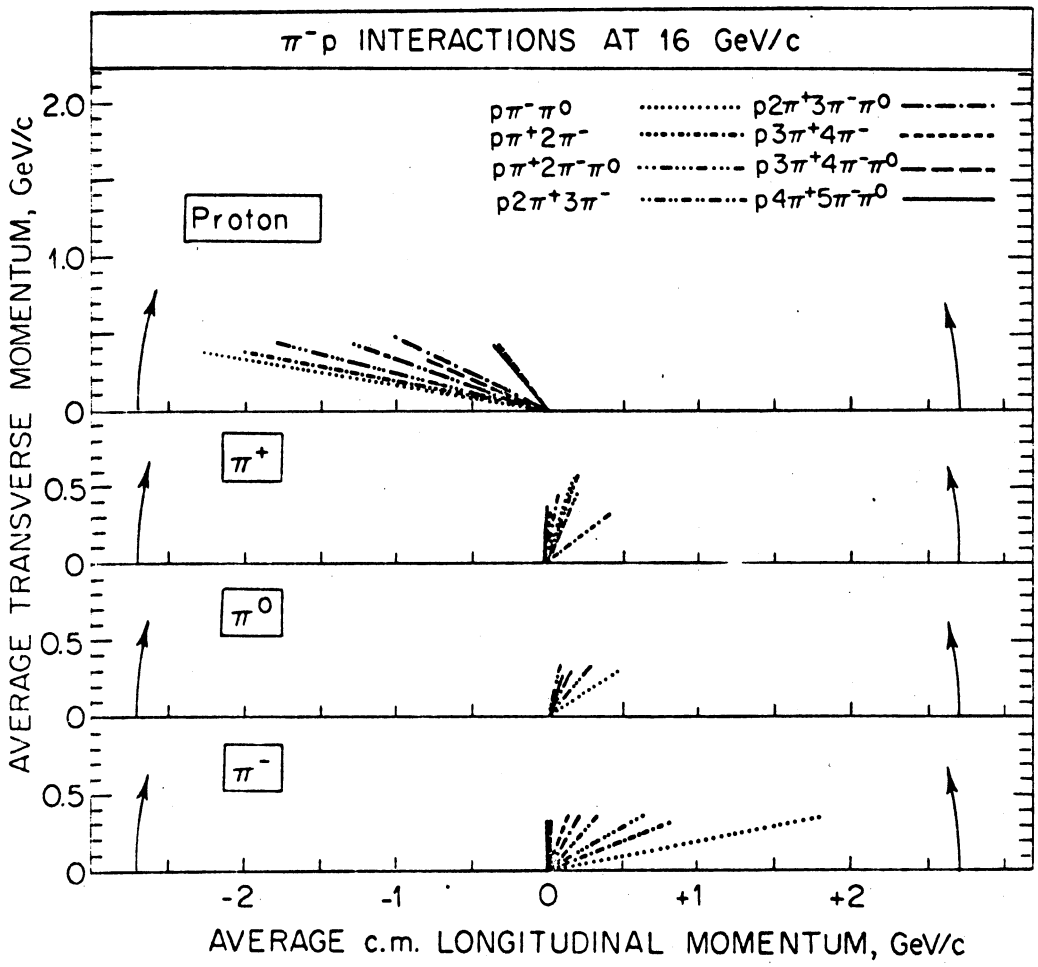
π⁻p INTERACTIONS AT 16 GeV/c
pπ⁻π⁰
pπ⁺2π⁻
pπ⁺2π⁻π⁰
p2π⁺3π⁻
p2π⁺3π⁻π⁰
p3π⁺4π⁻
p3π⁺4π⁻π⁰
p4π⁺5π⁻π⁰
Proton
π⁺
π⁰
π⁻
AVERAGE TRANSVERSE MOMENTUM, GeV/c
AVERAGE c.m. LONGITUDINAL MOMENTUM, GeV/c
2.0
1.0
0.5
0
-2
-1
+1
+2

- Figure 4 -

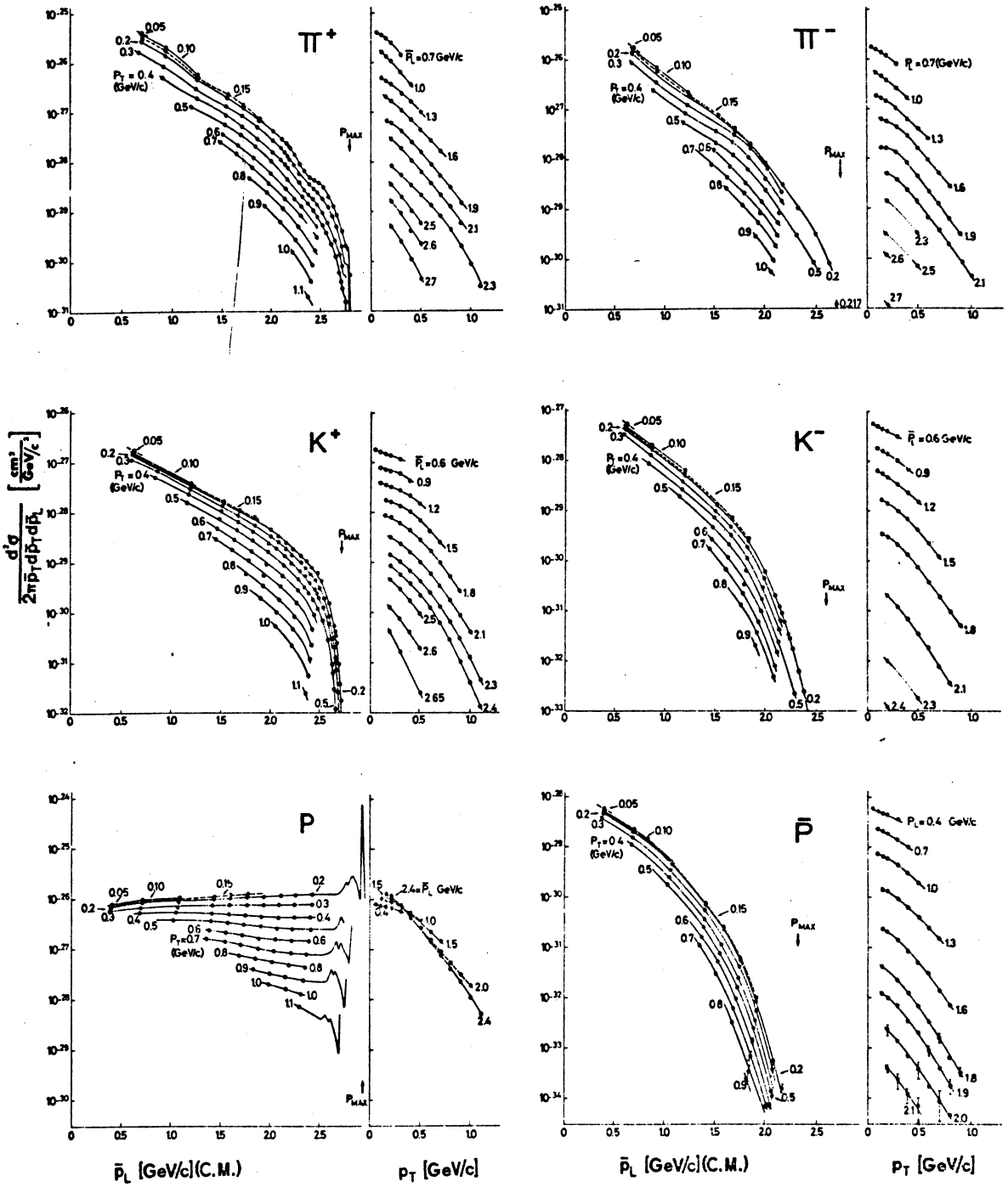
π^+
π^-
K^+
K^-
P
$\bar{P}$
$\frac{d^2\sigma}{2\pi \bar{p}_T d\bar{p}_T d\bar{p}_L}$ [cm²/(GeV/c)²]
$\bar{p}_L$ [GeV/c](C.M.)
p_T [GeV/c]

- Figure 5 -

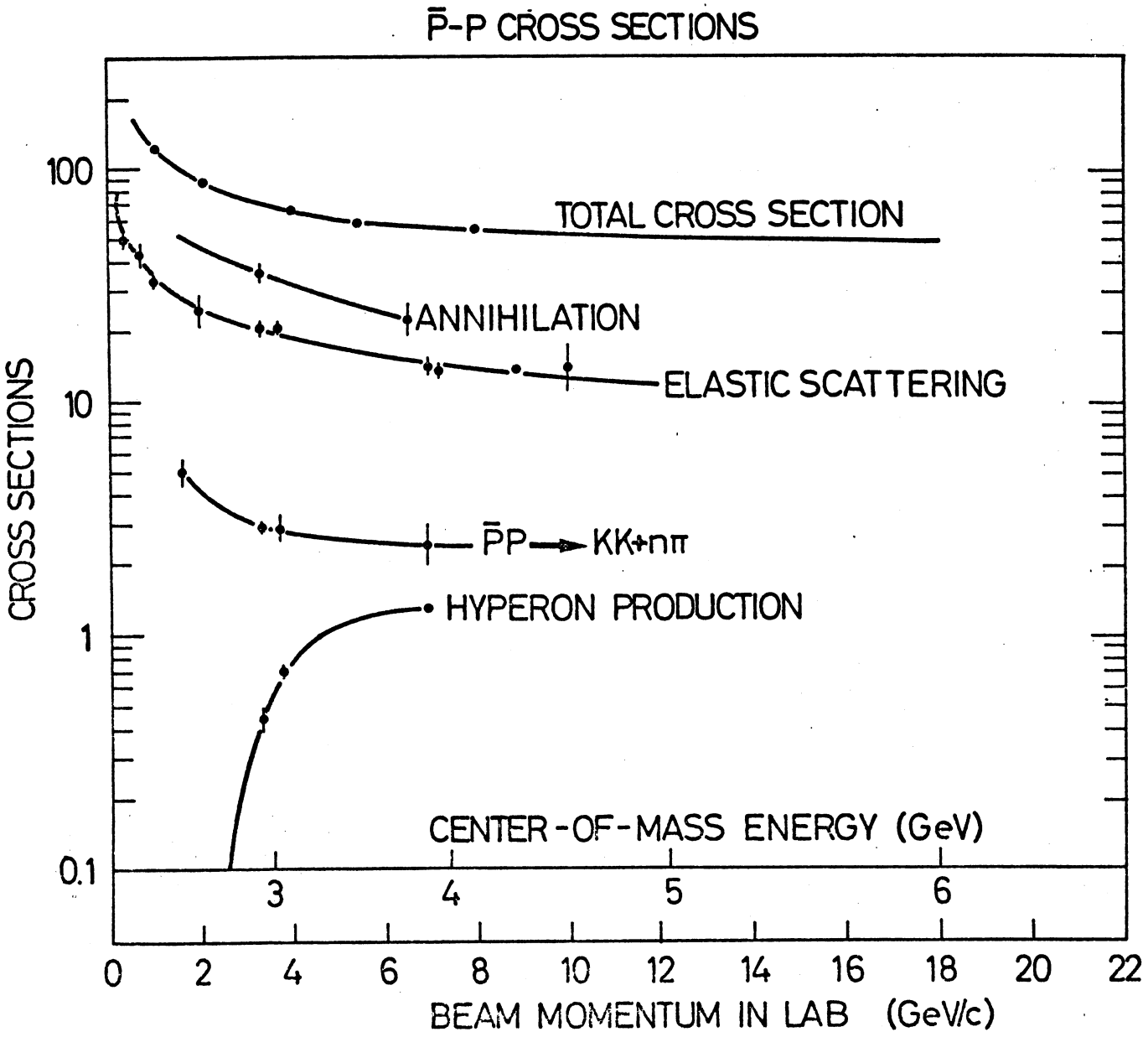
P̄-P CROSS SECTIONS
TOTAL CROSS SECTION
ANNIHILATION
ELASTIC SCATTERING
P̄P → KK+nπ
HYPERON PRODUCTION
CROSS SECTIONS
100
10
1
0.1
CENTER-OF-MASS ENERGY (GeV)
3
4
5
6
0
2
4
6
8
10
12
14
16
18
20
22
BEAM MOMENTUM IN LAB (GeV/c)

- Figure 6 -

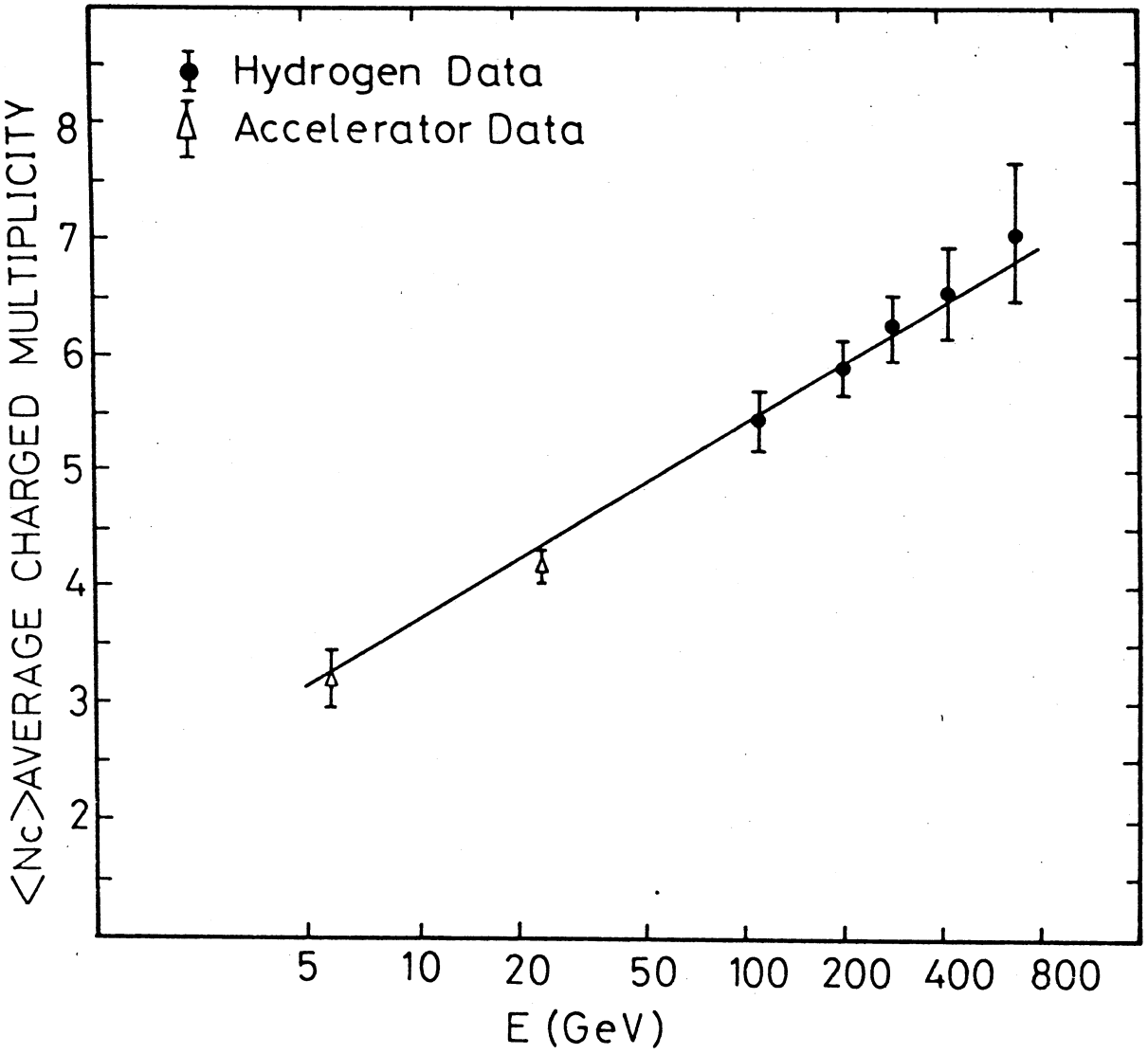
Hydrogen Data
Accelerator Data
<Nc>AVERAGE CHARGED MULTIPLICITY
2
3
4
5
6
7
8
5
10
20
50
100
200
400
800
E (GeV)

- Figure 7 -

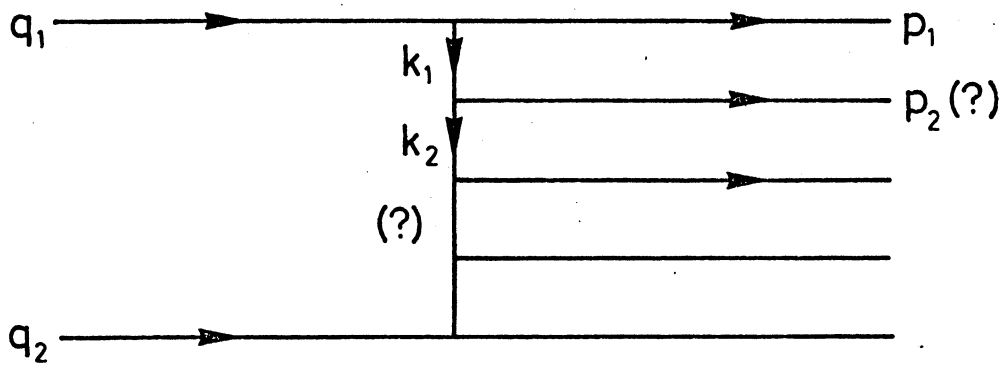

- Figure 8 -

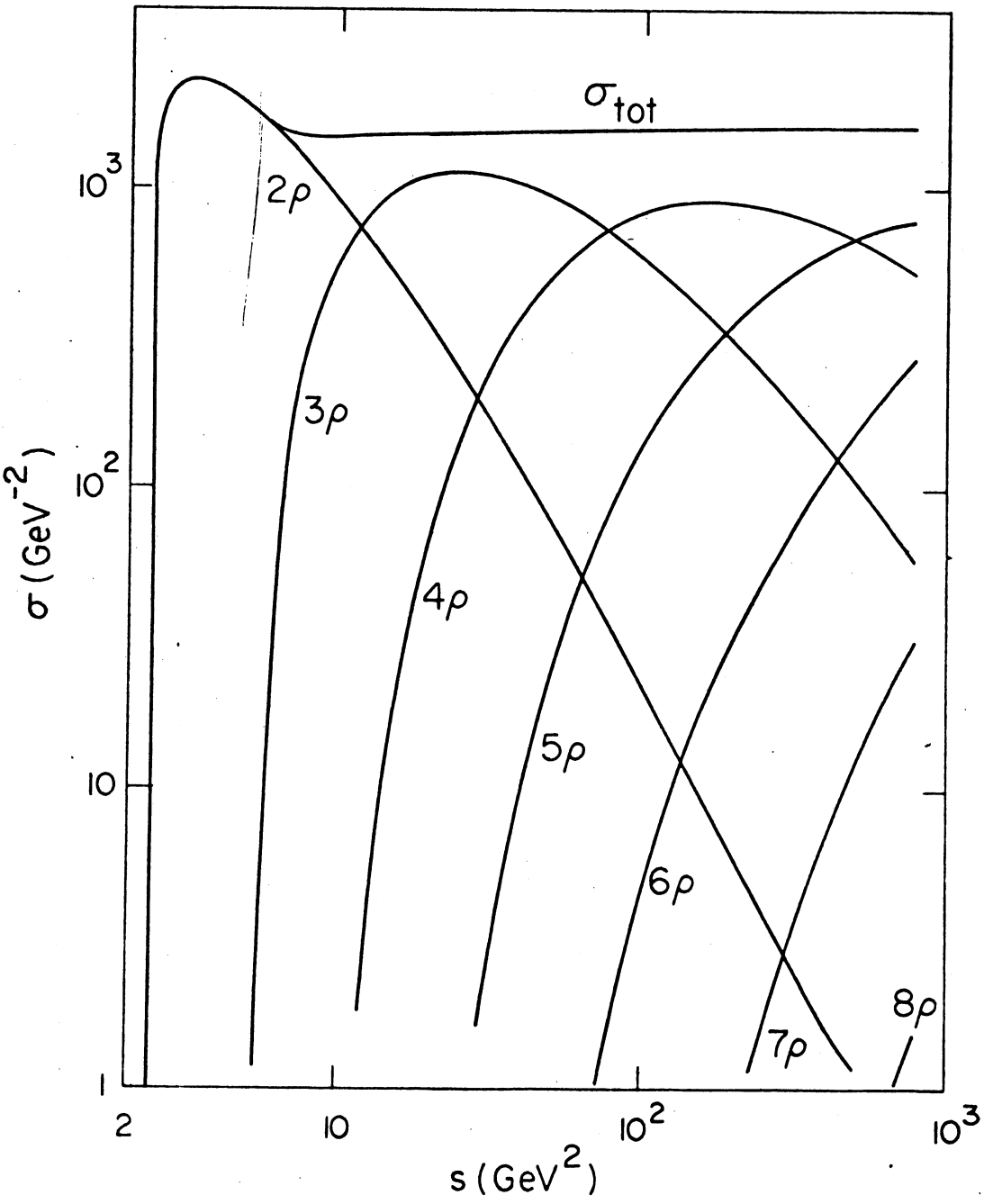
σ_{tot}
2ρ
3ρ
4ρ
5ρ
6ρ
7ρ
8ρ
10^3
10^2
10
1
σ (GeV^{-2})
2
10
10^2
10^3
s (GeV^2)

- Figure 9 -

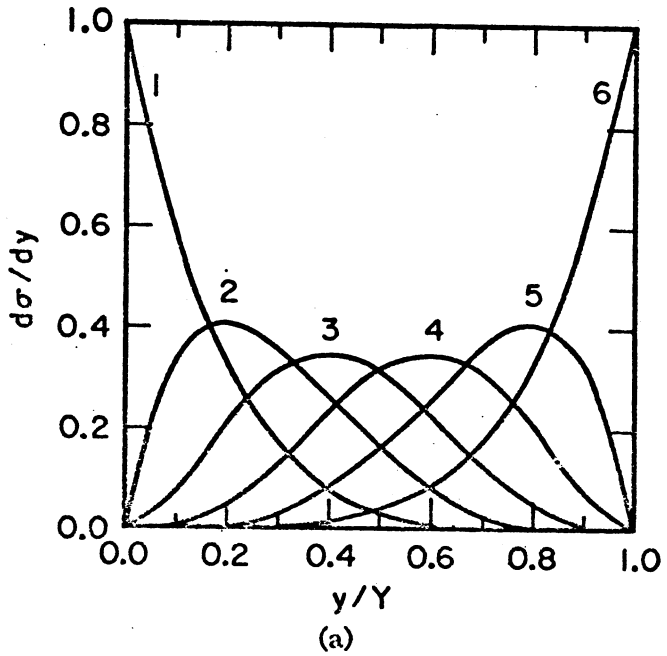
1.0
0.8
0.6
0.4
0.2
0.0
dσ/dy
1
2
3
4
5
6
0.0
0.2
0.4
0.6
0.8
1.0
y/Y

(a)

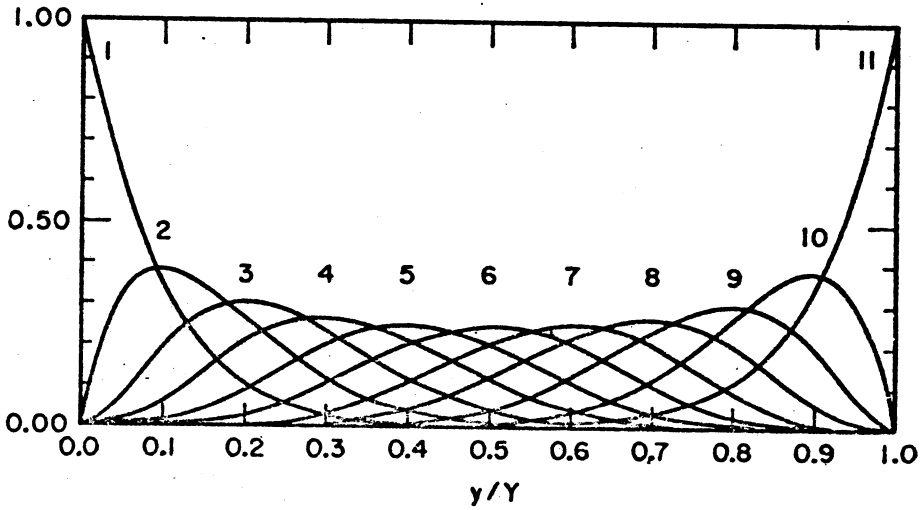
1.00
0.50
0.00
1
2
3
4
5
6
7
8
9
10
11
0.0
0.1
0.2
0.3
0.4
0.5
0.6
0.7
0.8
0.9
1.0
y/Y

(b)

- Figure 10 -

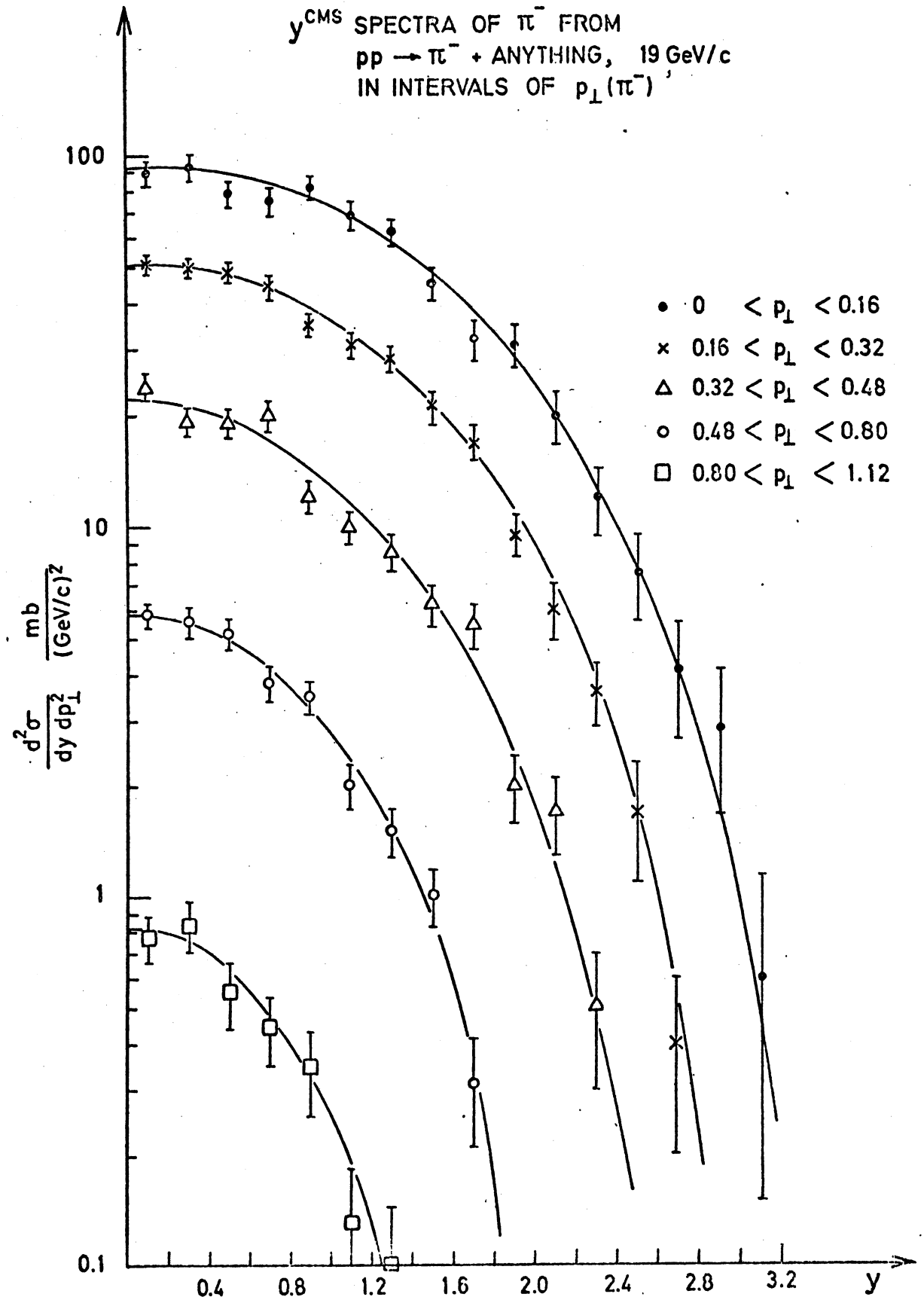
y^{CMS} SPECTRA OF π^- FROM
$pp \rightarrow \pi^- +$ ANYTHING, 19 GeV/c
IN INTERVALS OF $p_\perp(\pi^-)$
$\bullet$ $0 < p_\perp < 0.16$
$\times$ $0.16 < p_\perp < 0.32$
$\triangle$ $0.32 < p_\perp < 0.48$
$\circ$ $0.48 < p_\perp < 0.80$
$\square$ $0.80 < p_\perp < 1.12$
$\frac{d^2\sigma}{dy\,dp_\perp^2}$ $\frac{mb}{(GeV/c)^2}$
100
10
1
0.1
0.4
0.8
1.2
1.6
2.0
2.4
2.8
3.2
y

- Figure 11 -

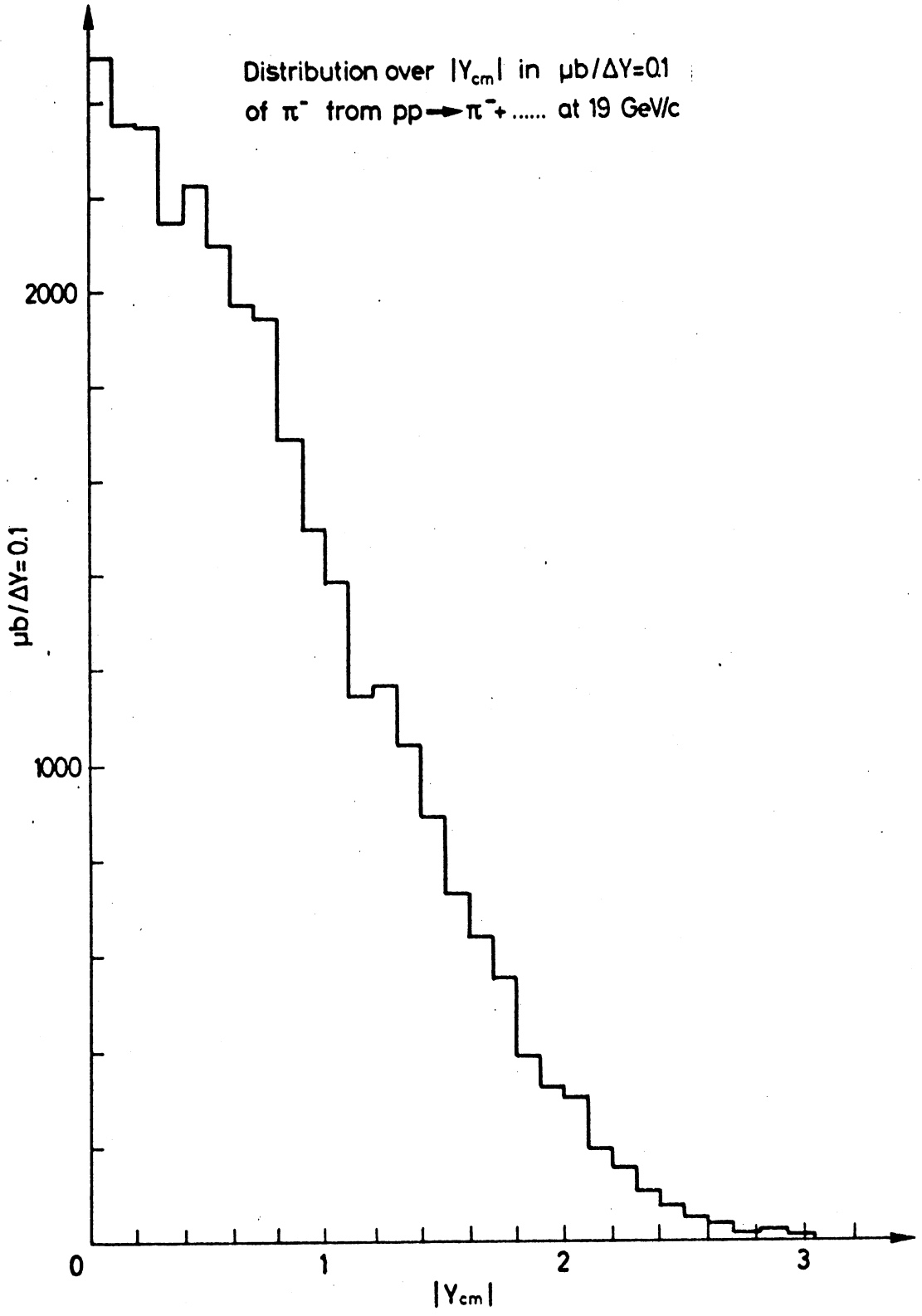
Distribution over |Ycm| in μb/ΔY=0.1
of π⁻ from pp→π⁻+..... at 19 GeV/c
2000
1000
μb/ΔY=0.1
0
1
2
3
|Ycm|

- Figure 12 -

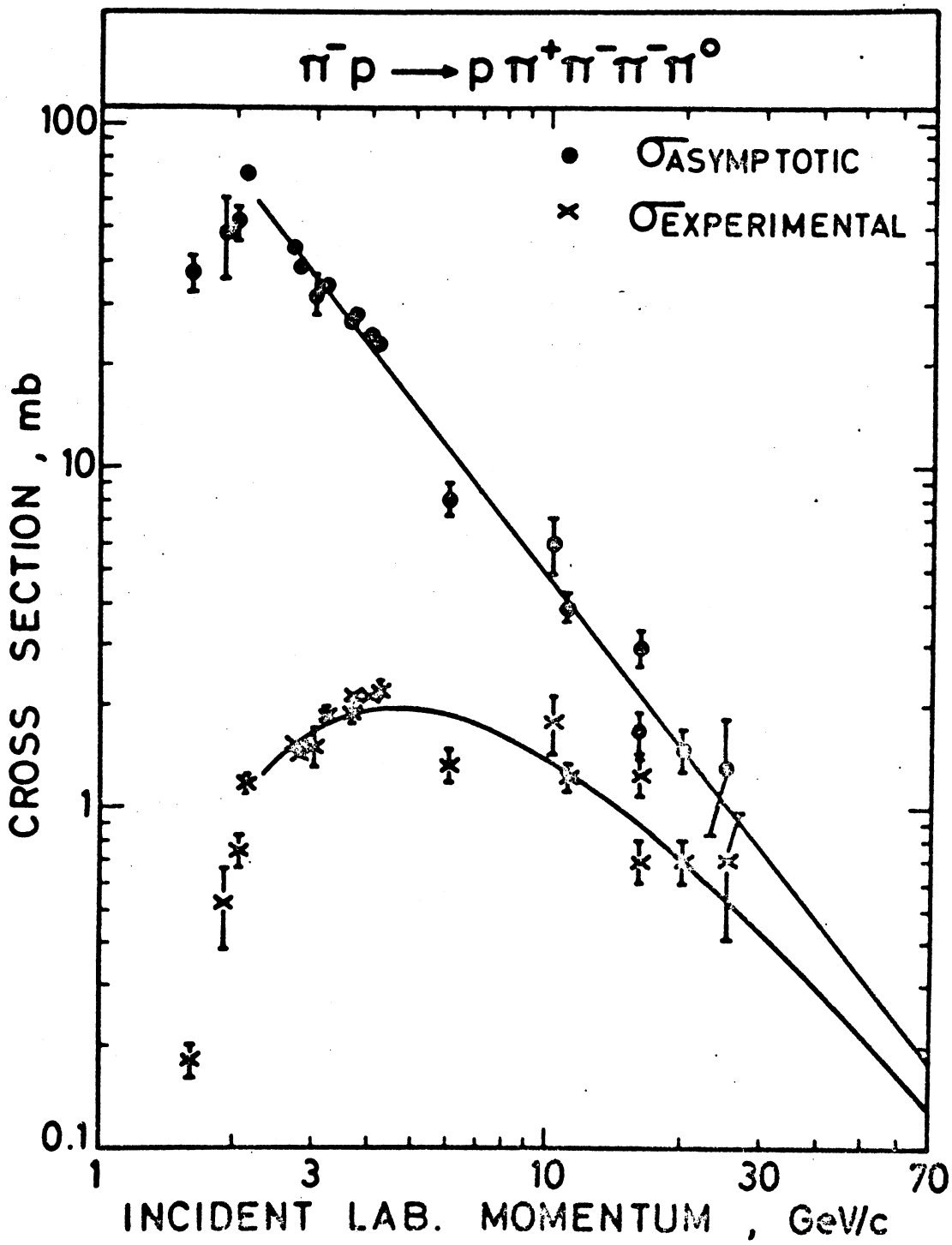
$\pi^- p \longrightarrow p\pi^+\pi^-\pi^-\pi^0$
$\sigma_{ASYMPTOTIC}$
$\sigma_{EXPERIMENTAL}$
CROSS SECTION , mb
100
10
1
0.1
1
3
10
30
70
INCIDENT LAB. MOMENTUM , GeV/c

- Figure 13 -

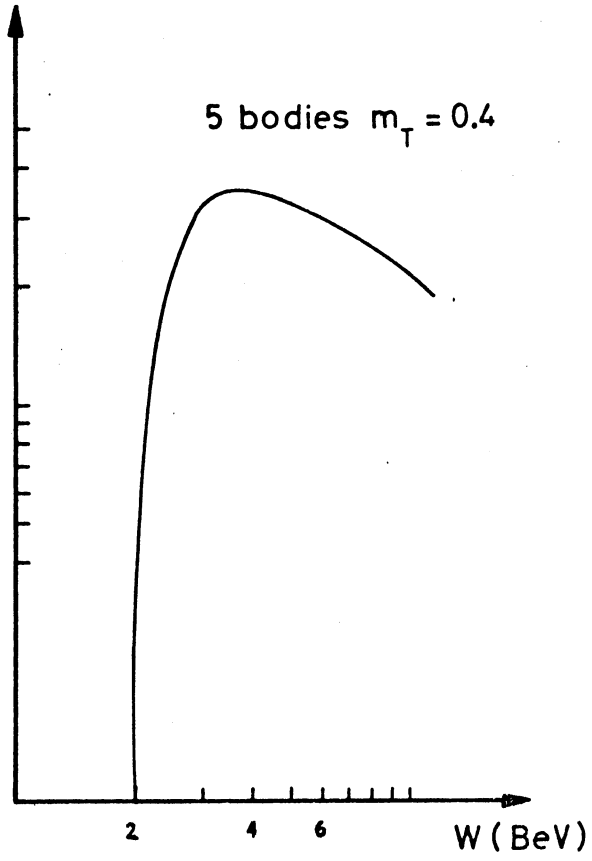

- Figure 14 -

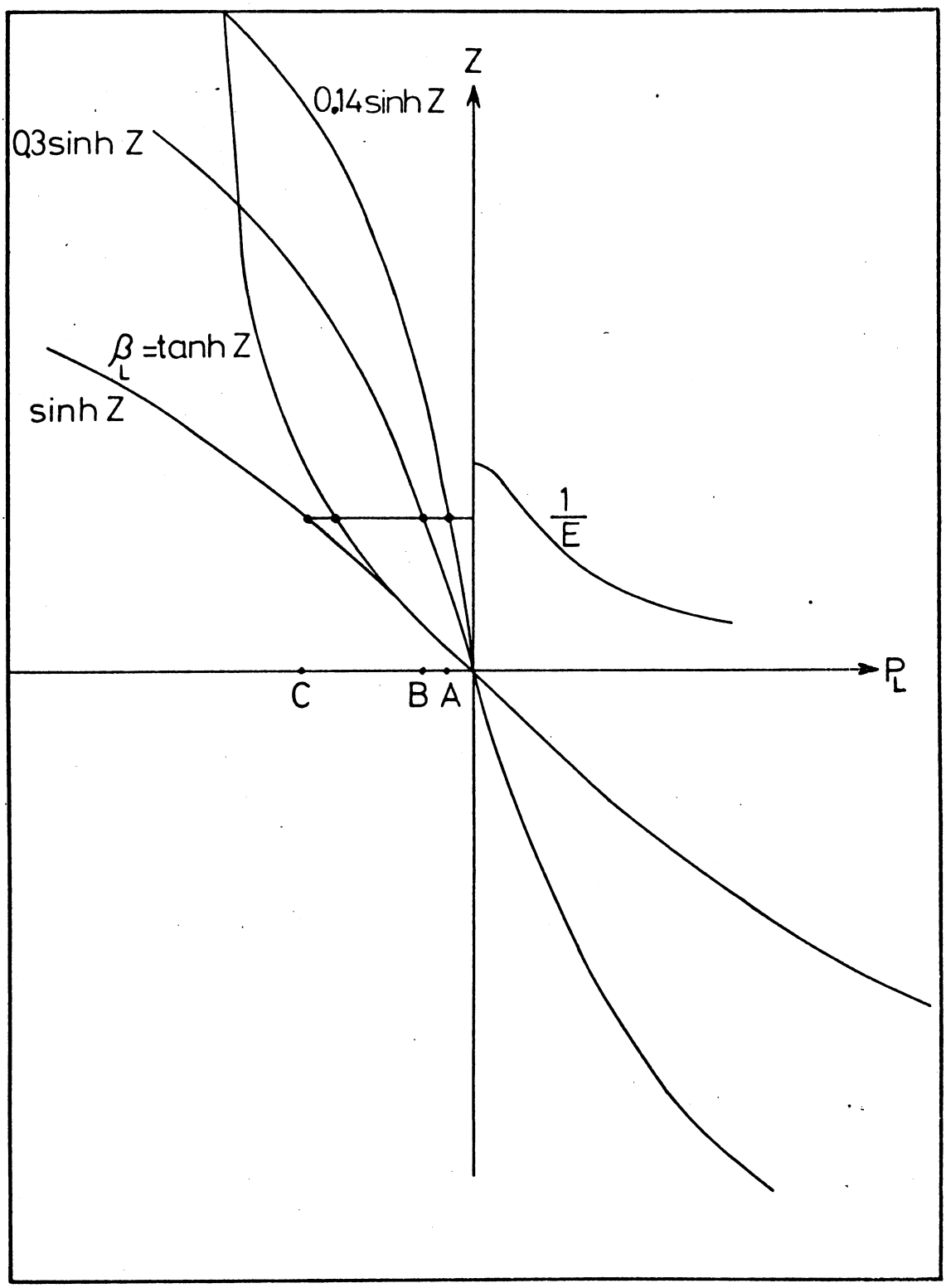

- Figure 15 -

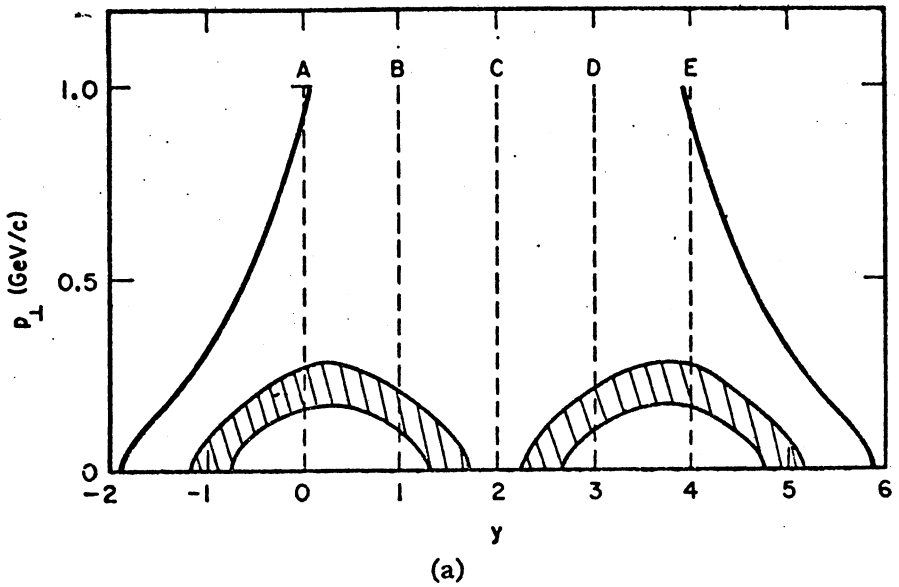

(a)

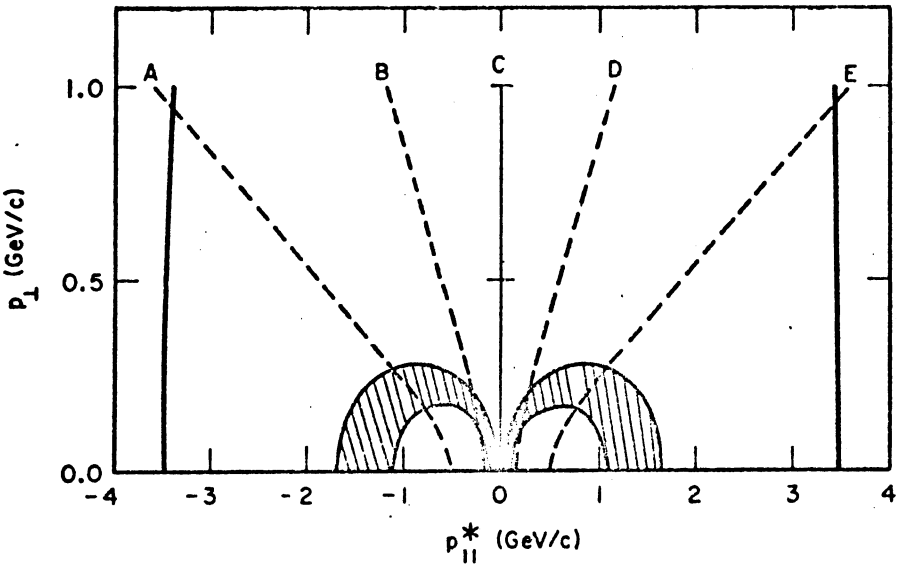

(b)

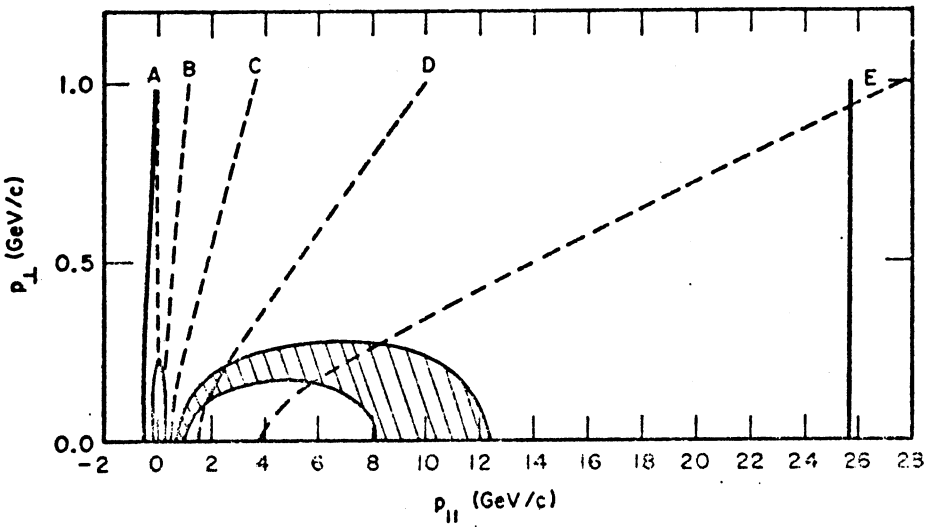

(c)

- Figure 16 -

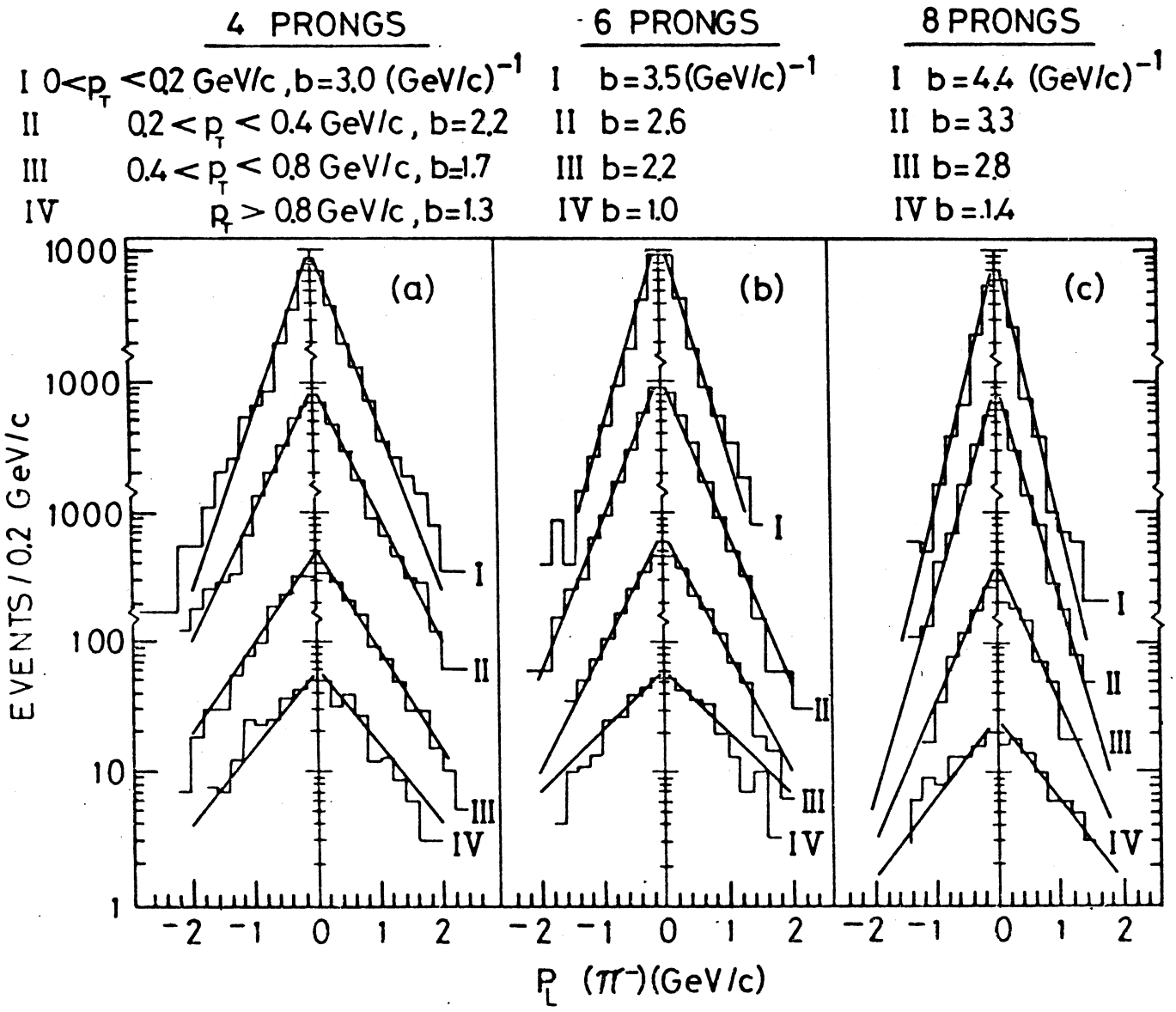
4 PRONGS
6 PRONGS
8 PRONGS
I 0<p_T<0.2 GeV/c, b=3.0 (GeV/c)^-1
II 0.2<p_T<0.4 GeV/c, b=2.2
III 0.4<p_T<0.8 GeV/c, b=1.7
IV p_T>0.8 GeV/c, b=1.3
I b=3.5 (GeV/c)^-1
II b=2.6
III b=2.2
IV b=1.0
I b=4.4 (GeV/c)^-1
II b=3.3
III b=2.8
IV b=1.4
(a)
(b)
(c)
EVENTS / 0.2 GeV/c
1000
1000
1000
100
10
1
I
II
III
IV
-2 -1 0 1 2
P_L (π⁻) (GeV/c)

- Figure 17 -

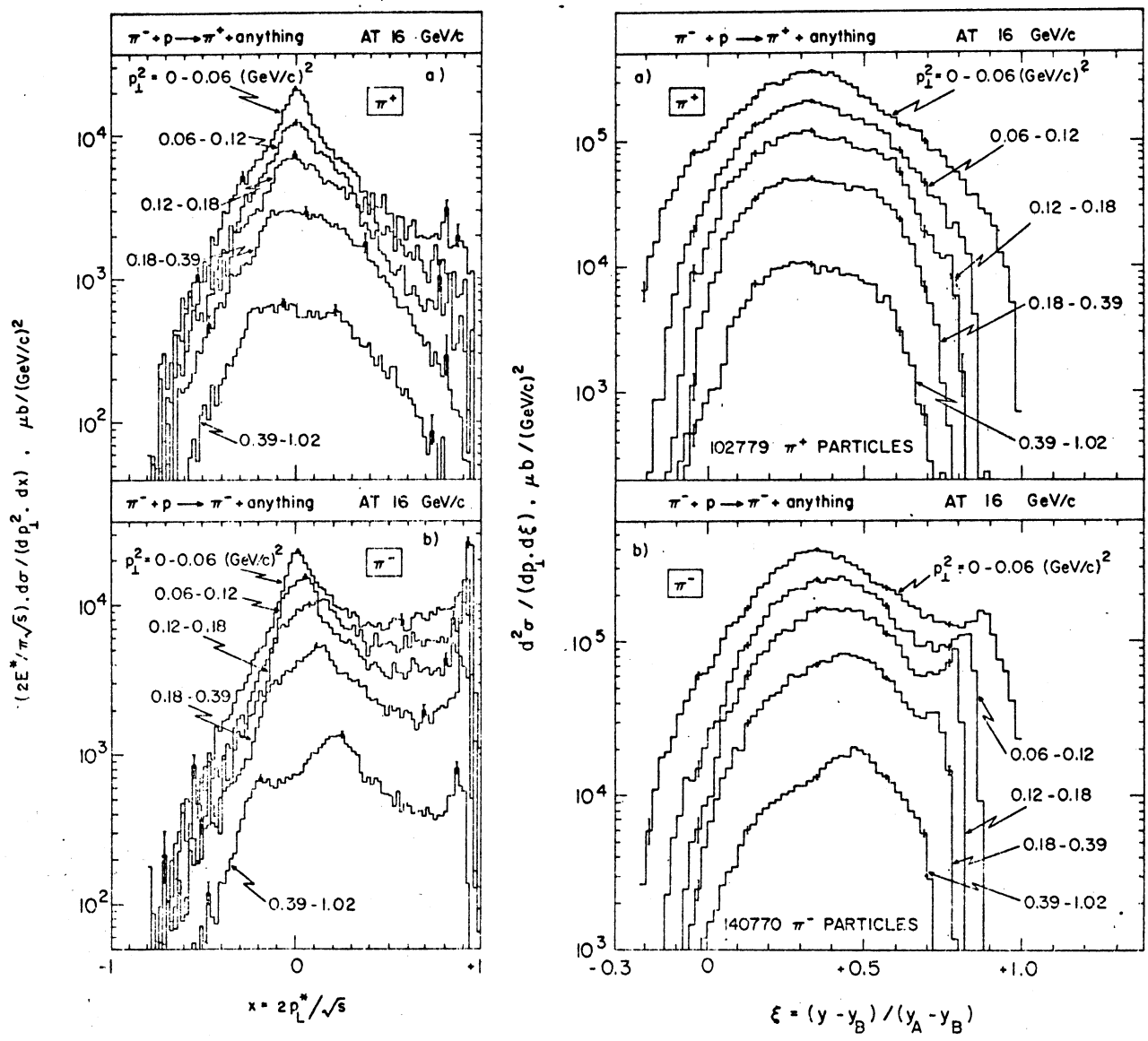
π⁻ + p → π⁺ + anything AT 16 GeV/c
a)
π⁺
p²⊥ = 0 - 0.06 (GeV/c)²
0.06 - 0.12
0.12 - 0.18
0.18 - 0.39
0.39 - 1.02
102779 π⁺ PARTICLES
π⁻ + p → π⁻ + anything AT 16 GeV/c
b)
π⁻
p²⊥ = 0 - 0.06 (GeV/c)²
0.06 - 0.12
0.12 - 0.18
0.18 - 0.39
0.39 - 1.02
140770 π⁻ PARTICLES
(2E*/π√s) . dσ/(dp²⊥ . dx) . μb/(GeV/c)²
x = 2p*L/√s
d²σ/(dp⊥ . dξ) . μb/(GeV/c)²
ξ = (y - yB)/(yA - yB)

- Figure 18 -

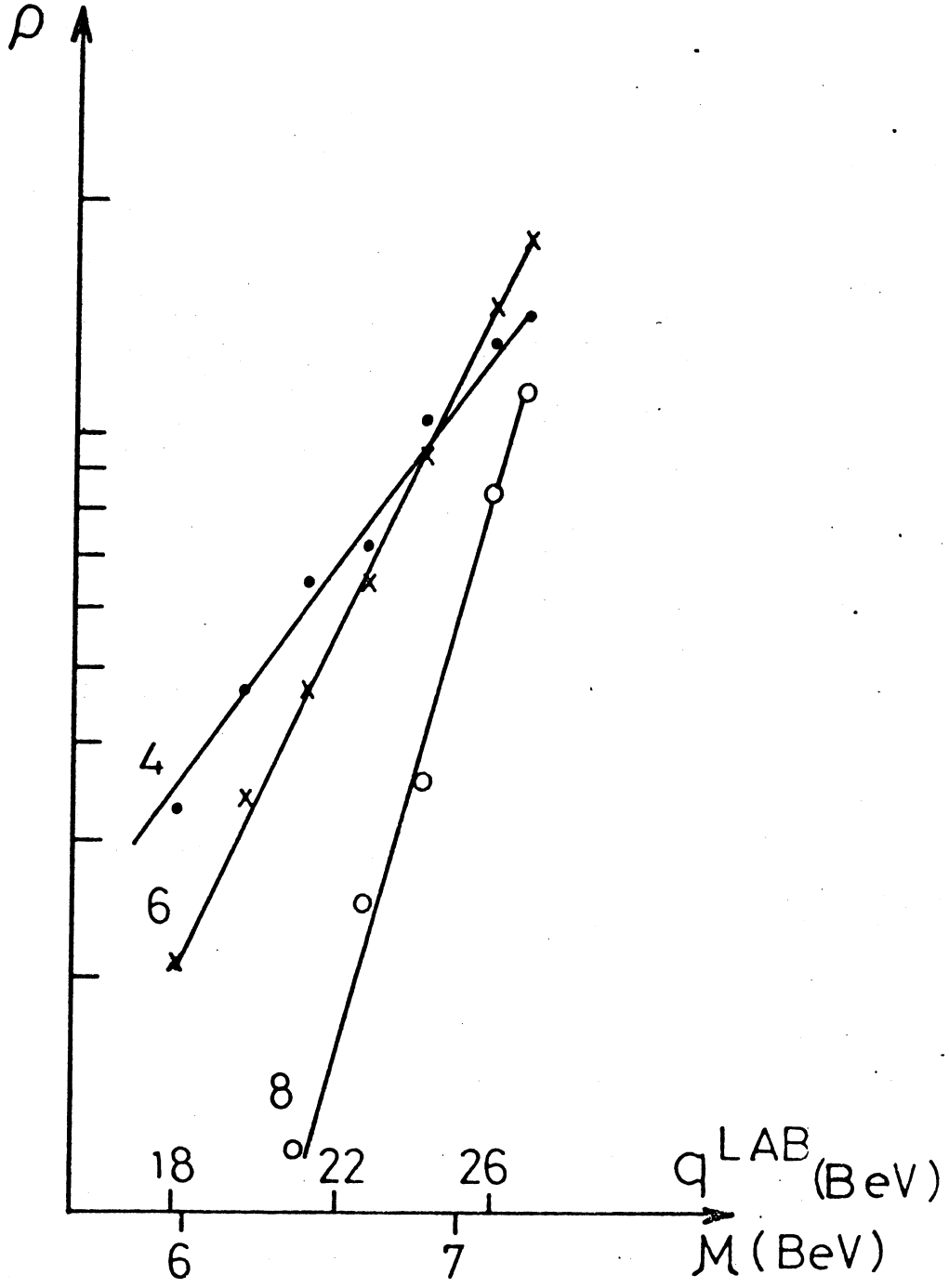

- Figure 19 -

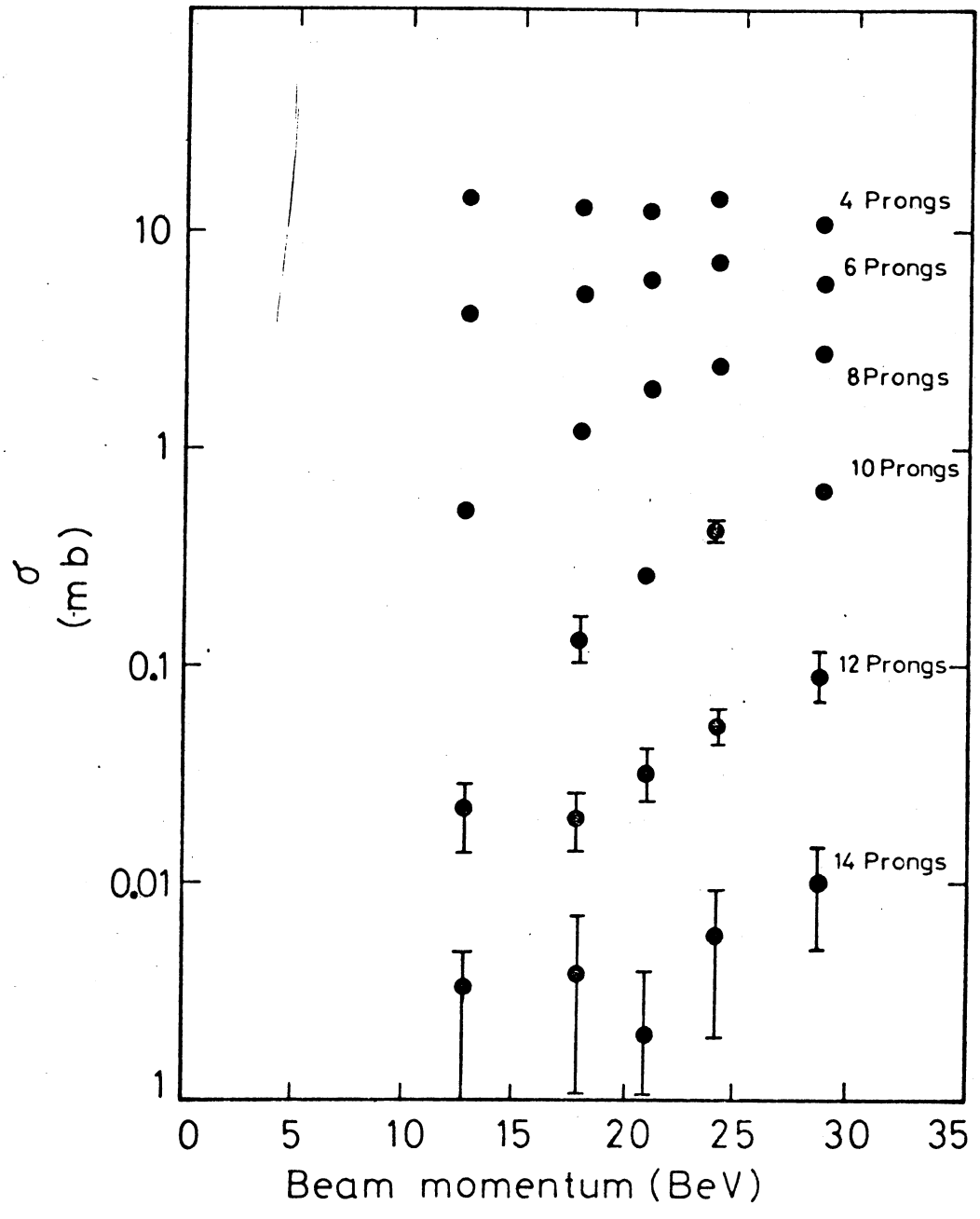
4 Prongs
6 Prongs
8 Prongs
10 Prongs
12 Prongs
14 Prongs
10
1
0.1
0.01
1
σ
(mb)
0
5
10
15
20
25
30
35
Beam momentum (BeV)

- Figure 20 -

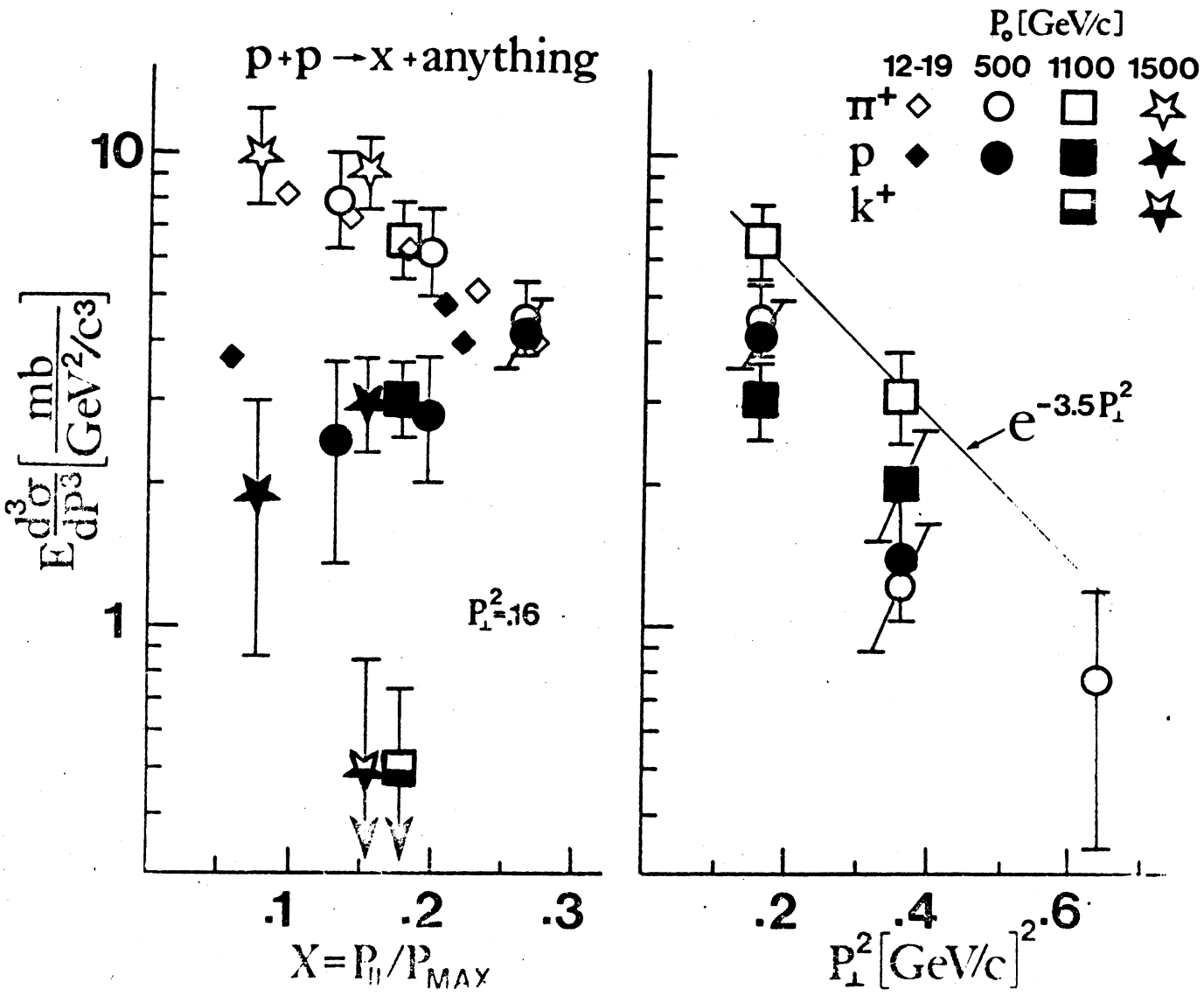
p+p → x + anything
$E\frac{d^3\sigma}{dP^3}\left[\frac{mb}{GeV^2/c^3}\right]$
10
1
$P_\perp^2$=.16
.1
.2
.3
$X = P_\parallel / P_{MAX}$
P_o [GeV/c]
12-19
500
1100
1500
π^+
p
k^+
$e^{-3.5P_\perp^2}$
.2
.4
.6
$P_\perp^2$ [GeV/c]^2

- Figure 21 -

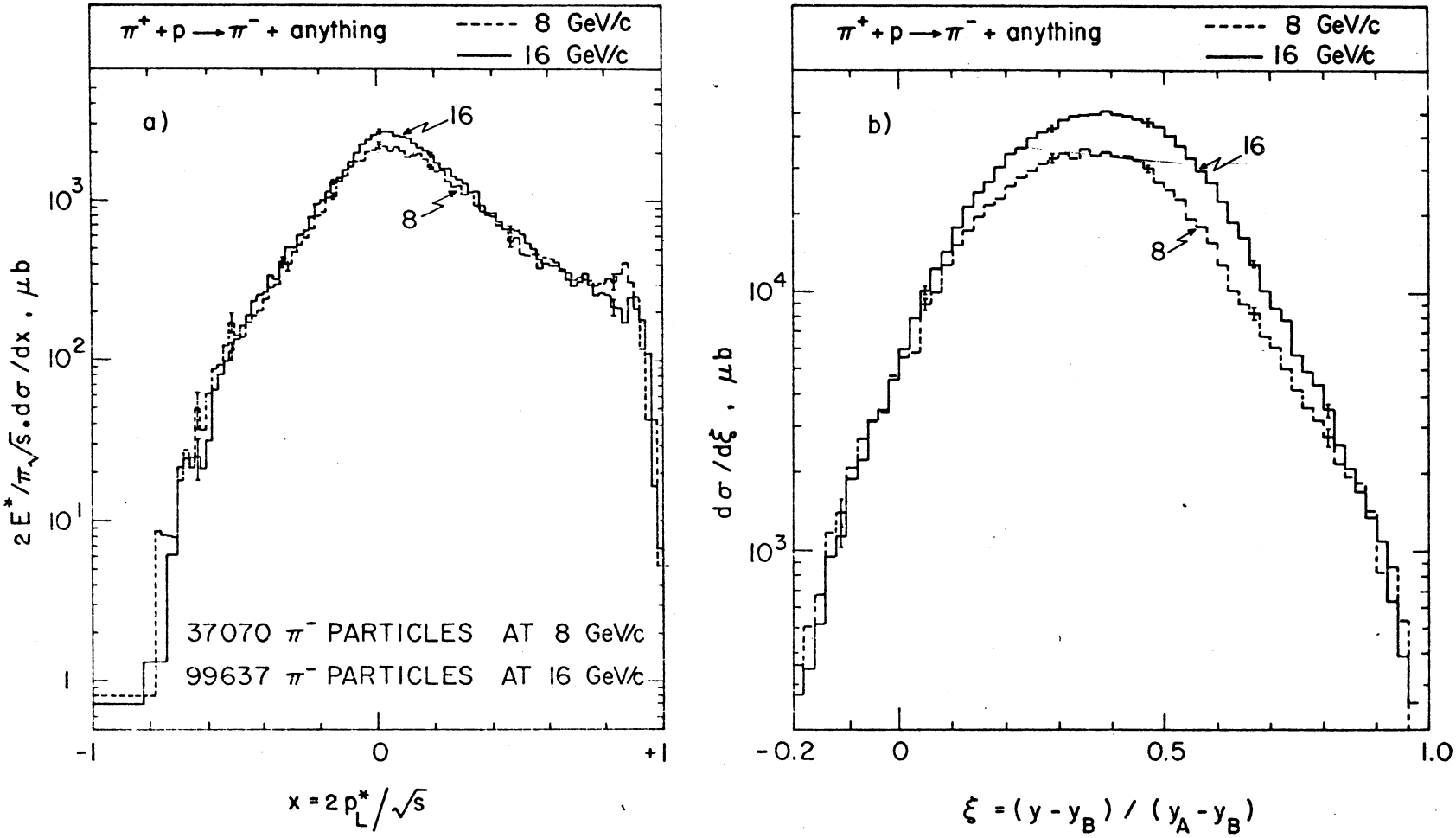
$\pi^+ + p \rightarrow \pi^- +$ anything
8 GeV/c
16 GeV/c
a)
16
8
10^3
10^2
10^1
1
37070 π^- PARTICLES AT 8 GeV/c
99637 π^- PARTICLES AT 16 GeV/c
-1
0
+1
$2E^*/\pi\sqrt{s} \cdot d\sigma/dx$, μb
$x = 2p_L^*/\sqrt{s}$
b)
10^4
10^3
-0.2
0
0.5
1.0
$d\sigma/d\xi$, μb
$\xi = (y - y_B) / (y_A - y_B)$

- Figure 22 -

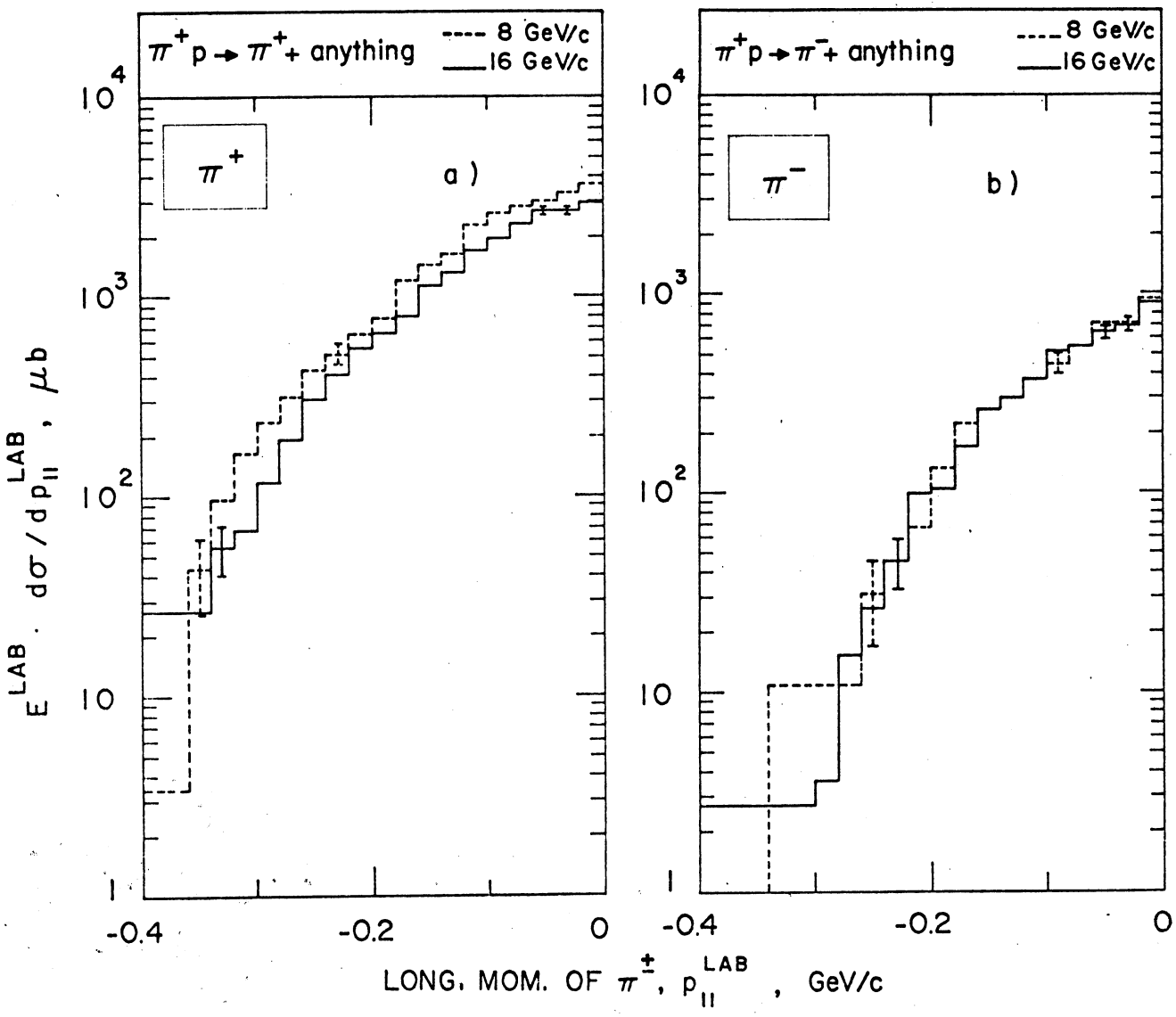
$\pi^+ p \to \pi^+ +$ anything
---- 8 GeV/c
—— 16 GeV/c
π^+
a)
$\pi^+ p \to \pi^- +$ anything
---- 8 GeV/c
—— 16 GeV/c
π^-
b)
$E^{LAB} \cdot d\sigma / d p_{\parallel}^{LAB}$, μb
10^4
10^3
10^2
10
1
-0.4
-0.2
0
LONG. MOM. OF $\pi^{\pm}$, $p_{\parallel}^{LAB}$, GeV/c

- Figure 23 -

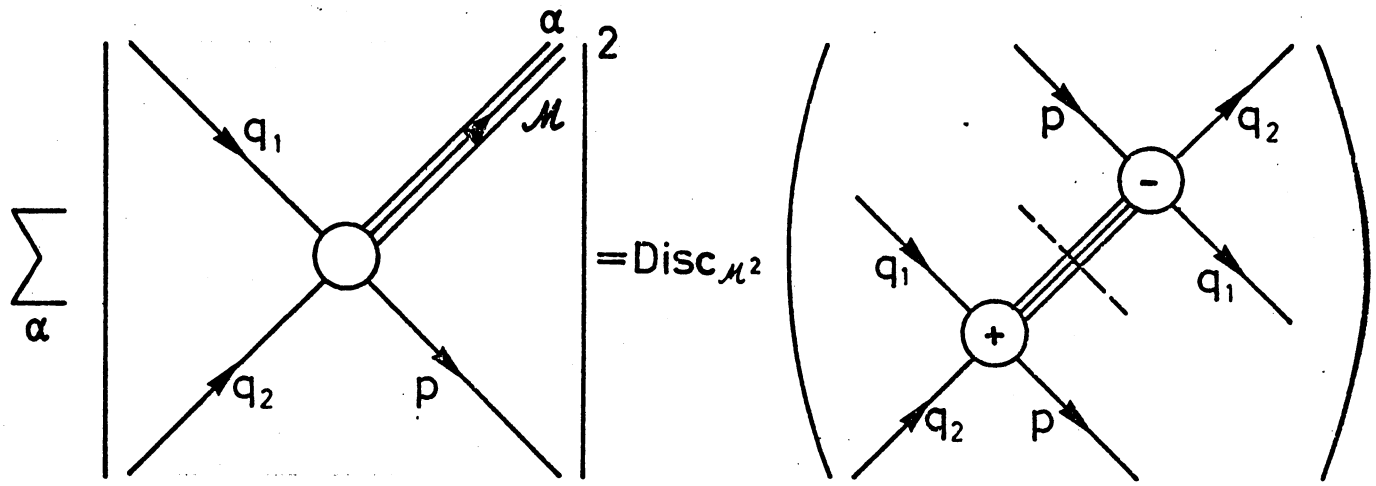

- Figure 24 -

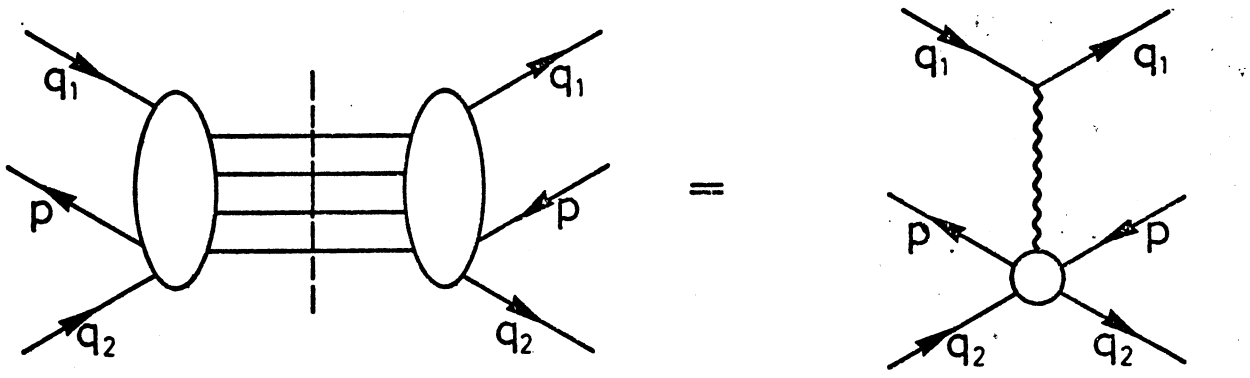

- Figure 25 -

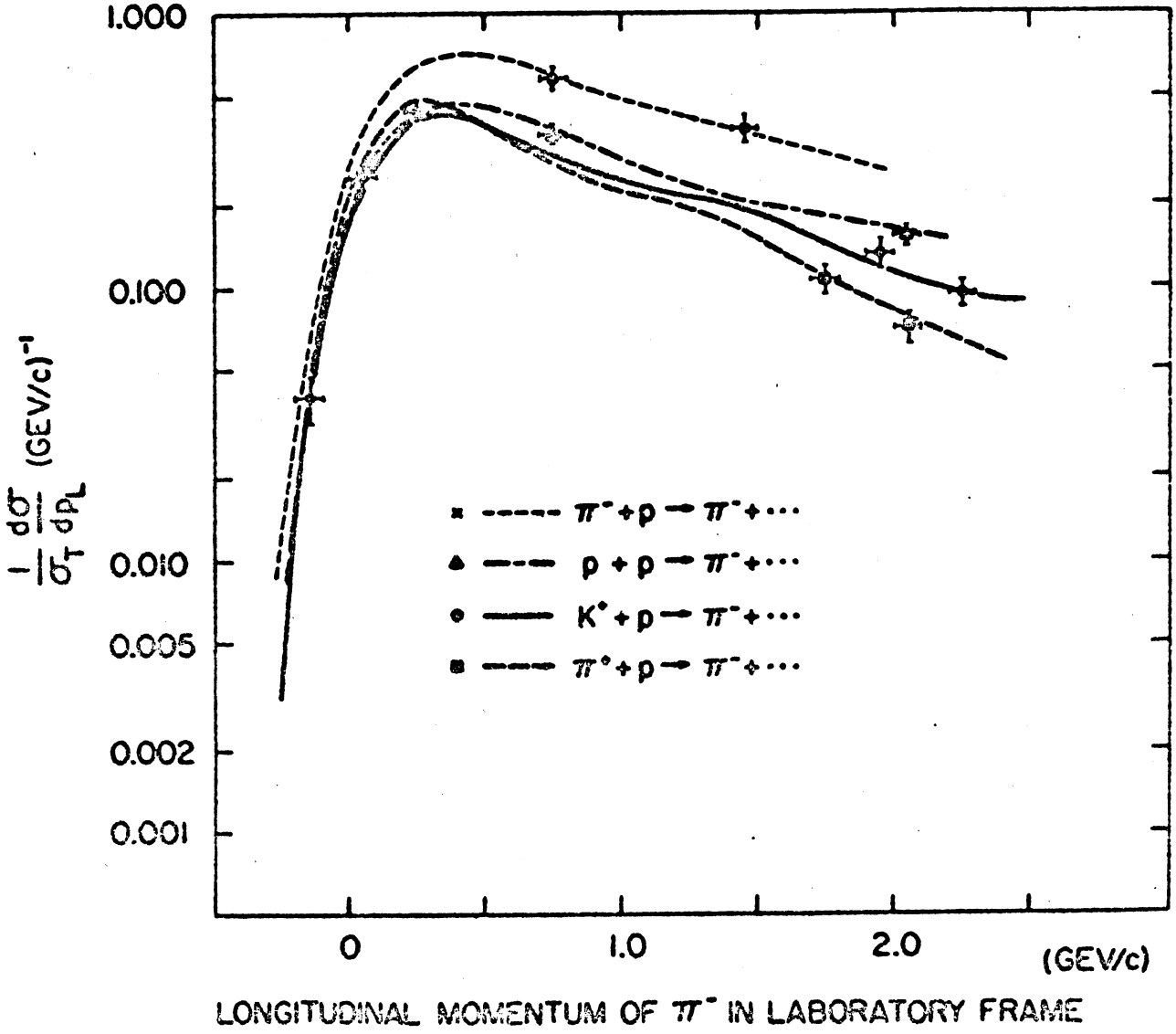
1.000
0.100
0.010
0.005
0.002
0.001
$\frac{1}{\sigma_T}\frac{d\sigma}{dp_L}$ (GEV/c)$^{-1}$
$\pi^- + p \rightarrow \pi^- + \cdots$
$p + p \rightarrow \pi^- + \cdots$
$K^\circ + p \rightarrow \pi^- + \cdots$
$\pi^\circ + p \rightarrow \pi^- + \cdots$
0
1.0
2.0
(GEV/c)
LONGITUDINAL MOMENTUM OF π^- IN LABORATORY FRAME

- Figure 26 -

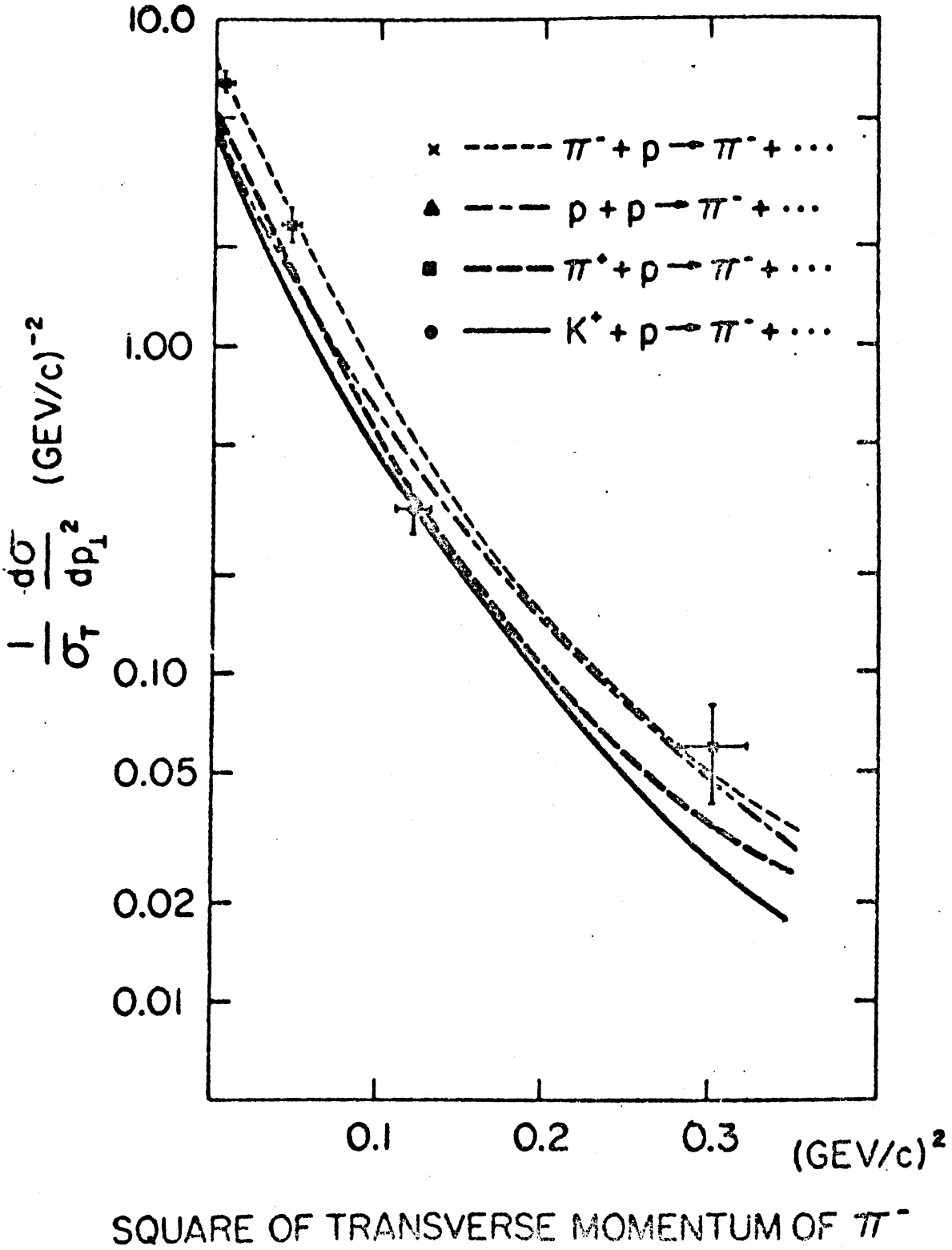
10.0
1.00
0.10
0.05
0.02
0.01
$\frac{1}{\sigma_T}\frac{d\sigma}{dp_1^2}$ (GEV/c)$^{-2}$
× ----- $\pi^- + p \rightarrow \pi^- + \cdots$
▲ — — $p + p \rightarrow \pi^- + \cdots$
■ — — $\pi^+ + p \rightarrow \pi^- + \cdots$
● —— $K^+ + p \rightarrow \pi^- + \cdots$
0.1
0.2
0.3
(GEV/c)^2
SQUARE OF TRANSVERSE MOMENTUM OF π^-

- Figure 27 -

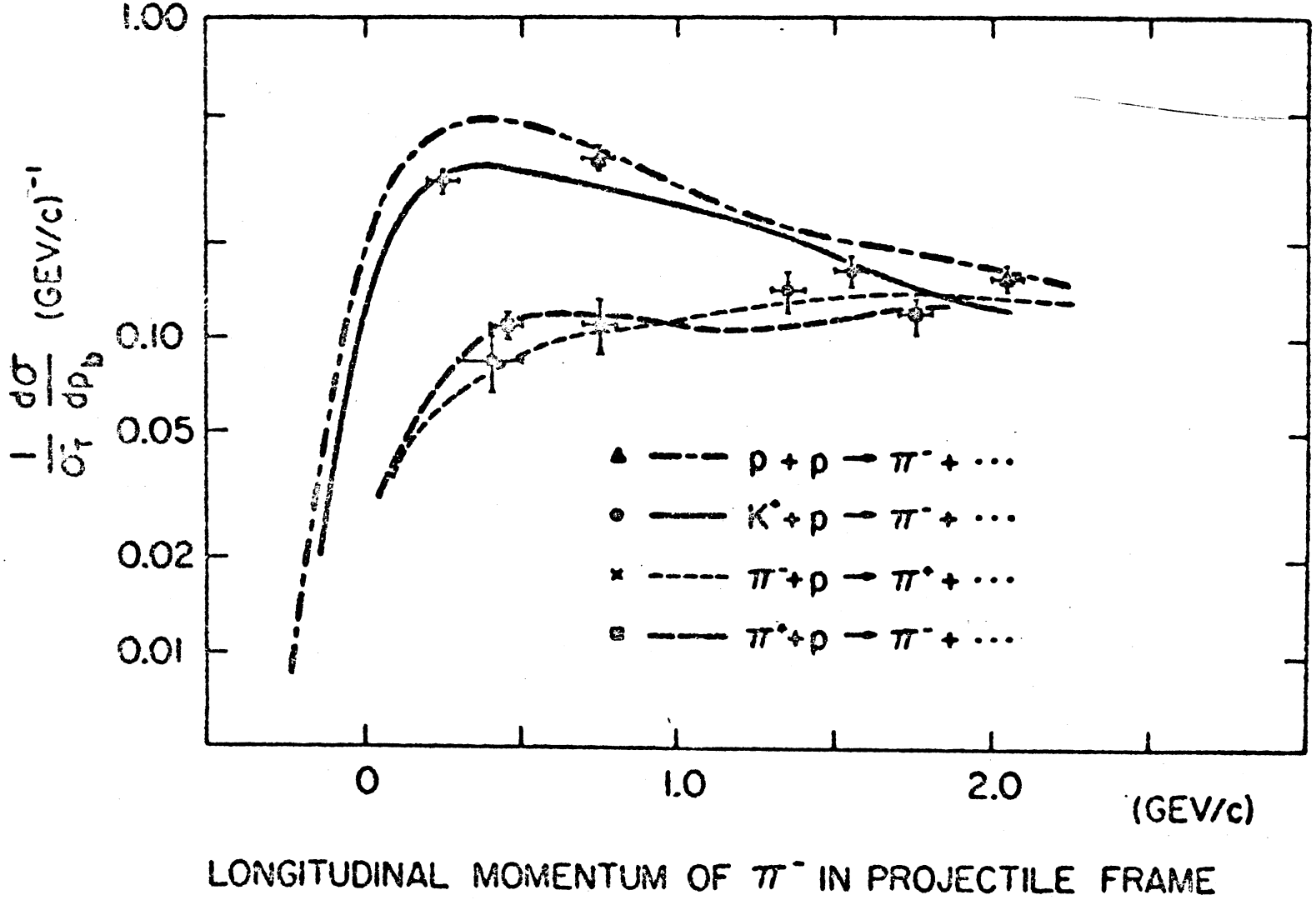
1.00
0.10
0.05
0.02
0.01
$\frac{1}{\sigma_T}\frac{d\sigma}{dp_b}$ (GEV/c)$^{-1}$
p + p → π⁻ + ···
K⁺ + p → π⁻ + ···
π⁻ + p → π⁺ + ···
π⁺ + p → π⁻ + ···
0
1.0
2.0
(GEV/c)
LONGITUDINAL MOMENTUM OF π⁻ IN PROJECTILE FRAME

- Figure 28 -

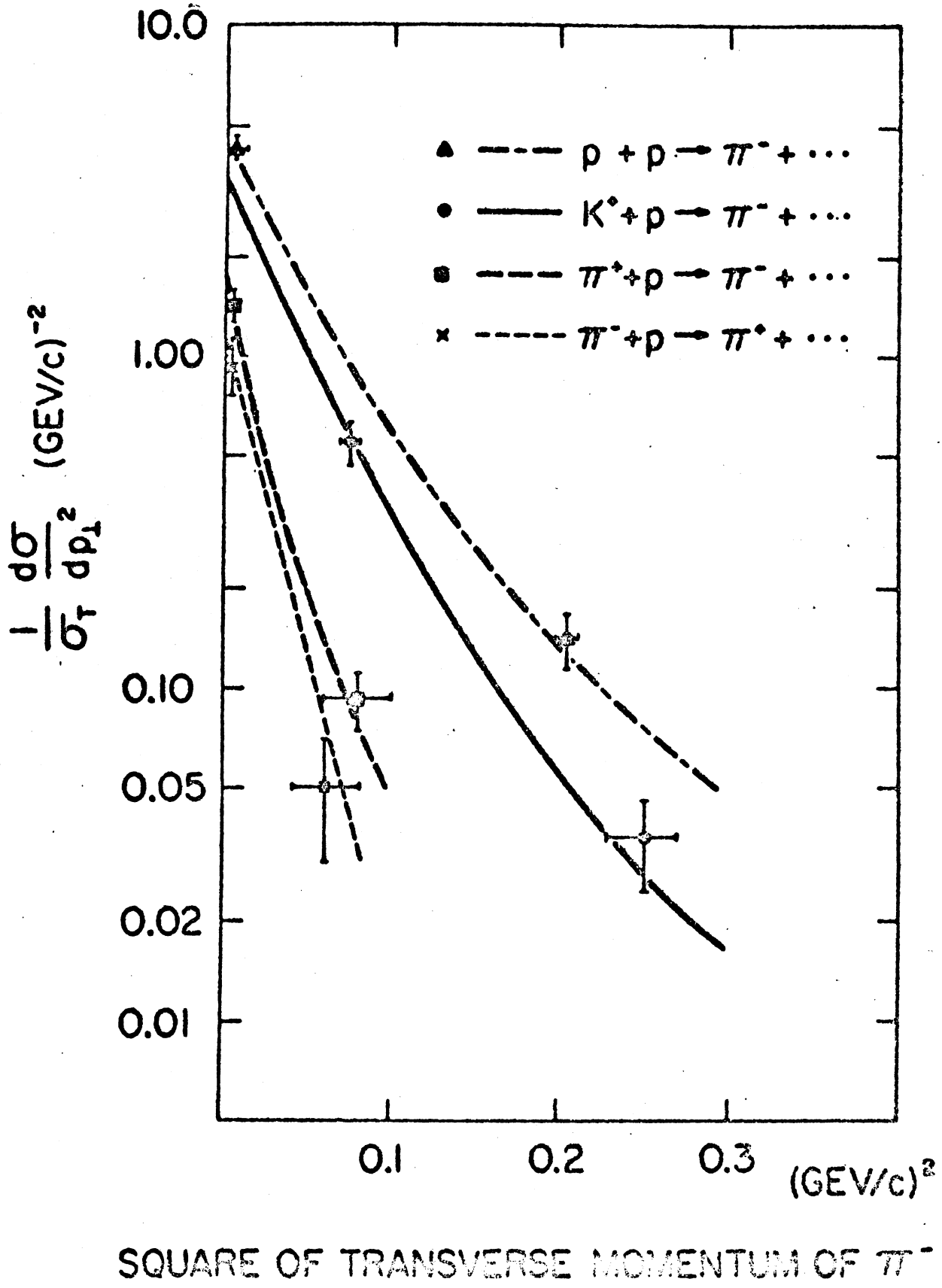
10.0
1.00
0.10
0.05
0.02
0.01
0.1
0.2
0.3
(GEV/c)²
(GEV/c)⁻²
1/σ_T dσ/dp_T²
p + p → π⁻ + ···
K⁰ + p → π⁻ + ···
π⁺ + p → π⁻ + ···
π⁻ + p → π⁰ + ···
SQUARE OF TRANSVERSE MOMENTUM OF π⁻

- Figure 20 -

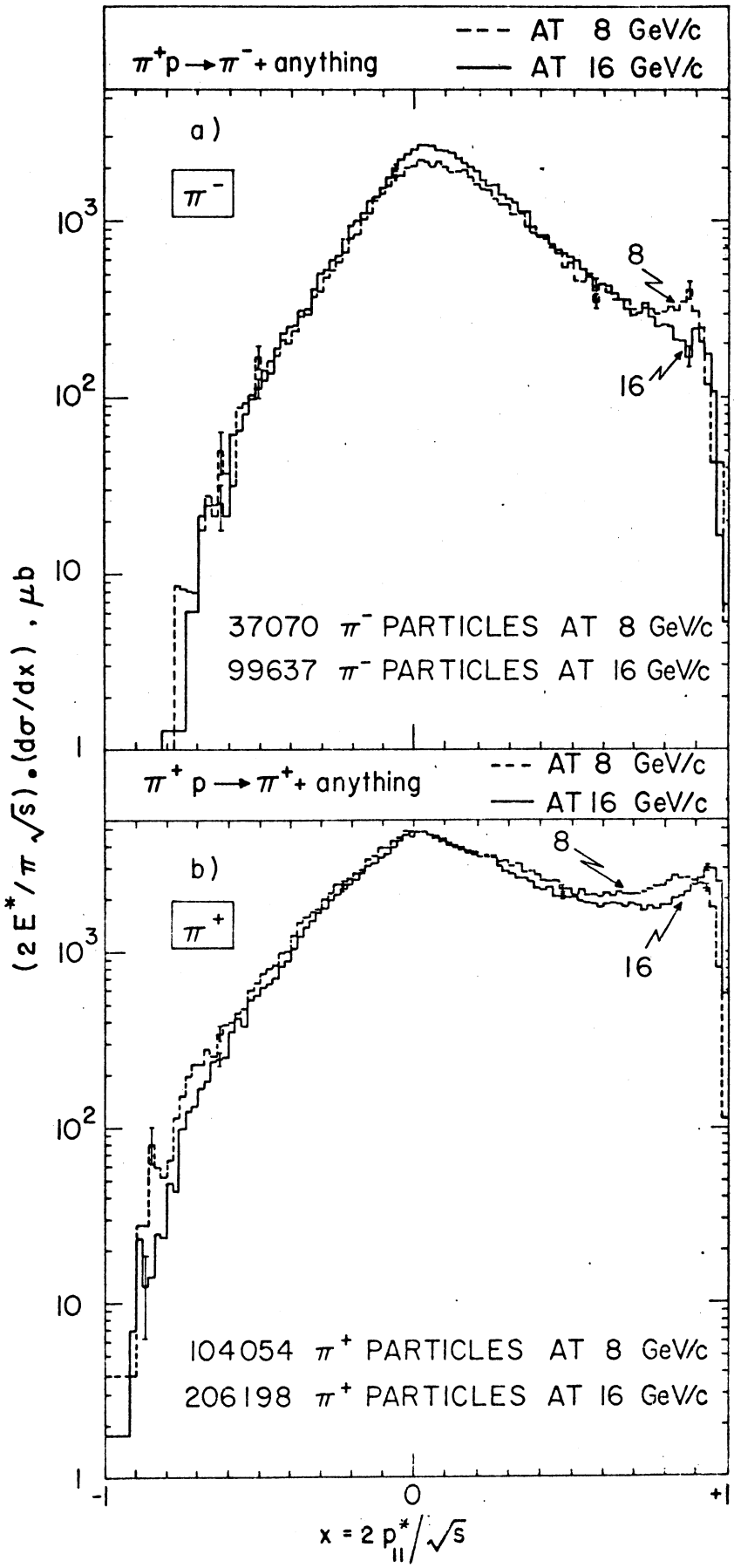
--- AT 8 GeV/c
—— AT 16 GeV/c
$\pi^+ p \to \pi^- +$ anything
a)
π^-
8
16
37070 π^- PARTICLES AT 8 GeV/c
99637 π^- PARTICLES AT 16 GeV/c
$\pi^+ p \to \pi^+ +$ anything
--- AT 8 GeV/c
—— AT 16 GeV/c
b)
π^+
8
16
104054 π^+ PARTICLES AT 8 GeV/c
206198 π^+ PARTICLES AT 16 GeV/c
$(2E^*/\pi\sqrt{s}) \cdot (d\sigma/dx)$. μb
10^3
10^2
10
1
-1
0
+1
$x = 2p^*_{11}/\sqrt{s}$

- Figure 30 -

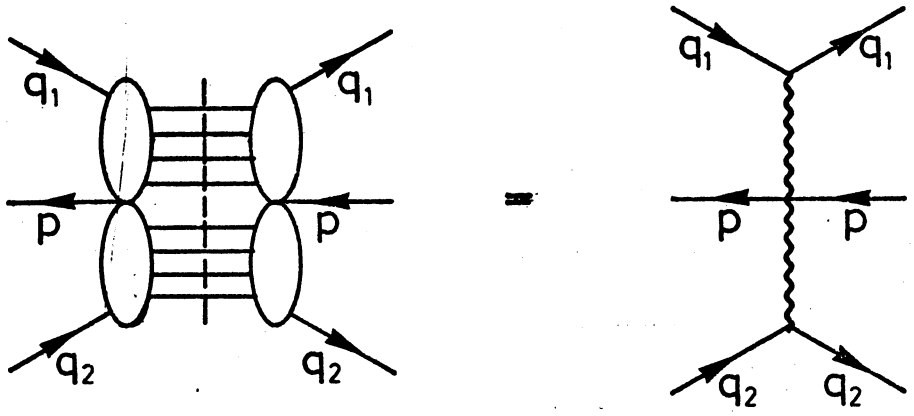

- Figure 31 -

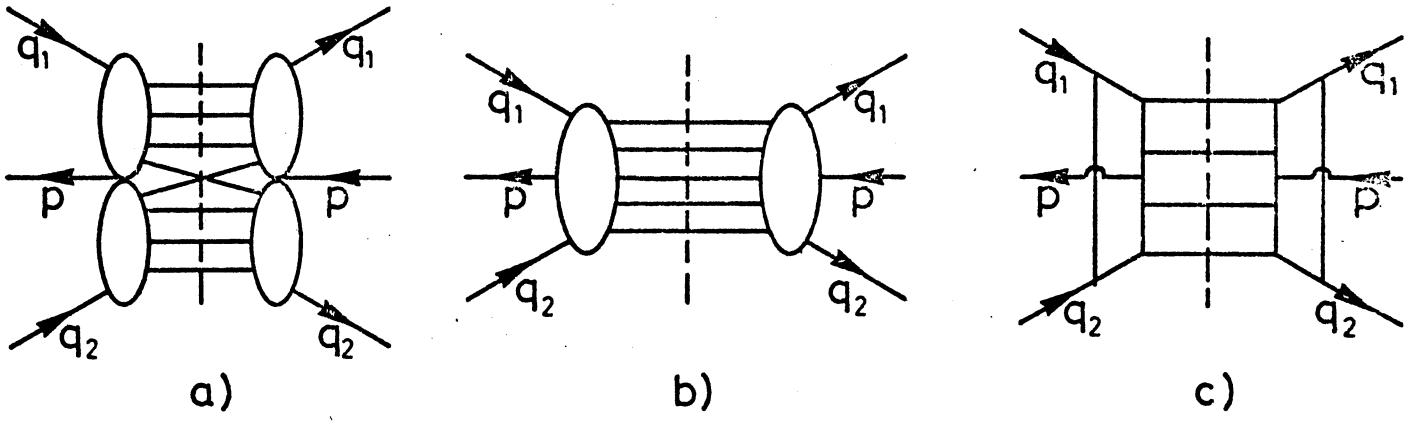

- Figure 32 -

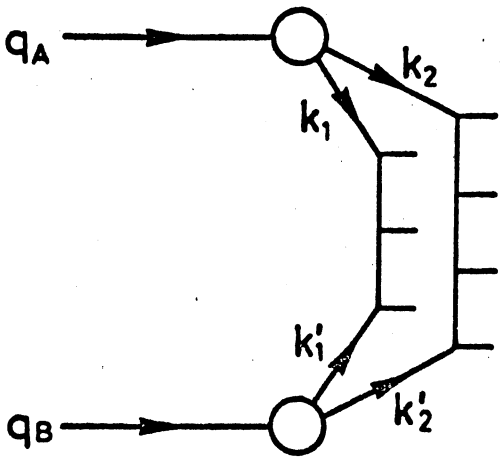

- Figure 33 a -

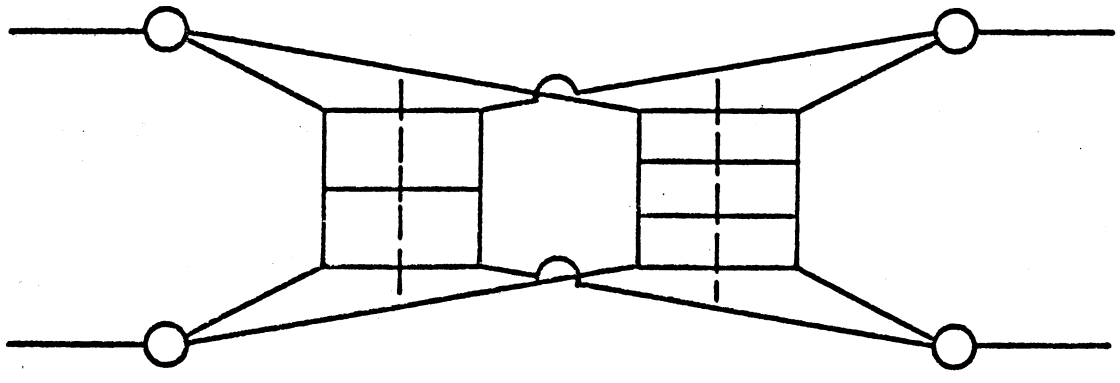

- Figure 33 b -

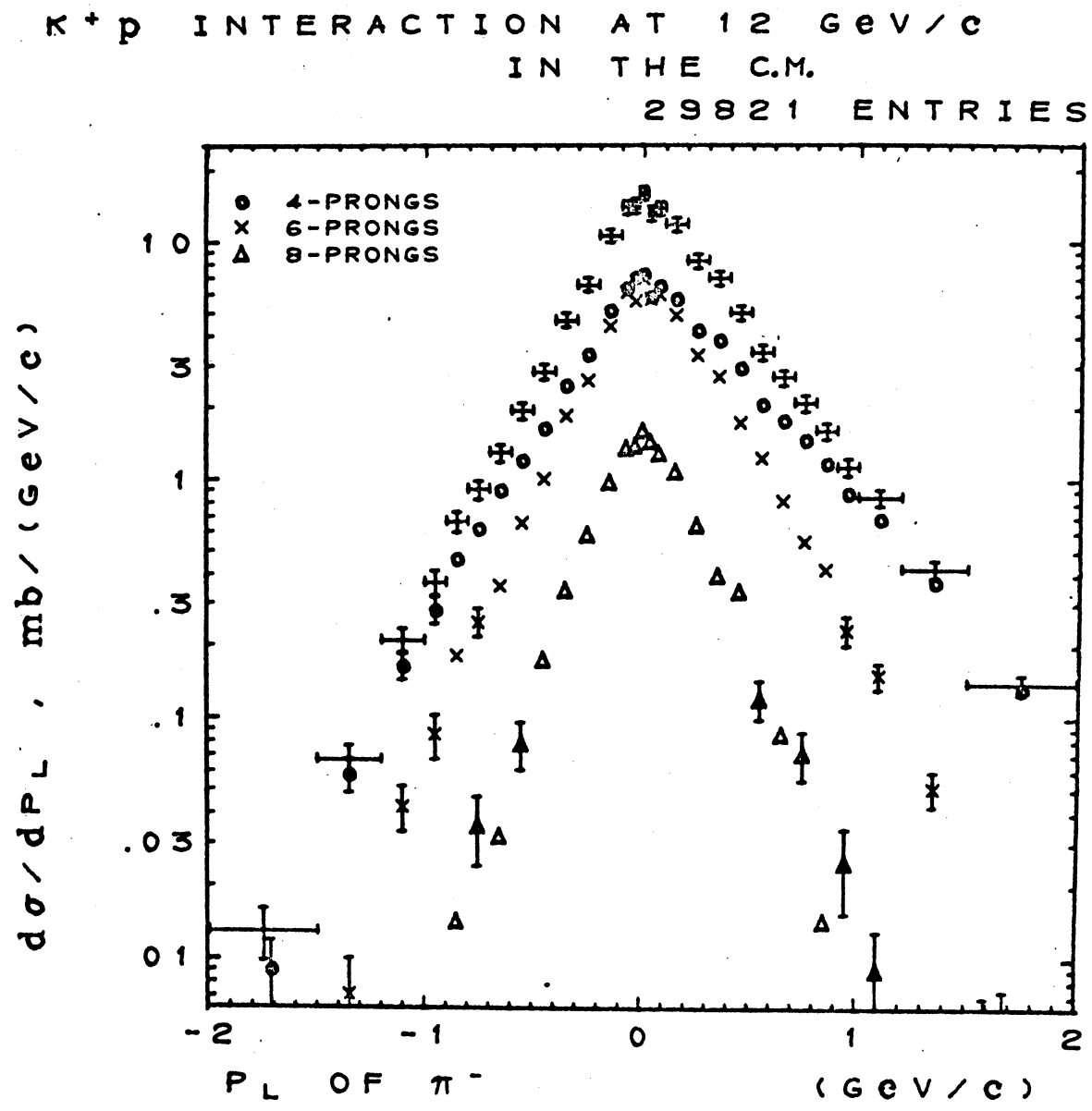
K⁺p INTERACTION AT 12 GeV/c
IN THE C.M.
29821 ENTRIES
4-PRONGS
6-PRONGS
8-PRONGS
dσ/dP_L , mb/(GeV/c)
10
3
1
.3
.1
.03
.01
-2
-1
0
1
2
P_L OF π⁻
(GeV/c)

- Figure 34 -

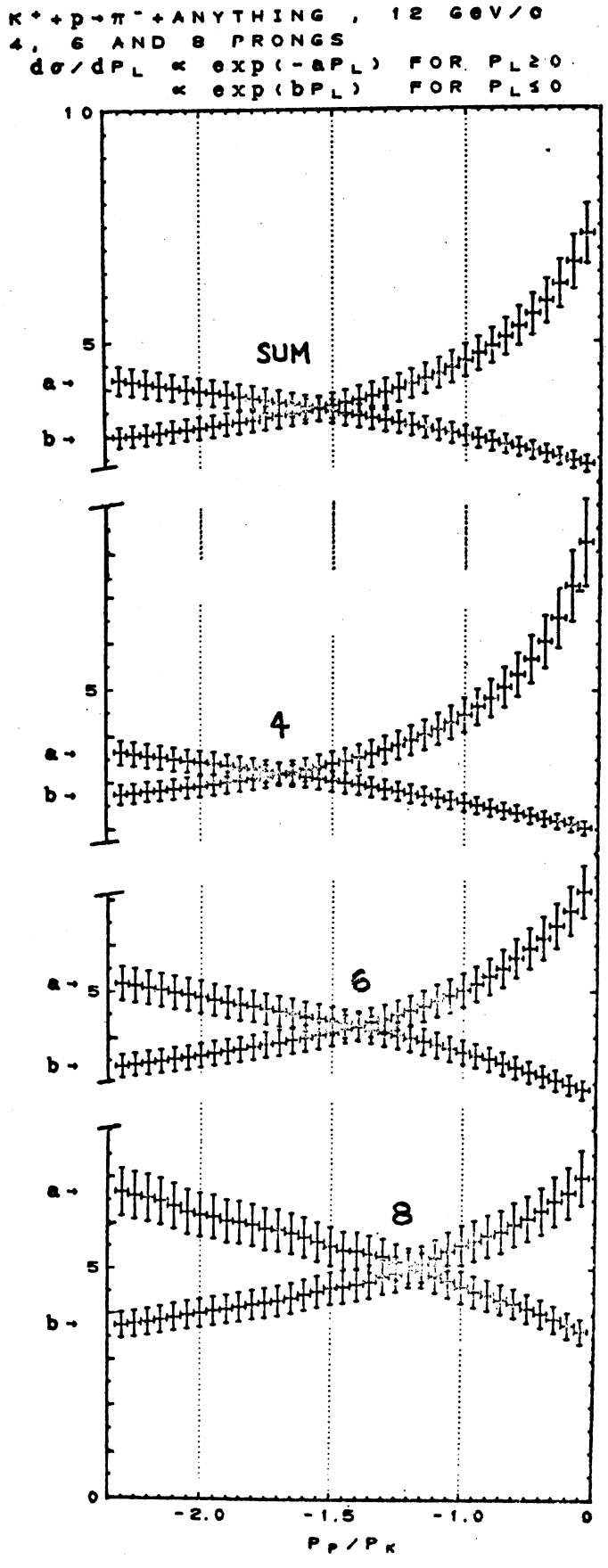
K⁺+p→π⁻+ANYTHING , 12 GeV/c
4, 6 AND 8 PRONGS
dσ/dP_L ∝ exp(-aP_L) FOR P_L≥0
∝ exp(bP_L) FOR P_L≤0
SUM
4
6
8
a→
b→
10
5
0
-2.0
-1.5
-1.0
0
P_P/P_K

- Figure 35 -

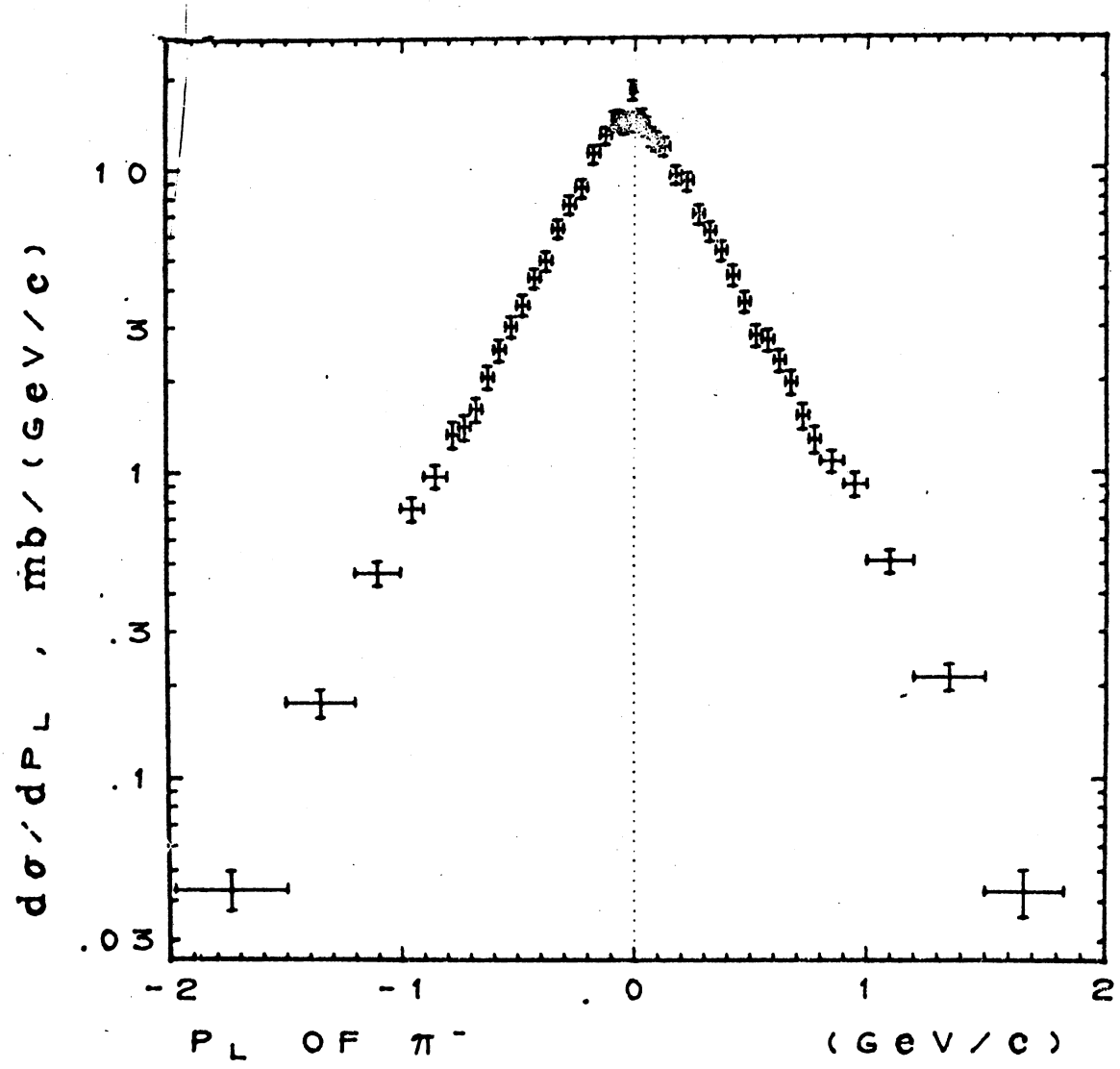

- Figure 36 -

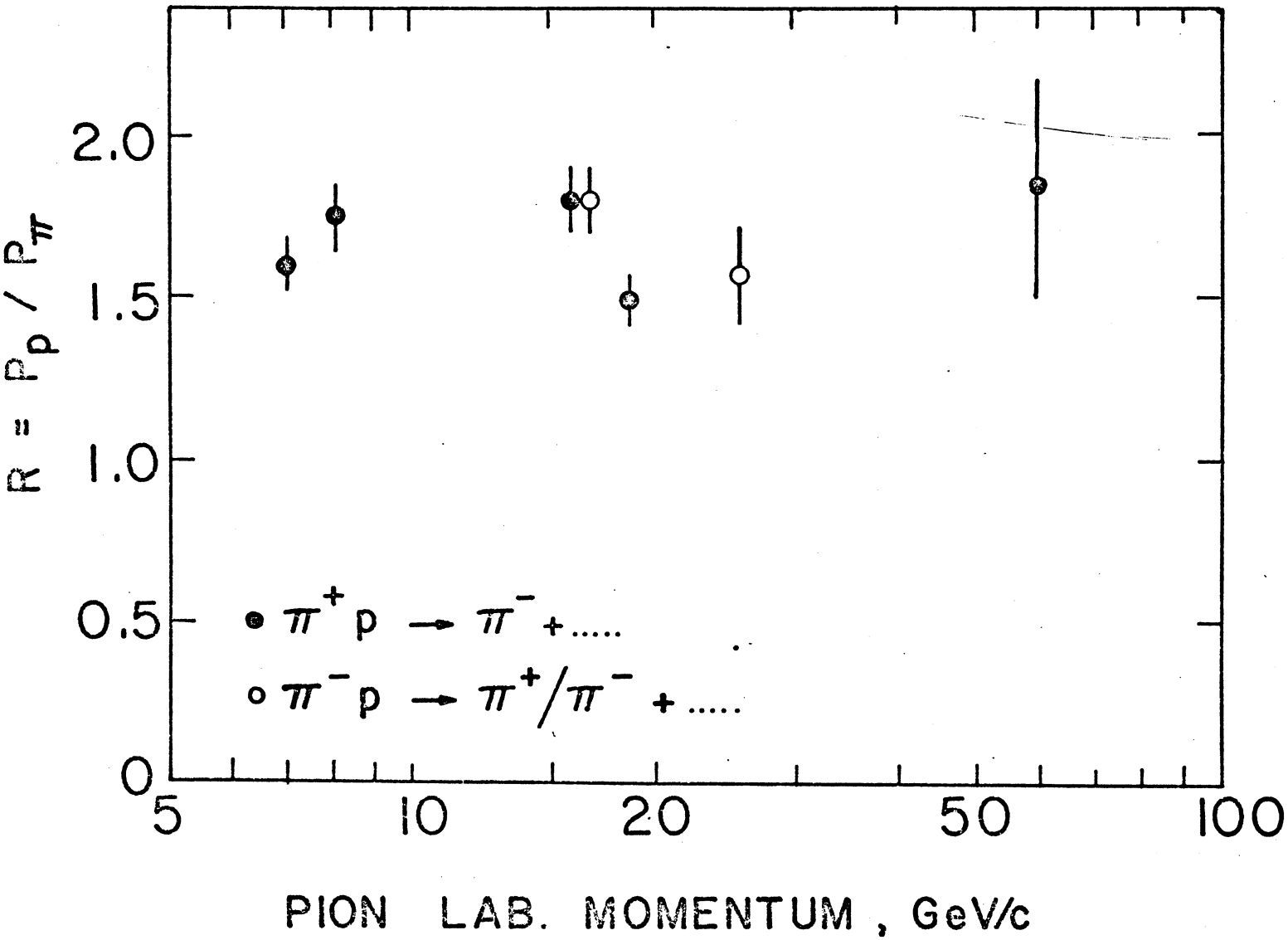
2.0
1.5
1.0
0.5
0
R = P_p / P_π
• $\pi^+ p \rightarrow \pi^- +$.....
○ $\pi^- p \rightarrow \pi^+/\pi^- +$.....
5
10
20
50
100
PION LAB. MOMENTUM , GeV/c

- Figure 37 a -

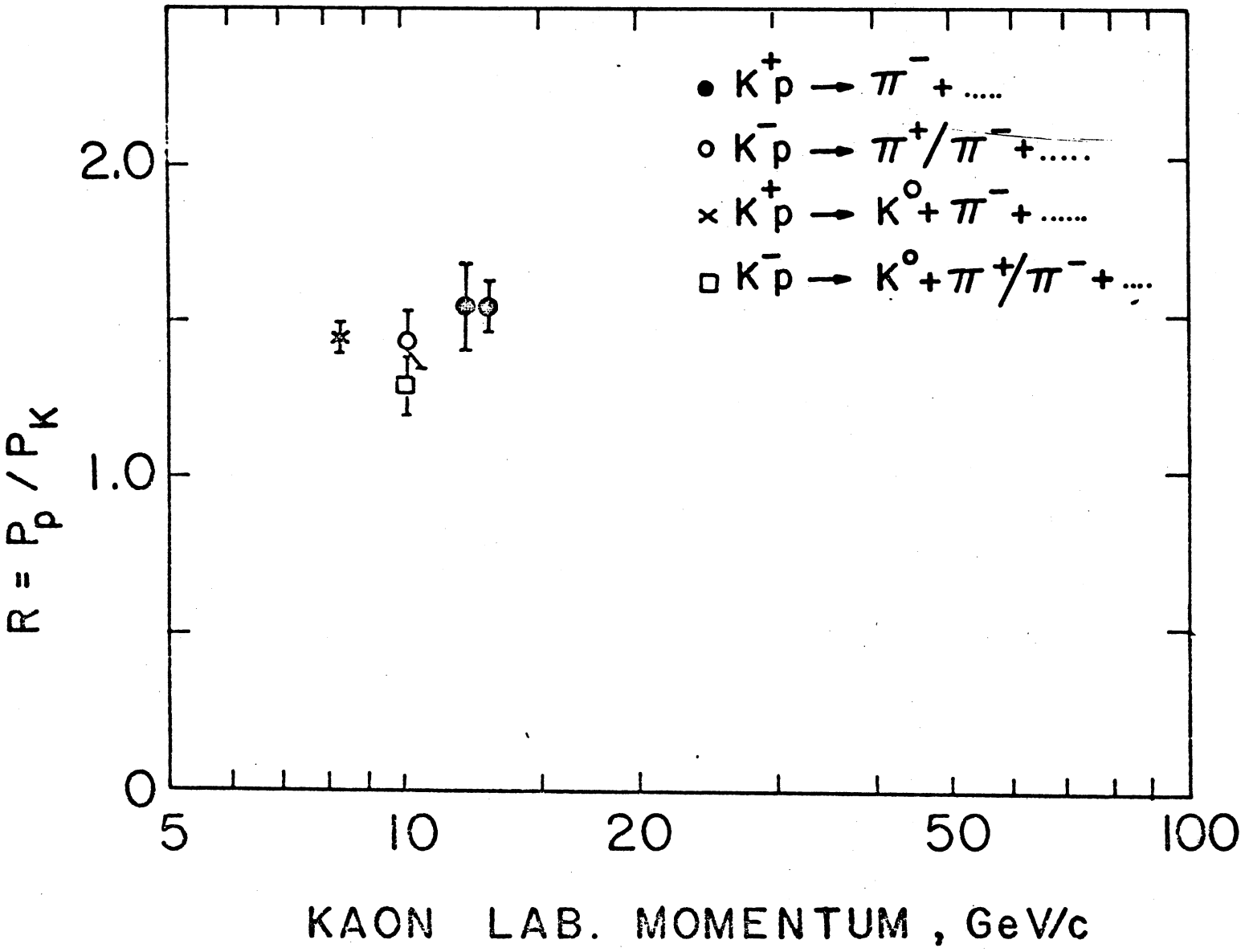
• $K^+p \rightarrow \pi^- + ...$
○ $K^-p \rightarrow \pi^+/\pi^- + ...$
× $K^+p \rightarrow K^o + \pi^- + ...$
□ $K^-p \rightarrow K^o + \pi^+/\pi^- + ...$
2.0
1.0
0
$R = P_p / P_K$
5
10
20
50
100
KAON LAB. MOMENTUM , GeV/c

- Figure 37 b -

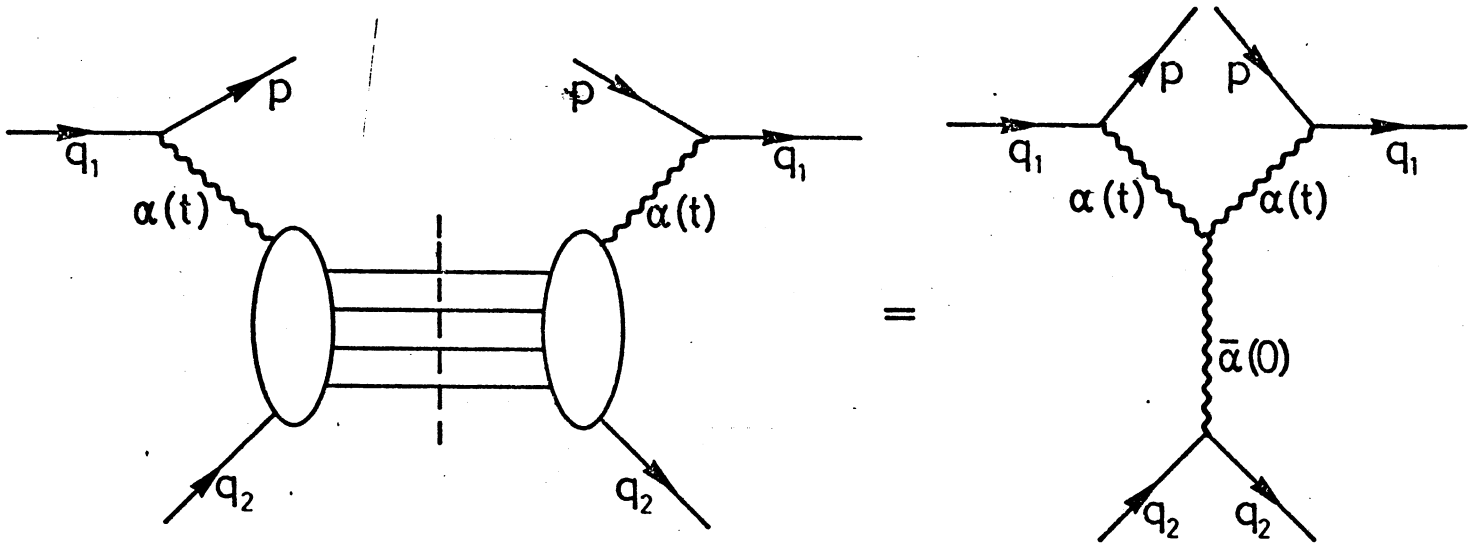
p
p
q_1
q_1
$\alpha(t)$
$\alpha(t)$
q_2
q_2
=
p
p
q_1
q_1
$\alpha(t)$
$\alpha(t)$
$\bar{\alpha}(0)$
q_2
q_2

- Figure 38 -

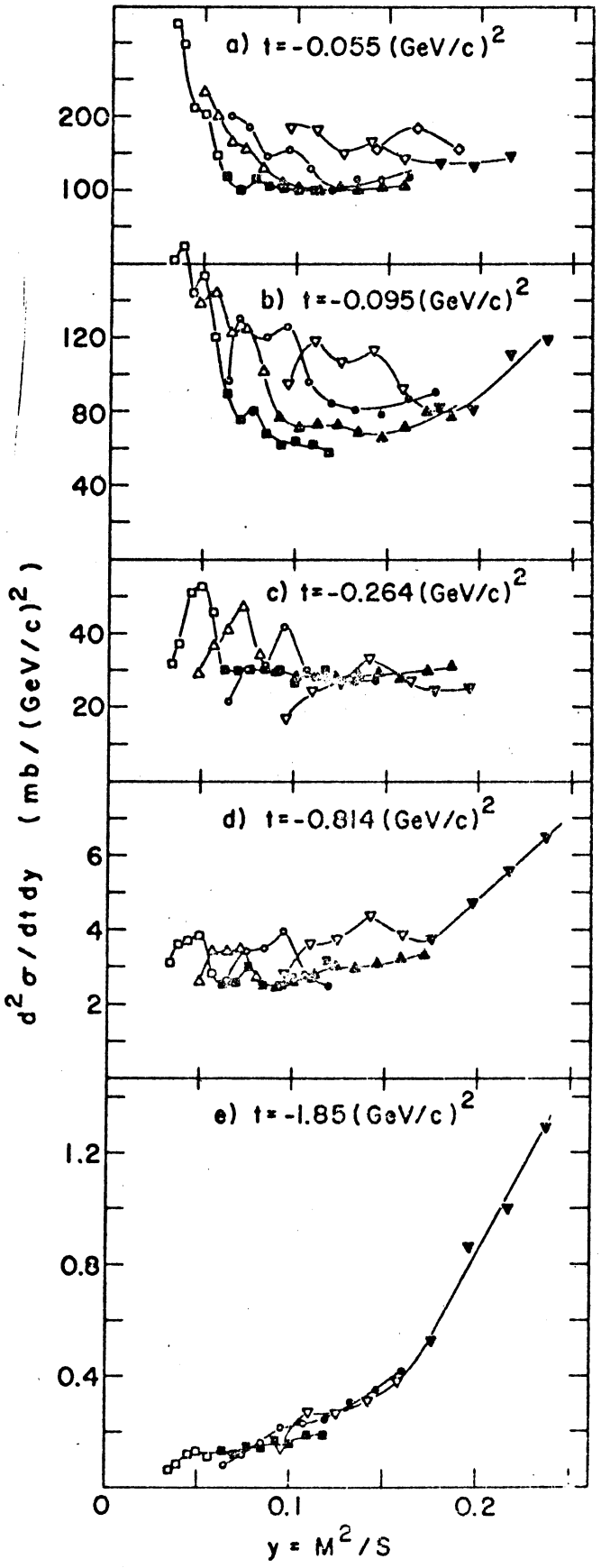
a) t=-0.055 (GeV/c)^2
b) t=-0.095 (GeV/c)^2
c) t=-0.264 (GeV/c)^2
d) t=-0.814 (GeV/c)^2
e) t=-1.85 (GeV/c)^2
200
100
120
80
40
40
20
6
4
2
1.2
0.8
0.4
0
0.1
0.2
$d^2\sigma/dtdy$ (mb/(GeV/c)^2)
$y = M^2/S$

- Figure 39 -

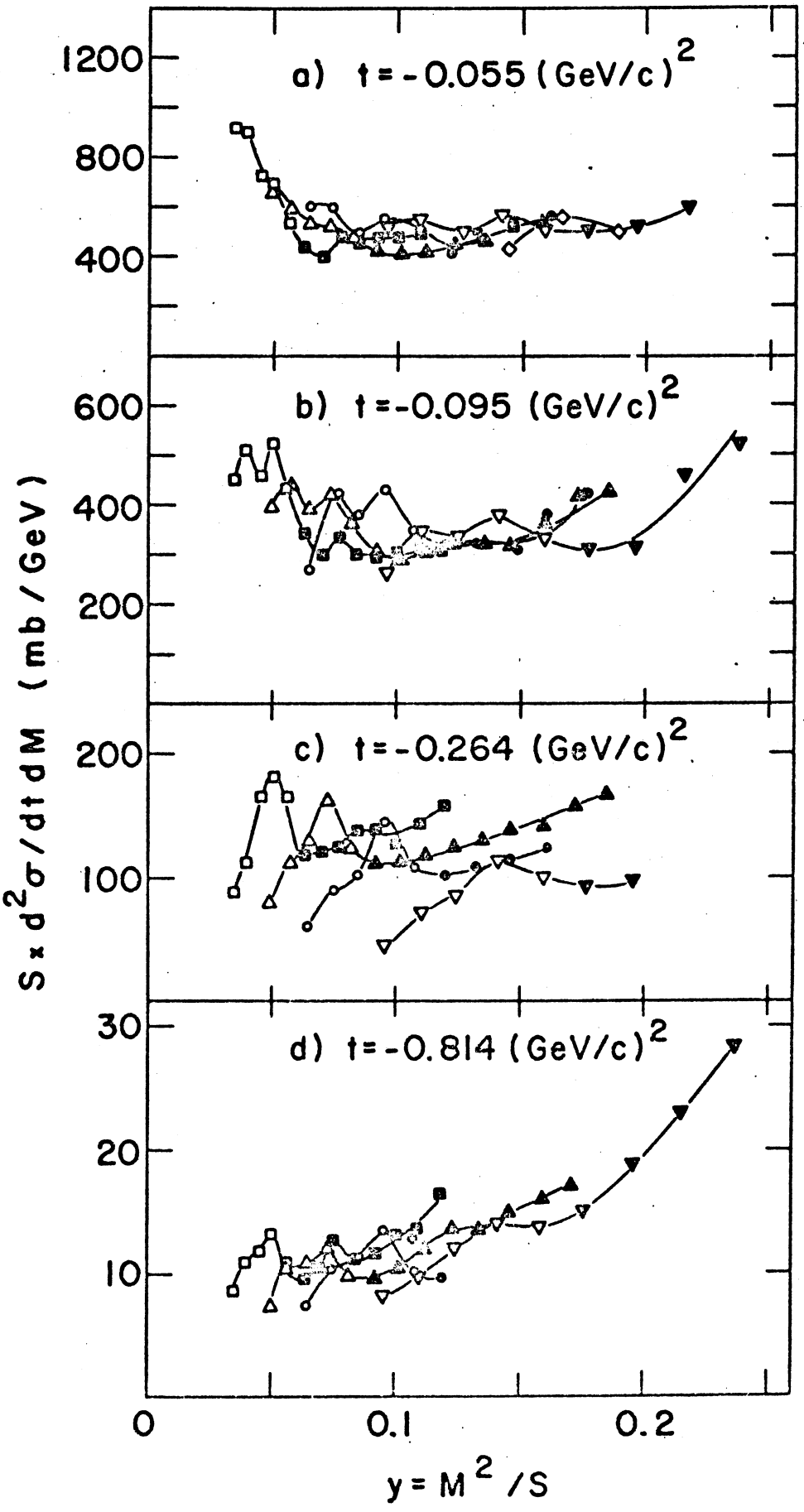
a) t = -0.055 (GeV/c)^2
b) t = -0.095 (GeV/c)^2
c) t = -0.264 (GeV/c)^2
d) t = -0.814 (GeV/c)^2
1200
800
400
600
400
200
200
100
30
20
10
0
0.1
0.2
$S \times d^2\sigma/dt\,dM$ (mb/GeV)
$y = M^2/S$

- Figure 40 -

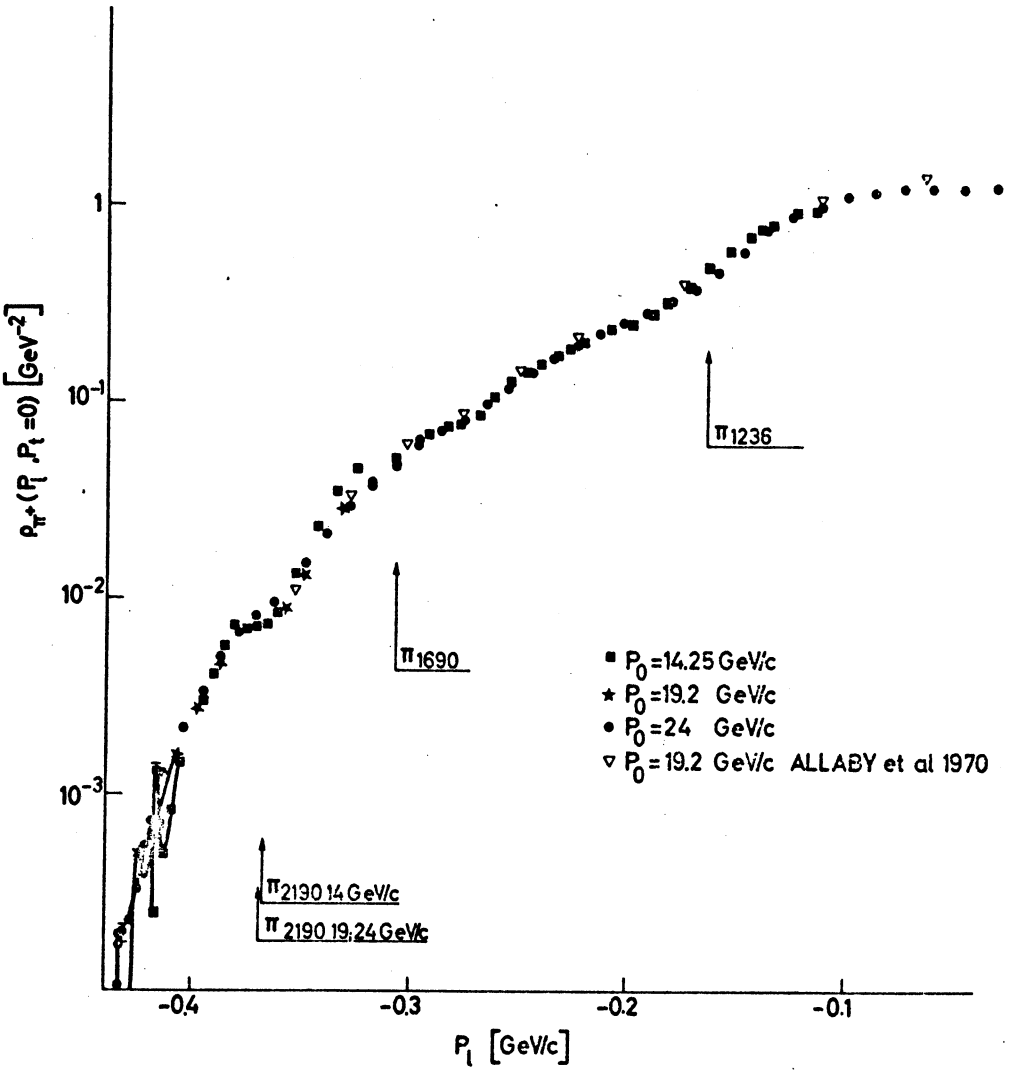
$\rho_{\pi^+}(P_l, P_t=0)$ [GeV^{-2}]
1
10^{-1}
10^{-2}
10^{-3}
-0.4
-0.3
-0.2
-0.1
P_l [GeV/c]
π_{1236}
π_{1690}
π_{2190} 14 GeV/c
π_{2190} 19;24 GeV/c
P_0 = 14.25 GeV/c
P_0 = 19.2 GeV/c
P_0 = 24 GeV/c
P_0 = 19.2 GeV/c ALLABY et al 1970

- Figure 41 -

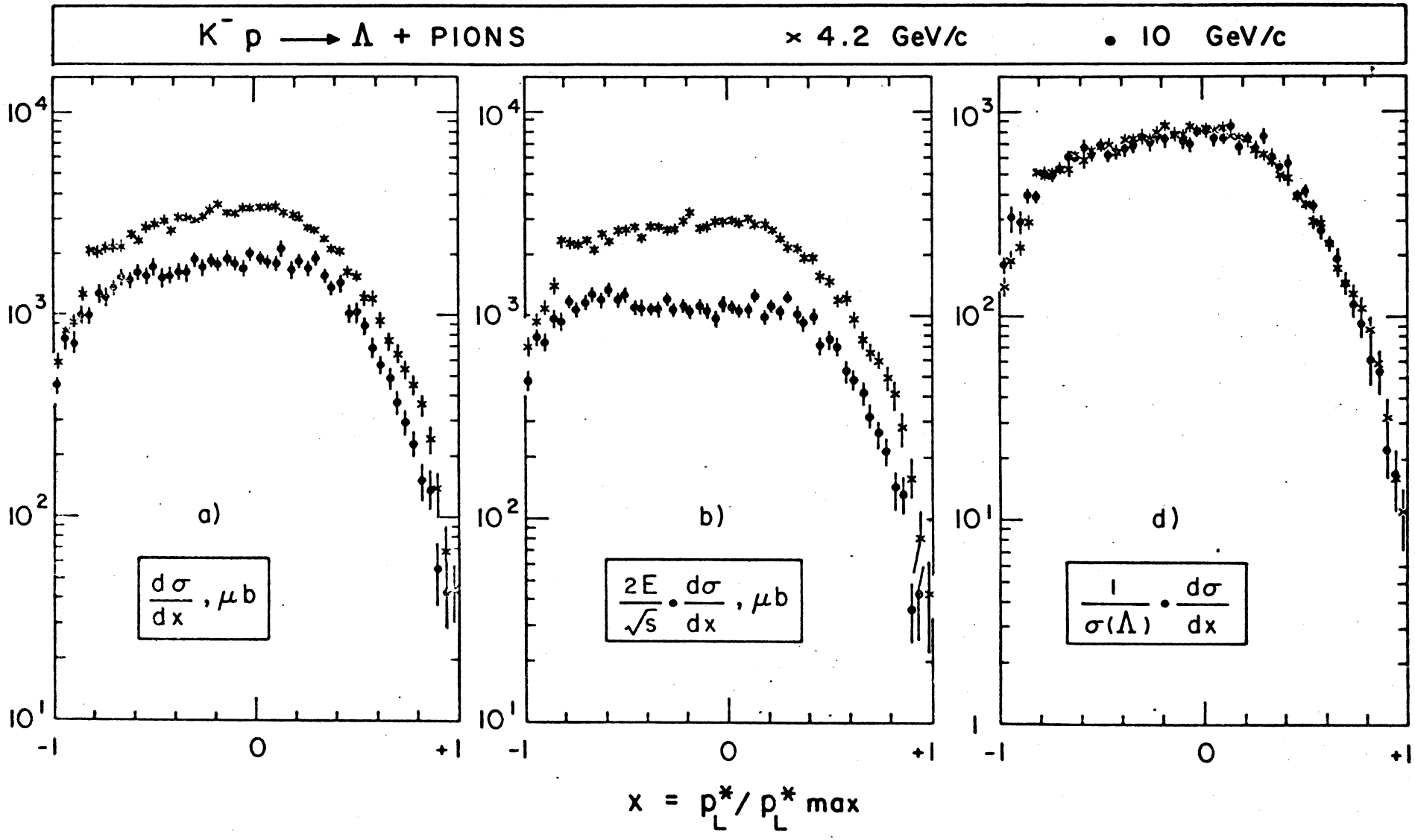
K⁻ p ⟶ Λ + PIONS
× 4.2 GeV/c
• 10 GeV/c
a)
b)
d)
dσ/dx , μb
2E/√s • dσ/dx , μb
1/σ(Λ) • dσ/dx
x = p*L / p*L max

- Figure 42 -

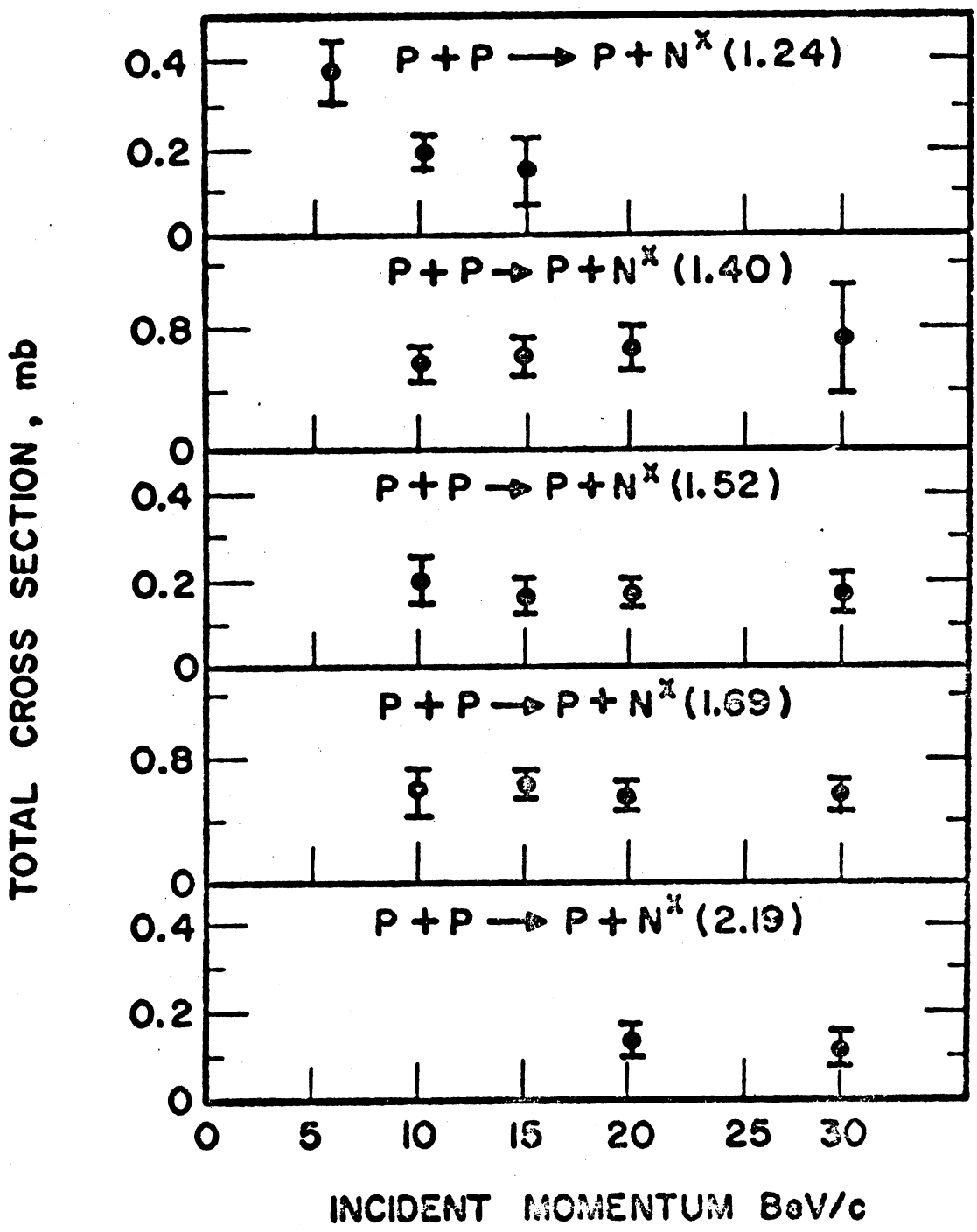
P + P → P + N* (1.24)
P + P → P + N* (1.40)
P + P → P + N* (1.52)
P + P → P + N* (1.69)
P + P → P + N* (2.19)
0.4
0.2
0
0.8
0
0.4
0.2
0
0.8
0
0.4
0.2
0
0 5 10 15 20 25 30
TOTAL CROSS SECTION, mb
INCIDENT MOMENTUM BeV/c

- Figure 43 -

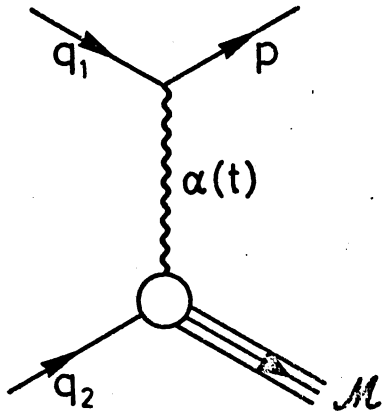

- Figure 44 -

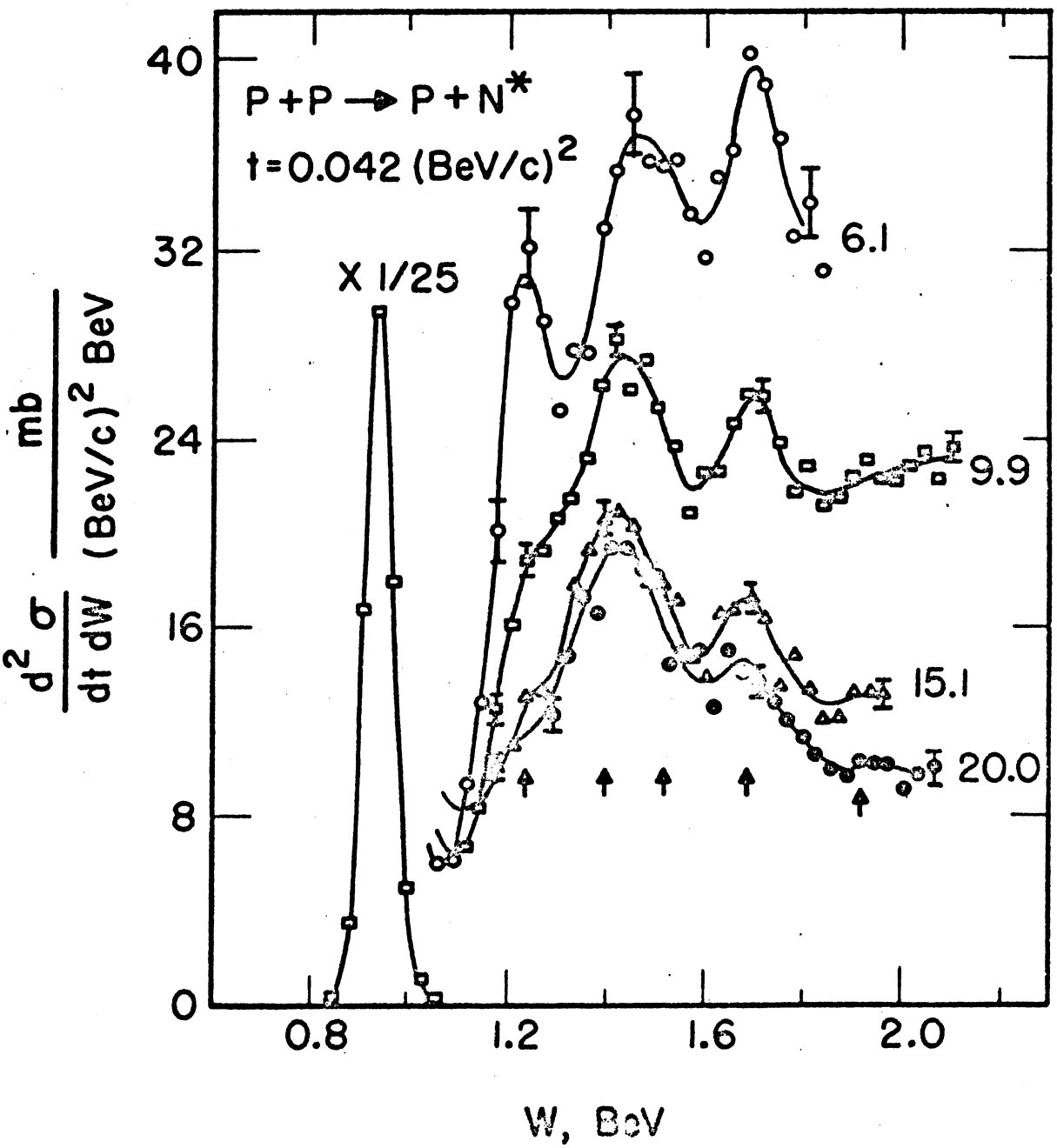
P+P → P+N*
t=0.042 (BeV/c)²
X 1/25
6.1
9.9
15.1
20.0
40
32
24
16
8
0
0.8
1.2
1.6
2.0
W, BeV
d²σ / dt dW mb / (BeV/c)² BeV

- Figure 45 -

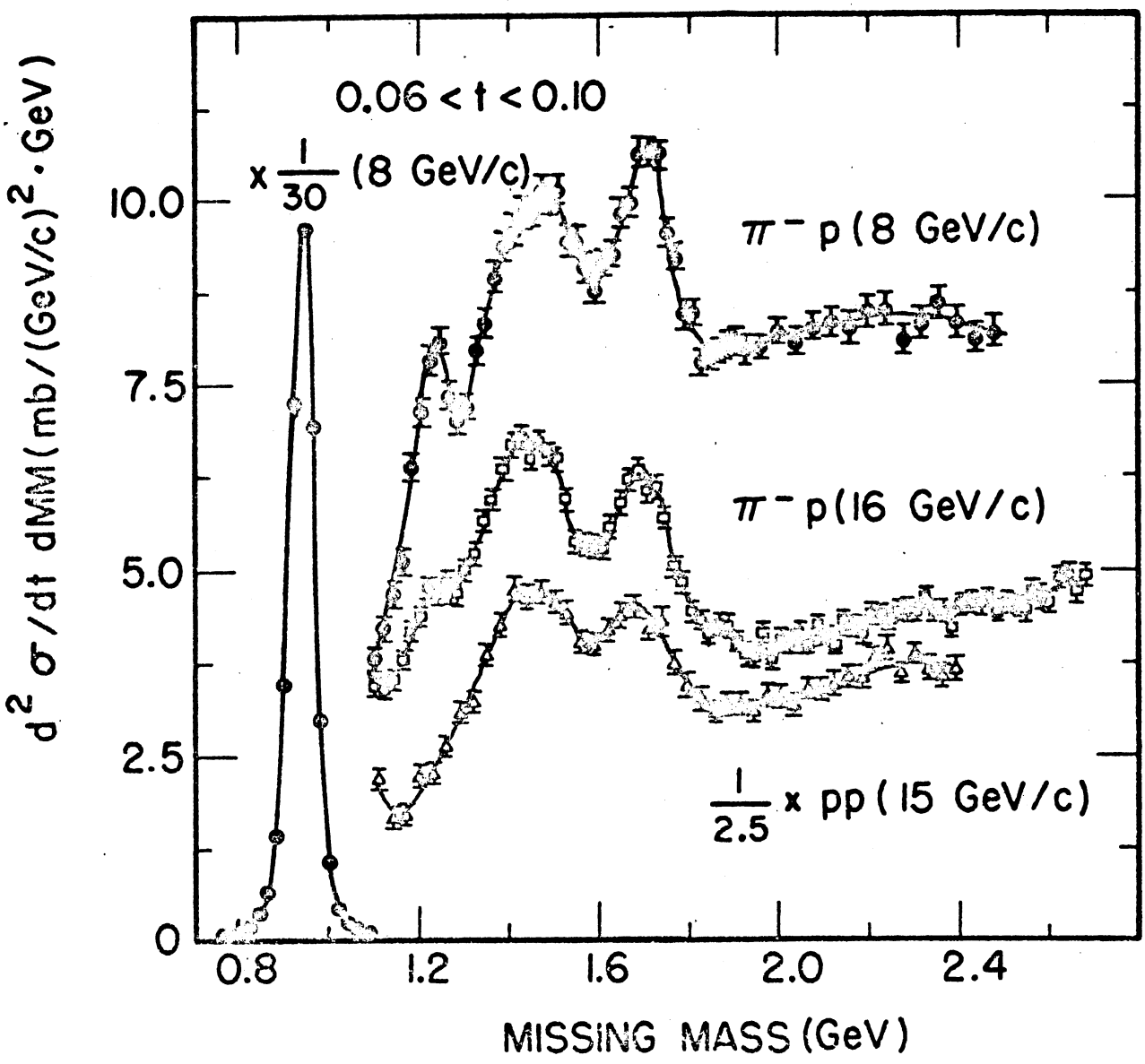
0.06 < t < 0.10
x 1/30 (8 GeV/c)
π⁻ p (8 GeV/c)
π⁻ p (16 GeV/c)
1/2.5 x pp (15 GeV/c)
d² σ/dt dMM (mb/(GeV/c)² · GeV)
10.0
7.5
5.0
2.5
0
0.8
1.2
1.6
2.0
2.4
MISSING MASS (GeV)

- Figure 46 -

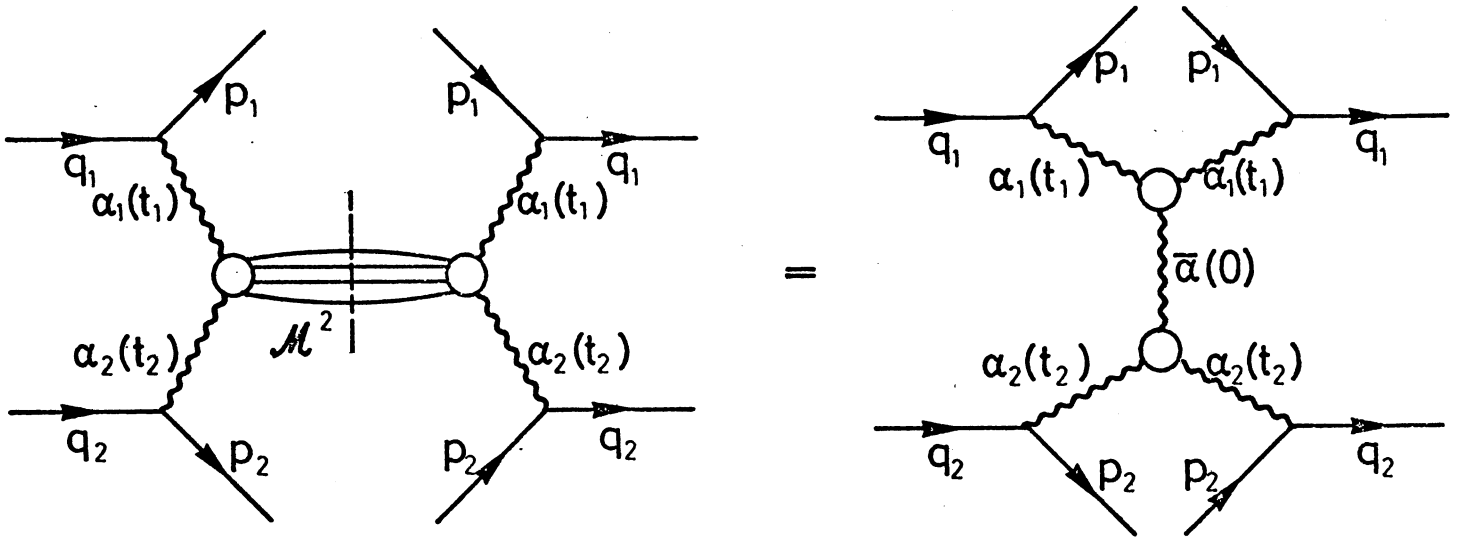
p1
p1
q1
α1(t1)
α1(t1)
q1
M2
α2(t2)
α2(t2)
q2
p2
p2
q2
=
p1
p1
q1
α1(t1)
ᾱ1(t1)
q1
ᾱ(0)
α2(t2)
α2(t2)
q2
p2
p2
q2

- Figure 47 -

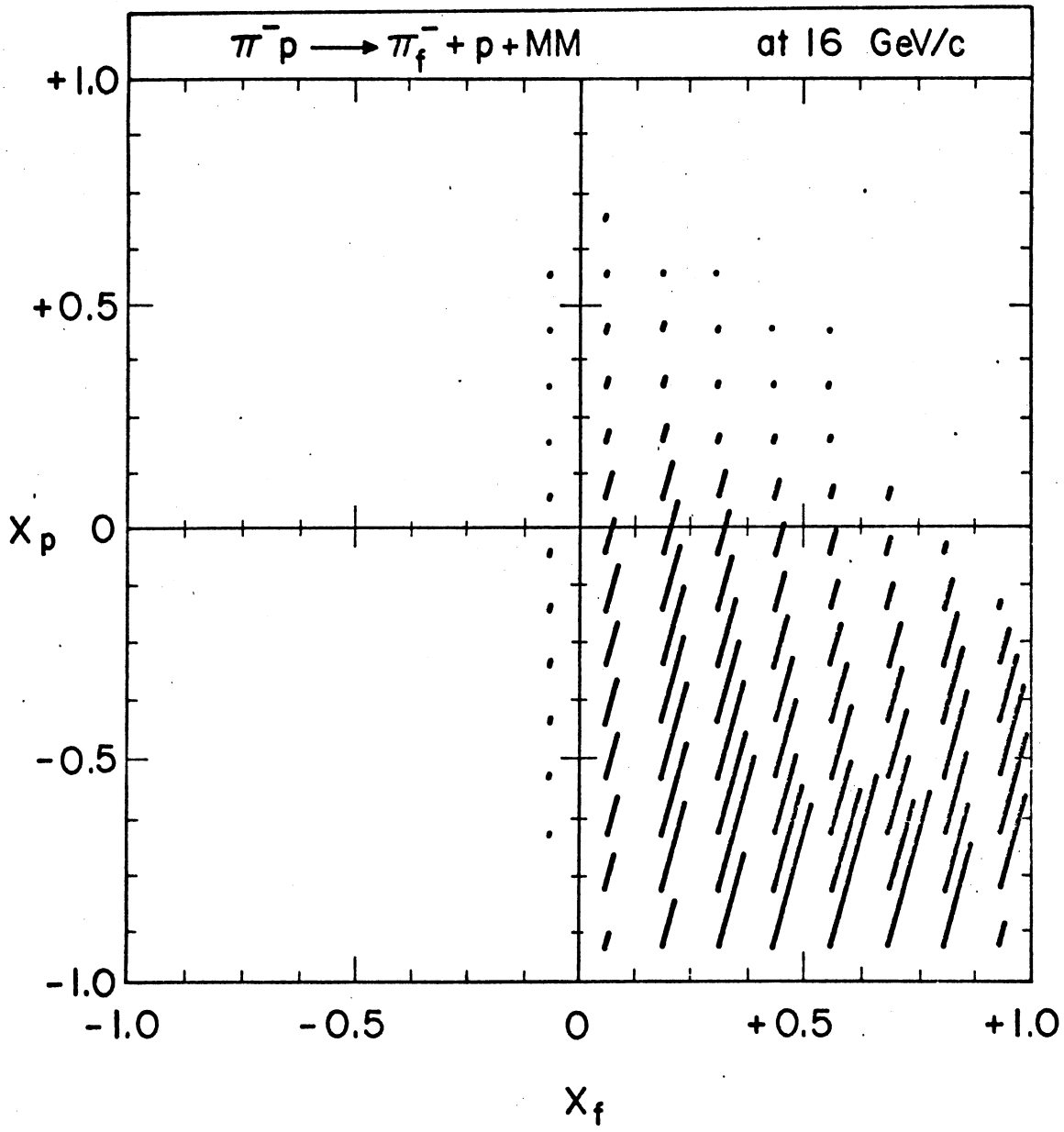
$\pi^- p \longrightarrow \pi_f^- + p + MM$
at 16 GeV/c
+1.0
+0.5
X_p 0
-0.5
-1.0
-1.0
-0.5
0
+0.5
+1.0
X_f

- Figure 48 -

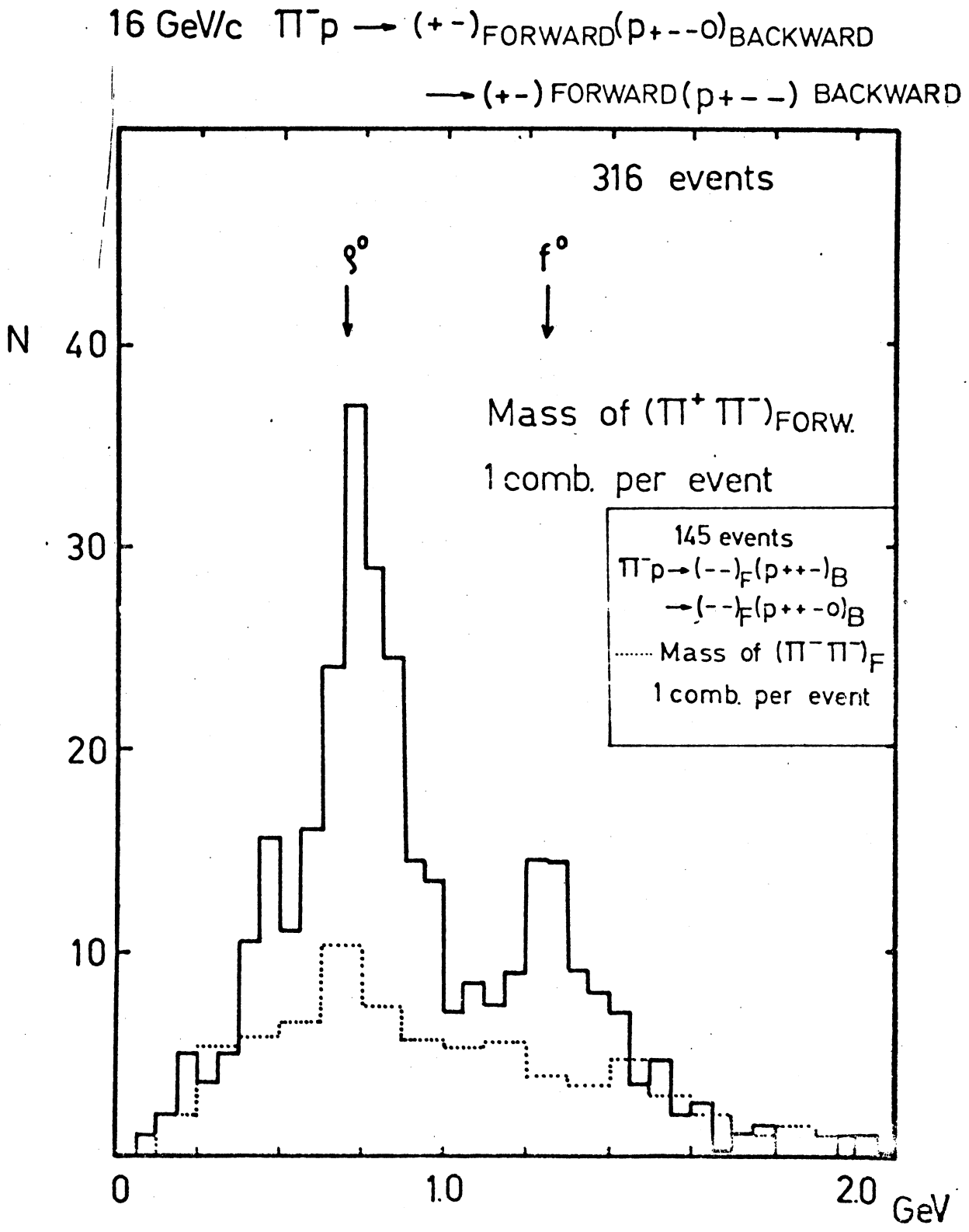
16 GeV/c $\pi^- p \rightarrow (+-)_{FORWARD}(p+--o)_{BACKWARD}$
$\rightarrow (+-)_{FORWARD}(p+--)_{BACKWARD}$
316 events
ϱ^0
f^0
N
40
30
20
10
Mass of $(\pi^+\pi^-)_{FORW.}$
1 comb. per event
145 events
$\pi^- p \rightarrow (--)_F(p++-)_B$
$\rightarrow (--)_F(p++-o)_B$
Mass of $(\pi^-\pi^-)_F$
1 comb. per event
0
1.0
2.0
GeV

- Figure 49 -

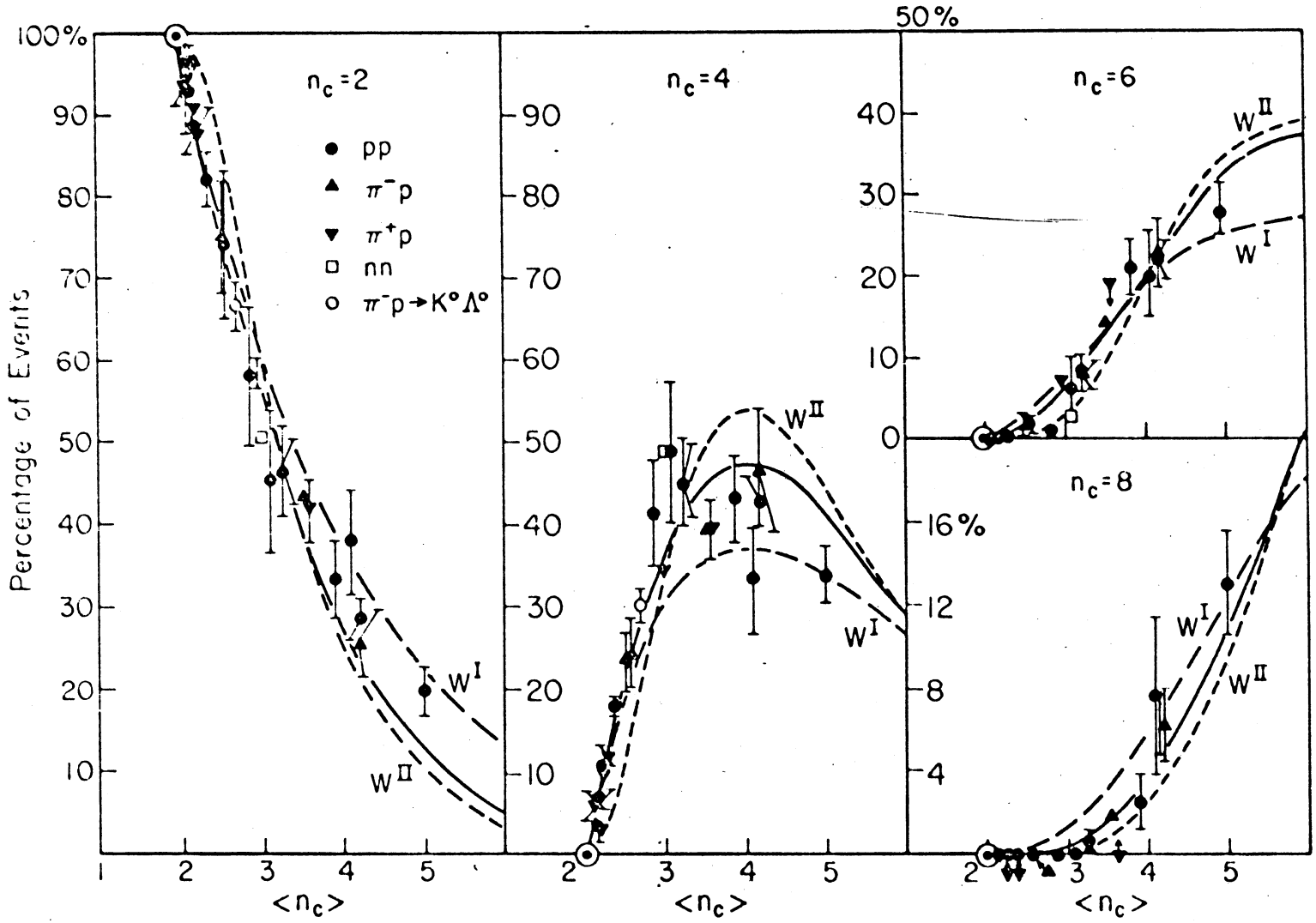
100%
90
80
70
60
50
40
30
20
10
Percentage of Events
$n_c=2$
pp
π^-p
π^+p
nn
$\pi^-p\to K^\circ\Lambda^\circ$
W^I
W^{II}
1
2
3
4
5
$\langle n_c\rangle$
$n_c=4$
W^{II}
W^I
$n_c=6$
50%
40
30
20
10
0
W^{II}
W^I
$n_c=8$
16%
12
8
4
W^I
W^{II}

- Figure 50 -

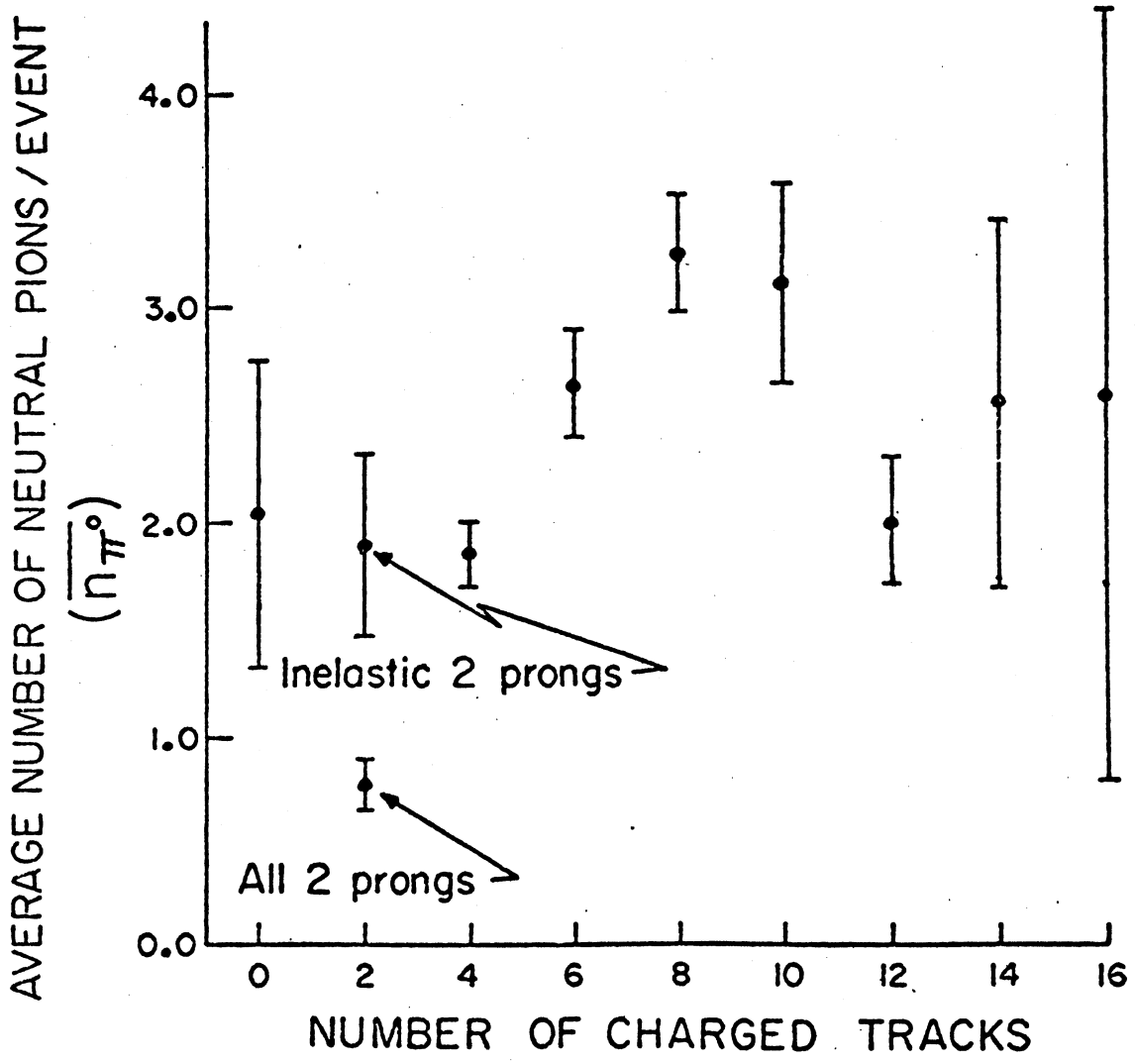
AVERAGE NUMBER OF NEUTRAL PIONS / EVENT
$(\overline{n_{\pi^0}})$
4.0
3.0
2.0
1.0
0.0
Inelastic 2 prongs
All 2 prongs
0
2
4
6
8
10
12
14
16
NUMBER OF CHARGED TRACKS

- Figure 51 -